Applied Catalysis B: Environmental 202 (2017) 217–261

Contents lists available at ScienceDirect

Applied Catalysis B: Environmental

journal homepage: www.elsevier.com/locate/apcatb

Review

Electrochemical advanced oxidation processes: A review on their application to synthetic and real wastewaters

Francisca C. Moreira[a,*], Rui A.R. Boaventura[a], Enric Brillas[b], Vítor J.P. Vilar[a,*]

[a] Laboratory of Separation and Reaction Engineering – Laboratory of Catalysis and Materials (LSRE-LCM), Departamento de Engenharia Química, Faculdade de Engenharia, Universidade do Porto, Rua Dr. Roberto Frias, 4200-465 Porto, Portugal

[b] Laboratori d'Electroquímica dels Materials i del Medi Ambient, Departament de Química Física, Facultat de Química, Universitat de Barcelona, Martí i Franquès 1-11, 08028 Barcelona, Spain

ARTICLE INFO

Article history:
Received 23 May 2016
Received in revised form 10 August 2016
Accepted 16 August 2016
Available online 18 August 2016

Keywords:
Anodic oxidation
Electro-Fenton
Photoelectro-Fenton
Synthetic wastewaters
Real wastewaters

ABSTRACT

Over the last decades, research efforts have been made at developing more effective technologies for the remediation of waters containing persistent organic pollutants. Among the various technologies, the so-called electrochemical advanced oxidation processes (EAOPs) have caused increasing interest. These technologies are based on the electrochemical generation of strong oxidants such as hydroxyl radicals (•OH). Here, we present an exhaustive review on the treatment of various synthetic and real wastewaters by five key EAOPs, i.e., anodic oxidation (AO), anodic oxidation with electrogenerated H_2O_2 (AO-H_2O_2), electro-Fenton (EF), photoelectro-Fenton (PEF) and solar photoelectro-Fenton (SPEF), alone and in combination with other methods like biological treatment, electrocoagulation, coagulation and membrane filtration processes. Fundamentals of each EAOP are also given.

Contents

Abbreviations: AC, activated carbon; ACF, activated carbon fiber; AO, anodic oxidation; AOP, advanced oxidation process; BDD, boron-doped diamond; BOD_5, 5-day biochemical oxygen demand; CF, carbon felt; CNT, carbon nanotube; COD, chemical oxygen demand; CPC, compound parabolic collector; DOC, dissolved organic carbon; DSA, dimensionally stable anode; EAOP, electrochemical advanced oxidation process; EC, electrocoagulation; EF, electro-Fenton; GDE, gas-diffusion electrode; LMCA, low-molecular-weight carboxylic acids; MCE, mineralization current efficiency; MF, microfiltration; MWWTP, municipal wastewater treatment plant; NF, nanofiltration; PAN, polyacrylonitrile; PC, peroxi-coagulation; PEF, photoelectro-Fenton; PF, photo-Fenton; PTFE, polytetrafluoroethylene; RO, reverse osmosis; ROS, reactive oxygen species; RSM, response surface methodology; RVC, reticulated vitreous carbon; SPC, solar heterogeneous photocatalysis; SPEF, solar photoelectro-Fenton; SPF, solar photo-Fenton; SS, stainless steel; TOC, total organic carbon; TSS, total suspended solids; UF, ultrafiltration; UV, ultraviolet; UVA, ultraviolet A; UVB, ultraviolet B; UVC, ultraviolet C; UV–vis, ultraviolet-visible; VSS, volatile suspended solids; WWTP, wastewater treatment plant; $[TDI]_0$, initial total dissolved iron concentration; [TDI], total dissolved iron concentration; E, electrode potential (V); EC_V, energy consumption per unit volume (kWh m^{-3}); EC_{DOC}, energy consumption per unit DOC mass (kWh (g DOC)$^{-1}$); E_{cell}, average cell potential (V); $E°$, standard redox potential (V/SHE); I, current intensity (mA); j, current density (mA cm^{-2}); j_{cat}, cathodic current density (mA cm^{-2}); Q, specific charge (Ah L^{-1}); T, temperature (°C); V, volume (L); λ, wavelength (nm); •OH, hydroxyl radical; Cl•, chorine radical; HO_2•, hydroperoxyl radical; SO_4•$^-$, sulfate radical.

* Corresponding authors.
E-mail addresses: francisca.moreira@fe.up.pt (F.C. Moreira), vilar@fe.up.pt (V.J.P. Vilar).

http://dx.doi.org/10.1016/j.apcatb.2016.08.037
0926-3373/

1. Introduction

One of the main current worldwide concerns is the growth of water pollution by organic compounds arising from many industrial, agricultural and urban human activities. The vast majority of these compounds are persistent organic pollutants, owing to their resistance to conventional treatments such as coagulation, biological oxidation, adsorption, ion exchange and chemical oxidation. As a result, they have been detected in rivers, lakes, oceans and even drinking waters all over the world. This constitutes a serious environmental health problem mainly due to their toxicity and potential hazardous health effects (carcinogenicity, mutagenicity and bactericidality) on living organisms, including human beings [1–4].

Over around the past three decades, research efforts have been made at developing more effective technologies to totally remove persistent organic pollutants from wastewaters. In this context, advanced oxidation processes (AOPs) acquired high relevance [5]. AOPs are based on the in situ production of highly reactive hydroxyl radicals (•OH) that non-selectively react with most organics, being able to degrade even highly recalcitrant compounds [6]. This radical is the second strongest oxidant known after fluorine, displaying a high standard redox potential of $E^{\circ}(^{\bullet}OH/H_2O) = 2.80$ V/SHE [7] and rate constants for reaction with several contaminants in the order of 10^6 to 10^{10} M^{-1} s^{-1} [8]. Moreover, •OH have a short lifetime, estimated as only a few nanoseconds in water [9], and so they can be self-eliminated from the treatment system. The most common AOPs are H_2O_2 with UVC radiation (H_2O_2/UVC), ozone and ozone based processes (O_3, O_3/UVC, O_3/H_2O_2 and O_3/H_2O_2/UVC), titanium dioxide based processes (TiO_2/UV and TiO_2/H_2O_2/UV) and Fenton's reaction based methods (Fenton – Fe^{2+}/H_2O_2 and photo-Fenton (PF) – Fe^{2+}/H_2O_2/UV) [10,11].

Over the last two decades, electrochemical advanced oxidation processes (EAOPs) have gained increasing attention as a promising class of AOPs [12–15]. The former, simplest and most popular EAOP is anodic oxidation (AO), where organics can be directly oxidized at the anode surface by electron transfer and/or indirectly oxidized by •OH weakly physisorbed at the anode surface and/or agents at the bulk solution such as active chlorine species, O_3, persulfates and H_2O_2 [16,17]. When AO is performed along with cathodic electrogeneration of H_2O_2, the process is called anodic oxidation with electrogenerated H_2O_2 (AO-H_2O_2) [18]. The electrochemical production of H_2O_2 with the addition of Fe^{2+} to the bulk originates the common and widely studied electro-Fenton (EF) process, in which additional •OH are produced in the bulk from Fenton's reaction. Furthermore, Brillas' group has proposed and extensively studied the photoelectro-Fenton (PEF) and solar photoelectro-Fenton (SPEF) processes, which combine the EF technique with irradiation provided by artificial light or natural sunlight, respectively [13]. Other EAOPs like peroxi-coagulation (PC), Fered-Fenton, electrochemical peroxidation and sonoelectro-Fenton have also been applied to the remediation of various wastewaters [19–21]. Due to the high capital and operating costs of EAOPs, the development of combined treatment strategies including biological processes, chemical coagulation, electrocoagulation (EC) and membrane processes have also been proposed to optimize the wastewater treatment [19,22–24].

Recently, Sirés et al. [20] exposed a general overview on the application of AO, EF, PEF, SPEF and sonoelectrochemical processes for the treatment of synthetic and real wastewaters, focusing on the most updated works and giving a look to the future, but without an exhaustive and critical analysis of treatments. Other reviews have focused mainly on the use of technologies like AO, EF, sonoelectro-Fenton, Fered-Fenton and/or electrochemical peroxidation for the remediation of different kinds of effluents [5,14,17,19,25–28]. Vasudevan and Oturan [29] reviewed the use of distinct elec-

trochemical technologies like electrocoagulation, electrodialysis, electroflotation and AO for water remediation, with only a brief mention to EF process and the influence of operational variables on its performance. Brillas et al. [13] presented a comprehensive review on the application of EF process and various electrochemical technologies based on Fenton's reaction chemistry to wastewater treatment, including the less mentioned PEF and SPEF processes, but up to then the number of works on these two last methods was very limited. More recently, Brillas [30,31] pointed out sound literature revisions on wastewater depollution by the application of PEF and SPEF processes, however few researches dated after 2010 were mentioned. Sirés and Brillas [32] presented a review on the remediation of water pollution caused by pharmaceuticals, embracing electrochemical separation technologies such as membrane technologies, electrocoagulation and internal micro-electrolysis, and technologies that allow the degradation of pharmaceuticals, among them AO, EF and PEF.

This paper intents to be a powerful tool for researchers in the pursuit for exhaustive information on the remediation of diversified synthetic and real wastewaters by AO, AO-H_2O_2, EF, PEF and SPEF processes from their origins up to now, alone or in combination with other technologies like biological treatment, chemical coagulation, EC and membrane filtration processes. It encompasses the treatment of several kinds of synthetic wastewaters containing dyes, pesticides, pharmaceuticals and other pollutants, and also various real wastewaters such as textile effluents, pharmaceutical effluents, wastewaters from secondary treatment of wastewater treatment plants (WWTPs), landfill leachates, among others. The remediation of each wastewater was assessed separately, regarding many features like wastewater composition, applied EAOPs, configuration of electrochemical reactor, anode and cathode characteristics and operational parameters such as applied current density (j), liquid flow rate, temperature, pH and initial total dissolved iron concentration ($[TDI]_0$). Fundamentals of each technology are initially described to better analyze its characteristics and oxidative properties.

2. Fundamentals of EAOPs

Theoretical aspects of AO, AO-H_2O_2, EF, PEF and SPEF processes are comprehensively discussed below. Fig. 1 summarizes the main reactions occurring in these EAOPs.

2.1. Anodic oxidation

AO involves the pollutants oxidation by: (i) direct electron transfer to the anode surface M, (ii) heterogeneous reactive oxygen species (ROS) produced as intermediates of oxidation of water to oxygen, including the powerful physisorbed $^{\bullet}OH$ at the anode surface, denoted M($^{\bullet}OH$), generated via Eq. (1), and weaker oxidants like H_2O_2 produced from M($^{\bullet}OH$) dimerization by Eq. (2) and O_3 formed from water discharge at the anode surface by Eq. (3), and/or (iii) other weaker oxidant agents electrochemically produced from ions existing in the bulk [17].

$$M + H_2O \rightarrow M(^{\bullet}OH) + H^+ + e^- \quad (1)$$

$$2M(^{\bullet}OH) \rightarrow 2MO + H_2O_2 \quad (2)$$

$$3H_2O \rightarrow O_3 + 6H^+ + 6e^- \quad (3)$$

The efficiency of AO is highly dependent on the mass transfer of pollutants from the bulk to the anode surface or its vicinity [17]. Furthermore, studies performed during the last twenty years have shown strong influence of the anode material nature on both efficiency and selectivity of AO. Two very distinct behaviors of organic pollutants degradation depending on the anode material have been reported: (i) partial organics degradation, along with the formation of many refractory species as final products, and (ii) large or total organics mineralization, i.e., conversion into CO_2, water and inorganic ions, together with the production of few or null amounts of refractory intermediates. The more accepted explanation for this behavior was proposed by Comninellis [33], slightly being modified afterwards by Marselli et al. [34]. The model considers the interaction of M($^{\bullet}OH$) with the anode surface as the responsible for the existence of two types of anode materials: (i) the so-called active anodes, with low O_2-overpotentials, in which the M($^{\bullet}OH$) is transformed into a higher state oxide or superoxide MO via Eq. (4) that in combination with the anode surface M (redox couple MO/M) acts as selective mediator in the oxidation of organics, and (ii) the so-called non-active anodes, with high O_2-overpotentials, in which M($^{\bullet}OH$) are so weakly physisorbed at the anode surface that can react with organics, providing their mineralization.

Table 1
Potential for O_2 evolution at various anodes materials used in AO [12,230,231].

Anode material	Potential for O_2 evolution (V/SHE)
RuO_2	1.4–1.7
IrO_2	1.5–1.8
Pt	1.6–1.9
Graphite	1.7
Ebonex® (Ti_4O_7)	1.7–1.8
PbO_2	1.8–2.0
SnO_2	1.9–2.2
BDD	2.2–2.6

$$M(^{\bullet}OH) \rightarrow MO + H^+ + e^- \quad (4)$$

As a general rule, the higher potential for O_2 evolution of the anode material, the weaker is the interaction of M($^{\bullet}OH$) with the anode surface and the higher is the chemical reactivity toward organics oxidation [17]. Ruthenium dioxide (RuO_2), iridium dioxide (IrO_2), platinum (Pt), graphite and other sp^2 carbon based electrodes are typical examples of active anodes and exhibit potentials for O_2 evolution in general lower than 1.8 V/SHE, as can be seen in Table 1. Carbon-based materials cannot be robust enough against incineration, sometimes even when low j is applied [35]. On the other hand, lead dioxide (PbO_2), tin dioxide (SnO_2), boron-doped diamond (BDD) and sub-stoichiometric TiO_2 electrodes can be considered as non-active electrodes, presenting potentials of O_2 evolution from 1.7 to 2.6 V/SHE (see Table 1). The BDD anode is the most potent non-active anode known, thereby being considered the most suitable anode for AO [17,34]. The characteristics of BDD electrodes, including the substrate nature, e.g. silicon (Si), titanium (Ti), niobium (Nb), the boron content, the sp^3/sp^2 ratio and the BDD layer thickness, can strongly influence the organics oxidation [36]. Recently, the sub-stoichiometric TiO_2 has been reported as a promising anode material. There are several sub-oxides of TiO_2, collectively known as Magneli phases (Ti_nO_{2n-1}, $4 \leq n \leq 10$), where the most conductive compounds of the series are Ti_4O_7 and Ti_5O_9. Ceramic Magneli phase electrodes mainly consisting of Ti_4O_7 are commercially available, being known by the trade name Ebonex® [37]. It has been used in lab-scale water treatment applications [38,39]. Recent work compared Ebonex® electrodes with BDD, showing that the former produces lower amounts of $^{\bullet}OH$ than the latter but with higher reactivity [40].

The AO process can be improved by the action of oxidants like active chlorine species, persulfate, perphosphate, percarbonate and H_2O_2 that are electrochemically generated from agents existing in the bulk solution such as chloride, sulfate (or hydrogen sulfate), phosphate, carbonate (or hydrogen carbonate) and oxygen, respectively [17]. While active chlorine, persulfate, perphosphate and percarbonate are produced from anodic oxidation, the H_2O_2 is generated from cathodic reduction. Salts can already compose the

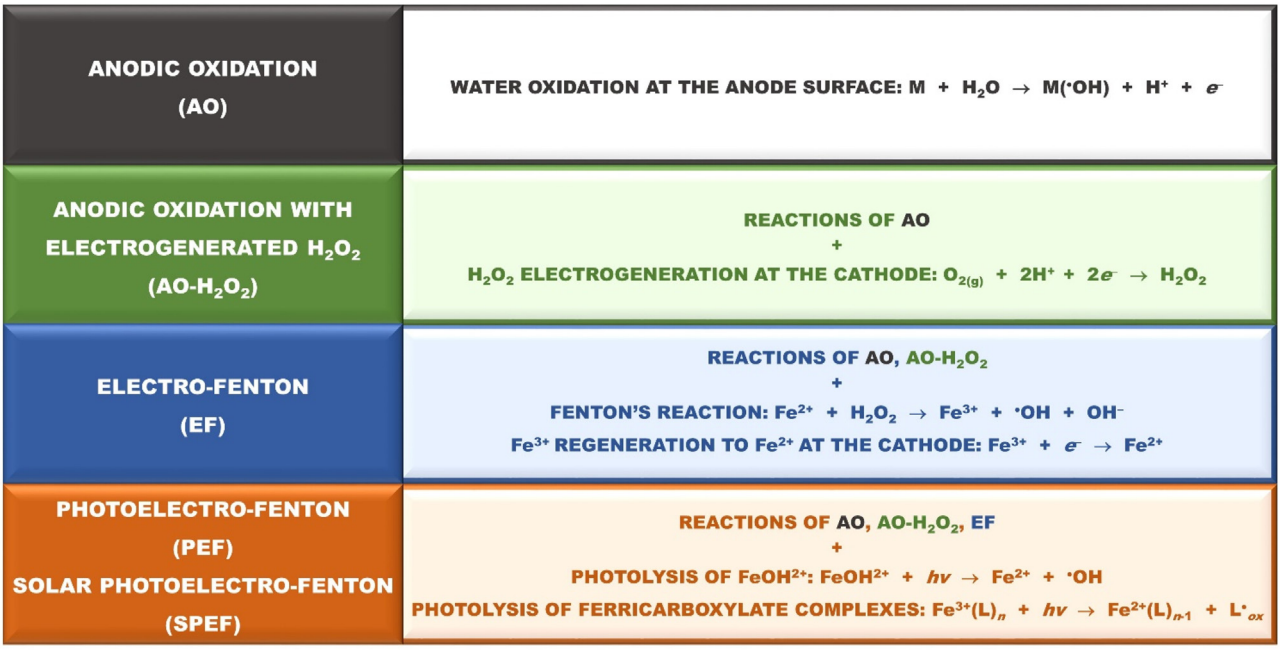

Fig. 1. EAOPs covered in this review and their main reactions.

wastewater matrix or, alternatively, they can be externally added. In the presence of these indirect oxidation processes, the AO is generally called mediated oxidation.

Active chlorine species are the main indirect oxidation agents employed in wastewater treatment. The mediated oxidation with active chlorine is based on the direct oxidation of chloride ions at the anode to yield chlorine (Cl_2) through Eq. (5), which diffuses away from the anode to be disproportionated to hypochlorous acid (HClO) and chloride via Eq. (6) [17].

$$2Cl^- \rightarrow Cl_2 + 2e^- \quad (5)$$

$$Cl_2 + H_2O \leftrightarrow HClO + Cl^- + H^+ \quad (6)$$

In the solution bulk, the HClO is in equilibrium with hypochlorite ion (ClO^-) with pK_a of 7.5, as shown in Eq. (7) [41].

$$HClO \leftrightarrow ClO^- + H^+ \quad (7)$$

Up to pH 3 the predominant active chlorine species is Cl_2, from pH 3–8 the dominant species is HClO and for pH above 8 the ClO^- prevails [42]. Since HClO (E° = 1.49 V/SHE) and Cl_2 (E° = 1.36 V/SHE) exhibit higher redox potentials than ClO^- (E° = 0.89 V/SHE), the oxidation of organics should be faster in acidic than in alkaline media [43]. HClO content can be decreased due to their electrochemically conversion to chlorate ion (ClO_3^-) according to Eq. (8), with consequent attenuation of organics degradation since ClO_3^- is not a good oxidant for organics at room temperature [44].

$$6HClO + 3H_2O \rightarrow 2ClO_3^- + 4Cl^- + 12H^+ + 1.5O_2 + 6e^- \quad (8)$$

For some electrodes, such as BDD, the perchlorate ion (ClO_4^-) is also formed during AO because of the action of M(•OH) via Eqs. (9)–(12) [44].

$$Cl^- + {}^\bullet OH \rightarrow ClO^- + H^+ + e^- \quad (9)$$

$$ClO^- + {}^\bullet OH \rightarrow ClO_2^- + H^+ + e^- \quad (10)$$

$$ClO_2^- + {}^\bullet OH \rightarrow ClO_3^- + H^+ + e^- \quad (11)$$

$$ClO_3^- + \rightarrow ClO_4^- + H^+ + e^- \quad (12)$$

ClO_4^- is the least reactive oxidant of the chloro-oxoanions and it is known for its hazardousness for human health [45]. The rates of electrode reactions (5) and (8)-(12) are a function of the electrocatalytic activity of the anode, chloride content, salt cation, stirring or liquid flow rate, temperature and applied current [46,47].

In addition, the formation of organochlorinated species, including chloramines, trihalomethanes, haloacetonitriles and haloketones, has been detected during AO due to reaction of active chlorine species with different functional groups of organic matter [48–50]. This is a major drawback of AO in the presence of active chlorine, because organochlorinated products are very toxic and usually more recalcitrant than parent molecules.

The strong persulfate, perphosphate and percarbonate oxidants can be efficiently produced by Eqs. (13), (14) and (15), respectively [17], only using non-active anodes such as BDD and PbO_2 [51,52].

$$2SO_4^{2-} \rightarrow S_2O_8^{2-} + 2e^- \quad (13)$$

$$2PO_4^{3-} \rightarrow P_2O_8^{4-} + 2e^- \quad (14)$$

$$2CO_3^{2-} \rightarrow C_2O_6^{2-} + 2e^- \quad (15)$$

H_2O_2 can be generated in the bulk from the two-electron reduction of oxygen (directly injected as pure gas or bubbled air) at the cathode surface in acidic/neutral media, according to Eq. (16) with E° = 0.68 V/SHE [53].

$$O_{2(g)} + 2H^+ + 2e^- \rightarrow H_2O_2 \quad (16)$$

Reaction (16) is easier than the four-electron reduction of oxygen to water (E° = 1.23 V/SHE). In alkaline solutions, oxygen is reduced to hydroperoxide ion (HO_2^-), the conjugate base of H_2O_2 (pK_a = 11.64) [54]. The electrogeneration of H_2O_2 sometimes is called electroperoxidation [55] and the AO process carried out with electrochemical production of this oxidant is named anodic oxidation with electrogenerated H_2O_2 (AO-H_2O_2) [18].

H_2O_2 production and stability depend on factors such as cell configuration, cathode properties and operational conditions. Parasitic reactions such as H_2O_2 electrochemical reduction at the cathode surface via Eq. (17) and, in much lesser extent, H_2O_2 disproportion in the bulk from Eq. (18) can occur using both undivided and

divided electrochemical cells, diminishing the H_2O_2 accumulation in the system [56].

$$H_2O_2 + 2H^+ + 2e^- \rightarrow 2H_2O \quad (17)$$

$$2H_2O_2 \rightarrow O_{2(g)} + 2H_2O \quad (18)$$

Furthermore, when an undivided cell is used, H_2O_2 can also be oxidized to oxygen at the anode according to Eqs. (19) and (20), producing the weak oxidant hydroperoxyl radical ($HO_2^\bullet$) as intermediate [57].

$$H_2O_2 \rightarrow HO^\bullet_2 + H^+ + e^- \quad (19)$$

$$HO^\bullet_2 \rightarrow O_2 + H^+ + e^- \quad (20)$$

To attain high H_2O_2 electrogeneration efficiency, the contact between cathode, oxygen and water must be maximized. For this reason, porous cathodes like gas-diffusion electrodes (GDEs) and three-dimensional electrodes of high specific surface area are preferred for H_2O_2 electrogeneration. Since carbon is non-toxic and exhibits a high overpotential for H_2 evolution and low catalytic activity for H_2O_2 decomposition, along with relative good stability, conductivity and chemical resistance, carbonaceous cathodes have been widely employed for H_2O_2 electrogeneration with high efficiency [13]. Good examples of these cathodes are carbon-polytetrafluoroethylene (PTFE) gas (O_2 or air) diffusion electrodes [58,59], carbon or graphite felts [60,61], carbon sponge [62,63], activated carbon fiber (ACF) [64], carbon nanotube (CNT) [65,66], reticulated vitreous carbon (RVC) [67,68] and BDD [69,70].

H_2O_2 itself is only a moderately strong oxidant, exhibiting $E°(H_2O_2/H_2O) = 1.77$ V/SHE in acidic medium and $E°(H_2O_2/OH^-) = 0.88$ V/SHE in alkaline medium [71]. It is able to only attack reduced sulfur compounds, cyanides and some organics such as aldehydes, formic acid and some nitro-organic and sulfo-organic compounds [72]. For this reason, electrochemical processes with H_2O_2 electrogeneration are usually performed in the presence of Fe^{2+} ion to yield the Fenton's reagent, whose chemistry is explained in the section below.

2.2. Electro-Fenton

The classical Fenton's reagent is a mixture of H_2O_2 and Fe^{2+}, discovered by Fenton [73] and later clarified by Haber and Weiss [74]. It leads to the formation of the powerful •OH by the so-called Fenton's reaction (21) [74].

$$Fe^{2+} + H_2O_2 \rightarrow Fe^{3+} + {}^\bullet OH + OH^- \quad (21)$$

Sun and Pignatello [75] showed that Fenton's reaction can be efficiently applied in acidic pH 2.8–3.0. For most of the aqueous solutions, precipitation does not take place yet.

In excess of H_2O_2, Fe^{3+} can be reduced to Fe^{2+} via Eqs. (22) and (23) [74].

$$Fe^{3+} + H_2O_2 \rightarrow Fe^{2+} + HO^\bullet_2 + H^+ \quad (22)$$

$$Fe^{3+} + HO^\bullet_2 \rightarrow Fe^{2+} + O_2 + H^+ \quad (23)$$

Both Eqs. (22) and (23) are much slower than Fenton's reaction (21). Furthermore, Eq. (22) scavenges H_2O_2 to generate $HO_2^\bullet$, which exhibits a much lower oxidation power than •OH, and so it can be regarded as a parasitic reaction competing with Fenton's reaction (21) [13]. Also other parasitic reactions (24) and (25) can occur in the presence of H_2O_2 and Fe^{2+} in excess, respectively, and, as a consequence, the ratio $[H_2O_2]/[Fe^{2+}]$ must be optimized for each specific case [76].

$$H_2O_2 + {}^\bullet OH \rightarrow H_2O + HO^\bullet_2 \quad (24)$$

$$Fe^{2+} + {}^\bullet OH \rightarrow Fe^{3+} + OH^- \quad (25)$$

Note that the oxidant in Fenton's chemistry may not only be H_2O_2 [77]. HClO is also able to react with Fe^{2+} in a Fenton-type reaction, producing large amounts of •OH in the bulk [78]. Furthermore, other catalytic active metal ions like chromium, cerium, copper, cobalt, manganese and ruthenium can directly decompose H_2O_2 into •OH through conventional Fenton-like pathways [79].

Some of the major drawbacks of classical Fenton process, in which chemical Fenton's reagent is added to solution, are related to (i) the cost and risks associated with the provision, storage and transport of H_2O_2, (ii) the use of high amounts of iron with further formation of iron sludge that must be removed and properly treated at the end of the treatment, and (iii) the operation at acidic pH, which usually results in the need for acidification and subsequent neutralization [80]. To overcome some of these drawbacks and increase the efficiency of pollutants removal, EAOPs based on Fenton's reaction have been developed. The EF process is the most known and popular EAOP based on Fenton's reaction chemistry and it was developed and extensively applied over the last 15 years by Brillas' and Oturan's groups [13,81,82]. It comprises: (i) the in situ and continuous electrogeneration of H_2O_2 at a carbonaceous cathode fed with pure oxygen or air via Eq. (16), (ii) the addition of Fe^{2+} catalyst to the solution, and (iii) the cathodically reduction of Fe^{3+} to Fe^{2+} by Eq. (26), with consequent continuous production of Fenton's reagent [13].

$$Fe^{3+} + e^- \rightarrow Fe^{2+} \quad (26)$$

When an undivided cell is used, the EF process also counts on ROS produced at the anode, mainly M(•OH). In this context, the use of the emergent BDD anode significantly enhances the EF oxidation power.

Several cathode materials such as carbon-PTFE gas (O_2 or air) diffusion electrodes [81,83], carbon felt (CF) [82], carbon sponge [62] and RVC [68] have been applied for H_2O_2 electrogeneration in the EF process. Regarding the efficiencies, two major EF versions based on the nature of the cathode material can be distinguished, namely EF with carbon-PTFE air-diffusion electrode and EF with CF, which represent two extreme behaviors. In the former process, large amounts of H_2O_2 are accumulated in the medium with low Fe^{2+} regeneration from Eq. (26), whereas in the second one, all Fe^{3+} is continuously transformed into Fe^{2+} because of the low H_2O_2 electrogeneration at the CF cathode [84].

Recently, Kishimoto's group [85–87] developed an EF-type process using HClO and Fe^{2+}, where HClO is generated at the anode according to Eqs. (5) and (6) and iron is added to the solution to be regenerated from Fe^{3+} to Fe^{2+} at the cathode via Eq. (26).

The EF process should not be confused with other variations like PC, Fered-Fenton and electrochemical peroxidation, often called EF. The PC process, firstly proposed by Brillas' group [88], utilizes an individual cell that electrogenerates H_2O_2 at a carbonaceous cathode from Eq. (16) and simultaneously releases Fe^{2+} from a sacrificial iron anode according to Eq. (27). During this process, pollutants are oxidized by the attack of •OH in the bulk and their coagulation can also take place via $Fe(OH)_{3\,(s)}$ formation depending on pH.

$$Fe \rightarrow Fe^{2+} + 2e^- \quad (27)$$

The Fered-Fenton process involves the addition of both H_2O_2 and Fe^{2+} to the solution in an undivided cell along with the cathodic Fe^{3+} regeneration to Fe^{2+} by Eq. (26) [89]. In turn, the electrochemical peroxidation, firstly proposed by Lemley's group [90] and latter patented by Chiarenzelli's group [91], generally involves an undivided cell composed of a sacrificial iron anode for Fe^{2+} electrogeneration according to Eq. (27) and an inert cathode where hydrogen is produced from water reduction. Fe^{2+} is cathodically regenerated by Eq. (26), simultaneously with the external addition of H_2O_2 to the solution. Pollutants can then be removed both by the

attack of •OH in the bulk and by coagulation with $Fe(OH)_3$ precipitate. When a divided cell is applied, this process is called anodic Fenton treatment and the cathodic Fe^{3+} regeneration to Fe^{2+} cannot take place [92]. Both electrochemical peroxidation and anodic Fenton treatment should be regarded as variants of the PC technology.

2.3. Photoelectro-Fenton and solar photoelectro-Fenton

The irradiation of a solution treated under EF conditions by artificial UV light or natural sunlight leads to the PEF or SPEF processes, respectively, both proposed and extensively studied by Brillas' group [13,93–99]. In these photo-assisted treatments the degradation of pollutants is mainly accelerated by (i) the photoreduction of Fe(III)-hydroxy complexes, such as the most photoactive $FeOH^{2+}$ at pH near 3 according to Eq. (28) [75], with consequent •OH production and Fe^{2+} regeneration, and (ii) the direct photolysis by ligand-to-metal charge transfer excitation of complexes formed between Fe^{3+} and some organics, namely carboxylic acids, according to the general Eq. (29) [100–102], allowing the regeneration of Fe^{2+} in parallel with the formation of weak oxidizing species such as superoxide anion radical, carbon dioxide anion radical and H_2O_2.

$$FeOH^{2+} + h\nu \rightarrow Fe^{2+} + {}^{\bullet}OH \quad (28)$$

$$Fe^{3+}(L)_n + h\nu \rightarrow Fe^{2+}(L)_{n-1} + L^{\bullet}{}_{ox} \quad (29)$$

Artificial lamps providing UVA (λ of 315–400 nm), UVB (λ of 280–315 nm) and UVC (λ < 280 nm) radiation can be employed in PEF treatments. Depending on the wavelength and intensity of the radiation source, the pollutants can be degraded by different mechanisms and with increasing degradation rates for higher radiation intensities up to a given value. The photoreduction of photoactive Fe(III)-hydroxy complexes by Eq. (28) and the photolysis of Fe^{3+} complexes with organics by Eq. (29) occur under UV–vis radiation and direct photolysis of pollutants can take place when the light source emits radiation at the same wavelength range as the contaminants can absorb radiation efficiently. The application of UVC light in the presence of symmetrical peroxides such as H_2O_2 can lead to the generation of additional •OH through the homolytic cleavage of the peroxide (—O—O—) bond via Eq. (30) [6,103,104]. Note that Eq. (30) only takes place under UVC radiation, a common confusion of many researchers that report that it occurs for any type of UV light. Furthermore, high H_2O_2 contents are needed to generate high amounts of •OH via Eq. (30) due to the low absorption coefficient.

$$H_2O_2 + h\nu \rightarrow 2\ {}^{\bullet}OH \quad (30)$$

Among artificial lamps, the UVA lamps have been the most widely employed [18,105–108]. The use of artificial lamps in PEF technique is commonly responsible for high electrical costs, which can be minimized by the application of SPEF process, where the solution is directly irradiated with free and renewable natural sunlight. When comparing SPEF with PEF using low energy power artificial lamps, it is common to achieve higher pollutants degradation for SPEF due to a higher UV intensity of natural sunlight in simultaneous with an emission in the visible region (λ > 400 nm), thereby also leading to Fe(III)-carboxylate complexes direct photolysis according to Eq. (29).

Furthermore, the light irradiation of other species can lead to the production of other oxidation agents. For instance, persulfate can lead to the production of sulfate radical ($SO_4^{\bullet-}$) by Eq. (31) [109] and ClO^- can generate chorine radical (Cl•) and •OH from Eqs. (32) and (33), respectively [110].

$$S_2O_8^{2-} + h\nu \rightarrow 2SO^{\bullet}{}_4^- \quad (31)$$

$$ClO^- + h\nu \rightarrow O^{\bullet-} + Cl^{\bullet} \quad (32)$$

$$O^{\bullet-} + H_2O \rightarrow OH^- + {}^{\bullet}OH \quad (33)$$

Sun and Pignatello [75] showed that Fenton's reaction based processes can be efficiently applied in acidic pH 2.8–3.0. For most of the aqueous solutions, at this pH precipitation does not take place yet and the dominant iron species in solution is $FeOH^{2+}$, the most photoactive Fe(III)-hydroxy complex, as can be seen in the speciation diagram of Fe^{3+} in Fig. 2a.

2.4. Influence of operational parameters on EAOPs

The degradation of organic pollutants in aqueous solution by all mentioned EAOPs depends on various operational parameters such as initial organics concentration, supporting electrolyte nature, current density (j) or applied current (I) or applied electrode potential (E), stirring rate or liquid flow rate, temperature and pH. When carbonaceous cathodes are employed for H_2O_2 electrogeneration in AO-H_2O_2, EF, PEF and SPEF processes, the oxygen or air feeding flow rate also influences the process efficiency. In addition, the $[TDI]_0$ affects the efficiency of EAOPs based on Fenton's reaction. The effect of each parameter on EAOPs will be discussed in detail below and it is summarized in Table 2.

2.4.1. Initial organics concentration

For all EAOPs, the logical outcome is that solutions with higher initial organics concentration need longer treatment times to achieve a given degradation degree, as reported by many authors [111–115]. This outcome is often referred to as the attainment of lower percentages or efficiencies of pollutants removal for larger initial organics concentrations [96,116–118]. Moreover, it is consensual that the employment of greater initial pollutants contents leads to the removal of more amounts of pollutants per unit of time, i.e. higher pollutants removal rates [108,119–122]. This can be attributed to a faster oxidation of organics with •OH, inhibiting parasitic reactions like Eqs. (24) and (25).

In terms of pseudo-first-order kinetic constants for pollutants removal and mineralization, it is theoretically expected that these values are independent of the substrate content. However, it has been experimentally observed lower pseudo-first-order kinetic constants for increasing pollutants concentrations [67,108,114,123,124]. This can be ascribed to: (i) the shift of the rate-determining step from the diffusion process to the charge-transfer process on the electrode, which results in the shift from the pseudo-first-order kinetic to the zero-order kinetic and lowers the apparent pseudo-first-order kinetic constant, (ii) lower diffusion and/or mass transport toward/from electrodes of H_2O_2 and Fe^{2+} species in the presence of higher organic matter content, simultaneously with possible formation of larger amounts of Fe^{3+} complexes with organic matter, thus diminishing the production of •OH, and/or (iii) some limitations of this kinetic model to describe precisely the decay profiles, considering that a comprehensive mechanistic kinetic model may include all chemical, photocatalytic and electrochemical reactions occurring for each contaminant in solution, especially involving its oxidation products.

2.4.2. Supporting electrolyte nature and concentration

Supporting electrolytes are employed in EAOPs used for the degradation of model compounds to allow the flow of electrical current. Furthermore, the efficiency of EAOPs for the remediation of real effluents can be enhanced by the addition of ions, not only to yield better electrical current flow but also to provide the electrogeneration of strong oxidizing agents like active chlorine species [48,49,125].

Sodium sulfate (Na_2SO_4), sodium chloride (NaCl), potassium chloride (KCl), sodium perchlorate ($NaClO_4$), sodium nitrate

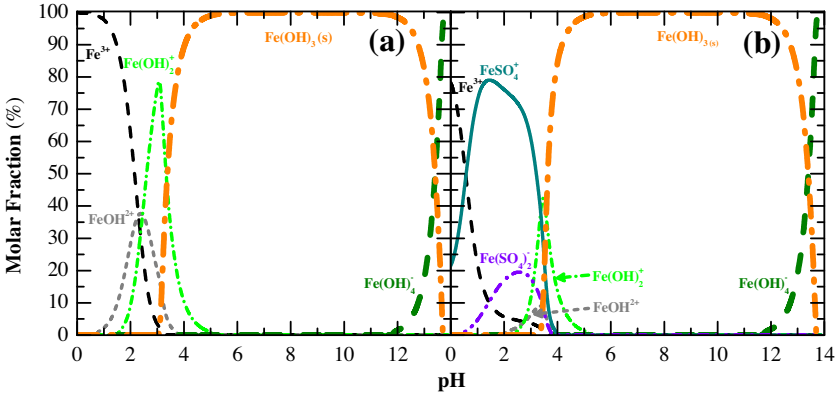

Fig. 2. Fe^{3+} speciation diagrams as a function of the solution pH in a calculated system containing: (a) 2.0 mg Fe^{3+} L^{-1} and (b) 2.0 mg Fe^{3+} L^{-1}, 4.7 g SO_4^{2-} L^{-1} and 2.3 g Na^+ L^{-1} (7.0 g L^{-1} Na_2SO_4). The formation of the solid iron phase $Fe(OH)_3$ was included in the calculation. Reprinted (adapted) from Moreira et al. [133], Copyright © (2014), with permission from Elsevier.

Table 2
Main EAOPs operational parameters and influence on degradation effectiveness.

Parameter	Influence on degradation efficiency
Initial organics concentration	All EAOPs – Higher initial organics concentrations require longer treatment times, lead to higher pollutants removal rates due to faster oxidation of organics with •OH and inhibition of parasitic reactions, and also result in lower pseudo-first-order kinetics constants.
Supporting electrolyte nature and concentration	Nature AO and AO-H_2O_2 – NaCl > Na_2SO_4 due to pollutants degradation by active chlorine species in the presence of chloride and/or scavenge of •OH by sulfate at higher rate than by chloride. EF and PEF – Controversial results: (i) NaCl > Na_2SO_4 due to pollutants degradation by active chlorine species in the presence of chloride, scavenging of •OH by sulfate at higher rate than by chloride and/or formation of sulfate-iron complexes; (ii) Na_2SO_4 > NaCl due to H_2O_2 consumption by reaction with HClO and/or formation of recalcitrant chloroderivatives; (iii) $NaClO_4$ > NaCl due to non-reactivity of ClO_4^- toward iron and •OH; or (iv) NaCl > $NaClO_4$. SPEF – Low influence of supporting electrolyte nature. The most applied supporting electrolyte is Na_2SO_4. Concentration Controversial results: higher degradation for larger contents of supporting electrolyte or higher degradation up to a given content.
Current density (or applied current or potential)	All EAOPs – Higher generation of oxidizing species, and consequent higher pollutants degradation, for larger j (or I or E) up to a value for which parasitic reactions occur in a such high extent that similar or even lower pollutants removal is attained for higher j.
Stirring rate or liquid flow rate	All EAOPs – High stirring rates or liquid flow rate lead to fast solution homogenization, prevention of solids deposition and assurance of proper mass transfer of pollutants toward electrodes, catalyst and, in case of light-assisted EAOPs, illuminated zone.
Temperature	AO and AO-H_2O_2 – Little influence. Increasing temperature enhances the mass transfer of reactants toward/from the electrodes and kinetic constants (both for •OH production and oxidation of organics by such species) are exponentially dependent on the temperature (Arrhenius law). EF, PEF and SPEF – Different influence depending on pH and wastewater composition since temperature affects not only the rate of Fe^{2+} generation and Fe^{3+} regeneration to Fe^{2+} by thermal reactions (22),(23) and (44) (higher rate for larger temperature) but also the amounts of $Fe(OH)_3$ precipitate, and, for light-induced EAOPs, the amount of photoactive species. Water evaporation and release of oxygen can occur for temperatures above 35 °C. Thermal decomposition of H_2O_2 into water and oxygen occurs in large extent for temperatures above 50 °C.
pH	AO and AO-H_2O_2 – Controversial results: (i) independency of pollutants degradation on pH or (ii) higher pollutants degradation at pH 3.0 or (iii) higher pollutants degradation at neutral pH. EF, PEF and SPEF: Commonly, maximum pollutants degradation at pH close to 3.0 due to predominance of Fenton's reaction, higher amounts of photoactive Fe(III)-hydroxy complexes, absence of iron precipitation, absence of scavenge of •OH by carbonate and bicarbonate species and null auto-decomposition of H_2O_2. Even though, some studies found similar process efficiency at pH 2.0–4.0. The addition of carboxylic acids can allow using higher pH values with high degradation efficiency.
O_2 or air feeding flow rate	AO-H_2O_2, EF, PEF and SPEF – High flow rates of oxygen (pure or air) ensure maximum H_2O_2 electrogeneration. Electrochemical cells with GDEs need to establish a compromise between liquid and oxygen flow rates to avoid cell flooding.
Initial total dissolved iron concentration	EF, PEF and SPEF – Higher degradation efficiency for increasing $[TDI]_0$ up to a value for which it is established an equilibrium between positive effects coming from the enhancement of Fenton's reaction and negatives effects arising from the growth of parasitic reactions and, for light-assisted EAOPs, inner filter effects and light attenuation along the photoreactor.

($NaNO_3$) and sodium carbonate (Na_2CO_3) are common supporting electrolytes. The nature of the supporting electrolyte can highly affect the degradation kinetics since the presence of some ions in solution can lead to: (i) the formation of strong oxidants such as active chlorine species produced by direct oxidation of chloride at the anode according to Eqs. (5) and (6), (ii) the scavenging of •OH in the presence of sulfate and chloride via Eqs. (34) and (35), respectively [126,127], (iii) the production of recalcitrant and toxic by-products like chloroderivatives that are only slowly degraded by •OH and active chlorine species, (iv) the consumption of H_2O_2

as it happens in the presence of $SO_4^{\bullet -}$ via Eqs. (36) and (37) and HClO at pH between 3 and 8 according to Eq. (38) [128], and (iv) the generation of complexes with iron like sulfato-iron and chloro-iron complexes [128], changing the amount of photoactive iron species like $FeOH^{2+}$, as exemplified in Fig. 2b, and also promoting the loss of free Fe^{2+} to participate in Fenton's reaction (21).

$$SO_4^{2-} + {}^{\bullet}OH \rightarrow SO^{\bullet}{}_4^{-} + OH^- \quad (34)$$

$$Cl^- + {}^{\bullet}OH \rightarrow [ClOH]^{\bullet -} \quad (35)$$

$$SO^{\bullet}{}_4^{-} + H_2O_2 \rightarrow SO_4^{2-} + H^+ + HO^{\bullet}{}_2 \quad (36)$$

$$SO^{\bullet}{}_4^{-} + HO^{\bullet}{}_2 \rightarrow SO_4^{2-} + H^+ + O_2 \quad (37)$$

$$HClO + H_2O_2 \rightarrow Cl^- + O_{2\,(g)} + H_2O + H^+ \quad (38)$$

For AO and AO-H_2O_2 processes, the removal of target compounds and mineralization were reported to occur more rapidly using NaCl when compared to Na_2SO_4 [23,129]. This can be mainly attributed to the pollutants degradation in the bulk by active chlorine species in the presence of chloride and/or the scavenging of $^{\bullet}OH$ by sulfate at higher rate than by chloride.

For EF and PEF processes, the degradation of primary compounds by applying NaCl and Na_2SO_4 has been attaining controversial results. While some studies achieved faster removal of target compounds using NaCl [23,130,131], others observed higher efficiency using Na_2SO_4 [67,68]. In terms of mineralization ability, the superiority of Na_2SO_4 over NaCl is consensual [23,131]. The faster target pollutants degradation by using NaCl instead of Na_2SO_4 was attributed to the attack of active chlorine species and the formation of sulfate-iron complexes in higher amount than chloro-iron complexes [128], leading to the loss of free Fe^{2+} to be used in Fenton's reaction. In contrast, the lower removal of primary compounds in chloride medium has been mainly related to the consumption of H_2O_2 by reaction with HClO via Eq. (38) and the slower mineralization has also been attributed to the generation of chloroderivatives that are hardly attacked by $^{\bullet}OH$ and active chlorine species.

The efficiency of EF and PEF using $NaClO_4$ and NaCl electrolytes has reached divergent results. In the work presented by Daneshvar et al. [130], the use of $NaClO_4$ showed superiority over NaCl, whereas in Thiam et al. [131] the achievements were antagonistic. Since ClO_4^- ion does not form complexes with Fe^{2+} and Fe^{3+} and is not reactive toward $^{\bullet}OH$ [128], the results attained by Daneshvar et al. [130] can seem more logical, but the action of Cl^- can be a function of its oxidation ability on the intermediates formed and this needs more research. Note that ClO_4^- ions are toxic and provoke damages in the environment and living organisms. In turn, Fan et al. [132] found decolorization ability in the order $Na_2SO_4 > NaNO_3 > Na_2CO_3$ for EF, which was ascribed to a higher ability of carbonate to scavenge $^{\bullet}OH$.

Under SPEF conditions, Thiam et al. [99] reported similar dye decays using Na_2SO_4, $NaClO_4$ and Na_2CO_3 supporting electrolytes and just a slightly lower mineralization using NaCl, which points to a low influence of the electrolyte nature in the presence of the beneficial effects of solar radiation.

Note that all the previous considerations were achieved for synthetic wastewaters contaminated with dyes.

Comparison between the employment of a 7.0 g Na_2SO_4 L^{-1} solution and a municipal wastewater from secondary treatment in the performance of a SPEF process to degrade trimethoprim antibiotic was carried out by Moreira et al. [133]. Slower drug and DOC removals were attained using the real wastewater compared to Na_2SO_4, which was attributed to the use of $^{\bullet}OH$ to oxidize the highly recalcitrant dissolved organic content of the real effluent and/or the filtration of photochemically active light by these dissolved organics.

The majority of studies employed Na_2SO_4 as supporting electrolyte and, with regards to the electrolyte concentration, most of them used 7.0 g L^{-1}. Thiam et al. [131] assessed a concentration range of 3.5–43 g Na_2SO_4 L^{-1} in the degradation of Allura Red AC azo dye by PEF process employing BDD anode under UVA radiation (PEF-UVA-BDD). The authors attained lower decolorization for Na_2SO_4 contents above 14 g L^{-1} and similar mineralization for all electrolyte contents. In contrast, Domínguez et al. [69] and González et al. [134] determined an optimum concentration of 70 g Na_2SO_4 L^{-1} by applying RSM in AO treatments.

2.4.3. Current density or applied current or potential

A constant j (in A m^{-2} or mA cm^{-2}) or I (in A or mA) is supplied to the cell when operating in galvanostatic mode, whereas a constant E (in V) is provided to the anode or the cathode of the cell *vs.* an electrode reference when working in potentiostatic mode. A constant potential can also be supplied to the electrochemical cell (E_{cell}), but this does not correspond to the operation in potentiostatic mode. Usually, EAOPs are operated in galvanostatic mode.

j (or I) is a key parameter in EAOPs since it regulates the amount of oxidizing species produced. For all EAOPs, j controls the amounts of M($^{\bullet}OH$) electrogenerated via Eq. (1) and indirect oxidation agents such as the active chlorine species generated from Eqs. (5) and (6). For EAOPs with H_2O_2 electrogeneration, it also regulates the quantity of electrogenerated H_2O_2 via Eq. (16). In the case of EAOPs based on Fenton's reaction, j sets the extent of cathodic Fe^{3+} regeneration to Fe^{2+} via Eq. (26), which, in parallel with the regulation of H_2O_2 electrogeneration, determines the amount of $^{\bullet}OH$ in the bulk produced from Fenton's reaction (21). In general, the rate of pollutants degradation increases with increasing j for all EAOPs since more oxidizing species are formed at a given time, as can be seen in Fig. 3a [98,135–138]. However, this parameter cannot be increased indefinitely since the rate of parasitic reactions is also promoted, leading to the decrease of current efficiency and similar or even lower pollutants removal than at inferior j value. The parasitic reactions can involve: (i) the dimerization of M($^{\bullet}OH$) to H_2O_2 by Eq. (2), (ii) the anodic oxidation of M($^{\bullet}OH$) to oxygen through Eq. (39), (iii) the dimerization of $^{\bullet}OH$ to H_2O_2 via Eq. (40), (iv) the H_2O_2 electrochemical reduction (in a divided cell) via Eq. (17), (v) the H_2O_2 electrochemical oxidation (in an undivided cell) according to Eqs. (19) and (20), (vi) the H_2O_2 reaction with Fe^{3+} via Eq. (22), and (vii) the destruction of $^{\bullet}OH$ with H_2O_2 and Fe^{2+} via Eqs. (24) and (25), respectively [20,34,75].

$$2M\,({}^{\bullet}OH) \rightarrow 2M + O_2 + 2H^+ + 2e^- \quad (39)$$

$$2\ {}^{\bullet}OH \rightarrow H_2O_2 \quad (40)$$

To choose the best j, it is necessary to take into account not only the degradation decays but also the current efficiency, i.e., the feasibility of EAOPs in terms of consumed electrical charge and/or the energy consumption for electrochemical cell operation at large scale. The mineralization current efficiency (MCE, in %) is a widely employed current efficiency parameter and it can be determined by Eq. (41) for single pollutant solutions for which the mineralization reaction is known [139]:

$$MCE = \frac{n\,F\,V_s\,\Delta(DOC)_{exp}}{4.32 \times 10^7 m\,I\,t}\,100 \quad (41)$$

where n is the theoretical number of electrons exchanged in the mineralization process of the organic compound, F is the Faraday constant (96 485 C mol^{-1}), V_s is the solution volume (in L), $\Delta(DOC)_{exp}$ is the experimental DOC abatement (in mg L^{-1}), 4.32×10^7 is a conversion factor to homogenize the units (3600 s h^{-1} × 12000 mg mol^{-1}), m is the number of carbon atoms of the molecule under study, I is the applied current (in A) and t is the electrolysis time (in h).

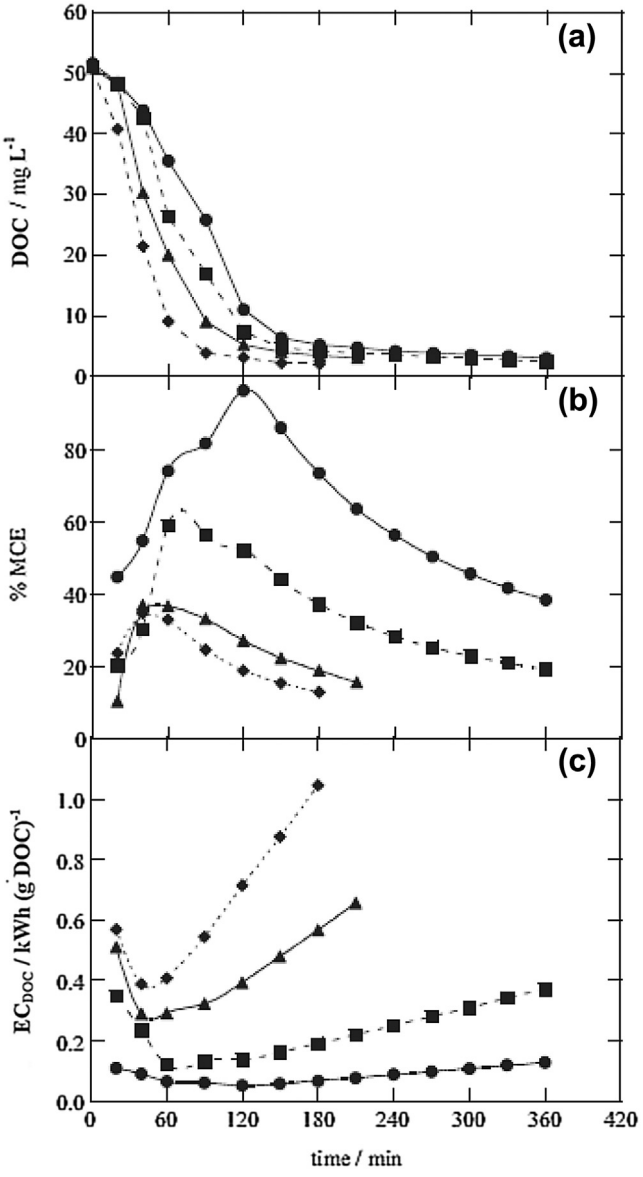

Fig. 3. Effect of current density on (a) DOC removal, (b) mineralization current efficiency and (c) energy consumption per unit DOC mass as a function of time for the treatment of 127 mg Acid Yellow 9 L^{-1} in 14 g Na_2SO_4 L^{-1} by SPEF using BDD anode, carbon-PTFE air-diffusion cathode, pH 3.0, 35 °C and $[TDI]_0$ of 28 mg L^{-1}. Current density: (●) 25, (■) 50, (▲) 100 and (◆) 150 mA cm^{-2}. Reprinted (adapted) from Ruiz et al. [170], Copyright © (2011), with permission from Elsevier.

The specific energy consumption for electrochemical cell operation per unit DOC mass (EC_{DOC}, in kWh (g DOC)$^{-1}$) and per unit volume (EC_V, in kWh m^{-3}) can be calculated from Eqs. (42) and (43), respectively, when operating at constant j [95]:

$$EC_{DOC} = \frac{E_{cell}\ I\ t}{V_s\ \Delta(DOC)_{exp}} \quad (42)$$

$$EC_V = \frac{E_{cell}\ I\ t}{V_s} \quad (43)$$

where E_{cell} is the average cell potential (in V), I is the applied current (in A), t is the electrolysis time (in h), V_s is the solution volume (in L) and $\Delta(DOC)_{exp}$ is the experimental DOC concentration decay (in mg L^{-1}).

In general, the rise in j come along with lower current efficiency and higher consumption of energy. An example of the decrease of MCE and increase of EC_{DOC} with higher j can be seen in Fig. 3b and c, respectively.

2.4.4. Stirring rate or liquid flow rate

The solution stirring rate in tank reactors and liquid flow rate in flow cells must be regulated to obtain fast homogenization of treated solution, avoid deposition of solids and ensure proper mass transfer of pollutants toward electrodes, catalyst and, in case of light-assisted EAOPs, illuminated zone. Ideally, the turbulent flow along the reactor should be guaranteed to provide a good mixing and avoid any sedimentation.

2.4.5. Temperature

The influence of temperature on AO and AO-H_2O_2 processes is rather little as found by Tsantaki et al. [140] and Boye et al. [135], although higher temperature enhances the mass transfer of reactants toward/from the electrodes and kinetic constants (for •OH generation by Eqs. (1) and (21), H_2O_2 production via Eq. (16) and oxidation of organics by such species) are exponentially dependent on the temperature (Arrhenius law). In addition to these two effects, the EAOPs based on Fenton's reaction can also count on the faster Fe^{3+} regeneration to Fe^{2+} by thermal reactions (22), (23) and (44) for higher temperature, which has been reported as the main cause for the increase of degradation kinetics with temperature in these processes [80,135,141]. Moreover, Moreira et al. [108] found distinct distribution of $Fe(OH)_3$ precipitate with temperature, and, for light-induced EAOPs, also the molar fraction of photoactive species changed with temperature. As a consequence, the influence of temperature on the system behavior depends on its composition and pH.

$$Fe^{3+} + O^{\bullet}{}_2^- \rightarrow Fe^{2+} + O_2 \quad (44)$$

Temperature can also be a limiting parameter for EAOPs with H_2O_2 electrogeneration on account of the decreasing dissolved oxygen concentration for higher temperatures, with consequent drop of the rate of H_2O_2 formation. For this reason, processes with electrogenerated H_2O_2 are usually performed at ambient temperature (20–30 °C). Temperatures above 35 °C should be taken with precaution [135,142]. Additionally, the thermal decomposition of H_2O_2 into water and oxygen (inactive species) may occur in large extent for temperatures above 50 °C [143]. Note that thermal reactions (22), (23) and (44) can also lead to H_2O_2 decomposition, with formation of less reactive species.

2.4.6. pH

A literature review on the influence of pH on AO and AO-H_2O_2 processes reveals discrepant results. Some studies point to the independency of mineralization rate by changing pH in the 2.0–6.0 or 4.0–10 range [48,135,144,145]; others achieved greater process efficiency at pH 3.0 compared to higher pH values [117,146,147], ascribing these results to the competitive electrogeneration of less powerful oxidizing species such as superoxide anion radical and, when chloride is available, to the formation of active chlorine species with higher oxidation ability at acidic pH [43]; and Hamza et al. [119] attained slightly faster mineralization at pH 7.4 than at pH 3.0. In contrast, the best pH value for EF, PEF and SPEF processes is in general close to 3.0 [97,114,135,148–152], mainly due to: (i) higher amounts of photoactive Fe(III)-hydroxy complexes in solution [102,153], (ii) absence of iron precipitation [102,153], (iii) absence of carbonate and bicarbonate species, which reduce the process efficiency due to their •OH scavenging effect [8], and (iv) null auto-decomposition rate of H_2O_2 to water and oxygen, typically occurring for pH above 5 [154]. However, some authors reported maximal and similar mineralization rates for pH values from 2.0 to 4.0 [105,132], 2.0 to 3.0 [96,113], 3.0 to 4.0 [94,155] and 3.5 to 4.0 [133].

To prevent or, at least, minimize the need for acidification to perform the EAOP and the necessity for subsequent neutralization to discharge the wastewater into the environment, the PEF process assisted by carboxylic acids, e.g. oxalic, citric, tartaric and malic, has been recently implemented [108,118,152,156]. The presence of carboxylic acids can improve PEF efficiency because: (i) they promote the formation of more soluble complexes with Fe^{3+}, allowing maintaining the iron in solution at higher pH values [157], (ii) Fe(III)-carboxylate complexes can absorb radiation in the UV–vis range, being photodecarboxylated according to the general Eq. (29) with higher quantum yields for Fe^{2+} generation than that of Fe(III)-hydroxy complexes [100–102,158], and (iii) the establishment of Fe(III)-carboxylate complexes can avoid the formation of Fe(III)-sulfate, Fe(III)-chloride and Fe(III)-pollutants complexes in view of their greater formation constants in comparison with that of these species [159,160].

2.4.7. Oxygen or air feeding flow rate

To electrogenerate H_2O_2 at carbonaceous cathodes according to Eq. (16), oxygen must be continuously provided during electrolysis either by means of expensive pure oxygen [135,161] or easily obtainable air [97,151]. In general, high flow rates of oxygen (pure or air) are employed for various types of carbonaceous cathodes in order to maintain oxygen-saturated solutions, thereby ensuring maximum H_2O_2 electrogeneration [67,70,115,151,162]. The oxygen gas is often provided during some minutes prior to electrolysis to saturate the aqueous solution [70,115,163,164]. For electrochemical cells with GDEs, it is necessary to establish a compromise between liquid and oxygen flow rates in order to apply similar pressures in both sides of the cathode and thus avoid cell flooding. Note that extremely high oxygen or air feeding flow rates are not recommended since they cause some operational problems such as: (i) the disruption of pumps used for liquid circulation, (ii) the fulfill of liquid compartments of filter-press cells with air, decreasing the contact between solution and electrodes and even obstructing ions transference, and (iii) the reduction of the irradiated volume in light-assisted EAOPs.

2.4.8. Initial total dissolved iron concentration

The $[TDI]_0$ (Fe^{2+}, Fe^{3+} or both species) is a crucial parameter for EAOPs based on Fenton's reaction chemistry since it determines the extent of Fenton's reaction (21) and, as a result, the pollutants degradation. For EF process, the best $[TDI]_0$ mainly depends on: (i) H_2O_2 concentration, (ii) system ability to regenerate Fe^{3+} to Fe^{2+} by means of cathodic reduction via Eq. (26) and thermal reactions (22),(23) and (44), and (iii) occurrence of parasitic reactions such as Eq. (25). For PEF and SPEF processes, it is also a function of: (i) Fe^{3+} regeneration to Fe^{2+} through photolysis of Fe(III)-hydroxy complexes by Eq. (28) and photolysis of complexes between Fe^{3+} and organics via Eq. (29), (ii) manifestation of inner filter effects, i.e., competitive absorption of photons between pollutants and Fe^{3+} photoactive species [80], and (iii) photoreactor geometry since the iron amount influences the light attenuation along the optical pathlength [80]. Note that the amount of iron added to the solution can diverge from $[TDI]_0$ since some precipitation can occur depending on pH and type and concentration of organic/inorganic compounds present in the solution.

For all wastewaters, it is expected the rise in process efficiency with increasing $[TDI]_0$ up to a value for which it is established an equilibrium between positive effects coming from the enhancement of Fenton's reaction (21) and negatives effects arising from the improvement of parasitic reactions and, for light-assisted EAOPs, inner filter effects and light attenuation along the photoreactor. Wherever possible, effluents with low organic contents up to few mg L^{-1} should use a total iron concentration in agreement with regulatory limits for the discharge of effluents into the environment to avoid the need for iron removal.

3. Degradation of synthetic wastewaters by EAOPs

3.1. Wastewaters containing dyes

Synthetic dyes are extensively used for coloring textiles, leather, paper, food, drinks, pharmaceuticals, cosmetics and inks and, consequently, large volumes of wastewaters with high contents of dyes are discharged into water bodies from industries. Among classes of synthetic dyes, azo dyes are by far the most commercialized ones, about 70% of total, and they are known by their resistance to conventional treatments, persisting in the environment and causing environmental damages and health risks for living organisms [1,165]. Table 3 collects information regarding thirty-five studies on the degradation of synthetic wastewaters containing dyes by EAOPs. To better explain the characteristics of the applied processes, this section will be divided in four subsections: dye content, process, electrochemical reactor and operational parameters. The same division was adopted in Sections 3.2, 3.3 and 4.3 to detail the performance of EAOPs on the treatments of other kind of pollutants related to pesticides, pharmaceuticals and landfill leachates, respectively.

3.1.1. Dye content

The majority of works refers to the degradation of azo dyes. In general, the synthetic wastewaters were produced using just one dye. Among the few studies regarding comparative degradations between two or more dyes [96,162,166], highlight can be given to Garcia-Segura et al. [166] that determined noticeable lower initial decolorization rates and dye removals for dye molecules with increasing number of azo bonds.

Distinct initial dye contents from 1.4 to 3580 mg L^{-1} have been employed. Half of the publications assessed the effect of initial dye concentration on the process efficiency, achieving results in agreement with Section 2.4.1.

3.1.2. Process

Most of the studies presented in Table 3 refer to the application of EF process, although a lot of works regarding AO are not included in it. AO-H_2O_2 and SPEF were the less applied processes. In general, processes efficiency in terms of mineralization could be arranged in the order SPEF > PEF-UVA > EF > AO-H_2O_2. The majority of studies employed low energy power UVA lamps. As illustrated in Fig. 4, Moreira et al. [167] found DOC removals of 93%, 84%, 60% and 29% after 150 min of SPEF, PEF-UVA, EF and AO-H_2O_2 processes, respectively, for the treatment of a 290 mg Sunset Yellow FCF L^{-1} solution in 7.0 g Na_2SO_4 L^{-1}. In this study, the SPEF-Pt process at pilot-scale reached 92% DOC removal after 240 min with an EC_{DOC} of 0.77 kWh (g DOC)$^{-1}$ and an EC_V of 7.2 kWh m^{-3}. Solano et al. [168] found DOC removals of 99%, 92% and 39% after 360 min of PEF-UVA, EF and AO-H_2O_2 processes, respectively, for the treatment of a 181 mg Congo Red L^{-1} solution in 7.0 g Na_2SO_4 L^{-1} using an undivided cell, BDD anode, carbon-PTFE air-diffusion cathode, pH 3.0, 25 °C, $[TDI]_0$ of 28 mg L^{-1} for EF and PEF-UVA and j_{cat} of 100 mA cm^{-2}.

In terms of decolorization and dye removal, controversial results have been reported. Some studies proved superiority of SPEF and PEF-UVA over EF [96,99,169], but other investigations found quite similar efficiencies for these three EAOPs [131,167,168,170,171]. The identical dye and color removals under EF and light-assisted EAOPs means that parent compounds and their colored by-products can be efficiently destroyed by M(•OH) and •OH produced in the bulk from Fenton's reaction (21), with little contribution of photoreduction reactions (28) and (29). Moreover, the dye removal is usually faster than solution decolorization, indicating that some

Table 3
Examples on the treatment of synthetic wastewaters contaminated with dyes by EAOPs.

Pollutant	Wastewater characteristics	Process	Electrochemical reactor		Electrodes/ Operational parameters	Maximum DOC decay (%)/ EC_{DOC} (kWh (g DOC)$^{-1}$)[a]	Refs.
			Configuration	V (L)			
4-amino-3-hydroxy-2-*p*-tolylazo-naphthalene-1-sulfonicacid (AHPS) azo dye	88–263 mg AHPS L^{-1} in 7.0 g Na_2SO_4 L^{-1}	EF catalyzed by pyrite	UC	0.2	Anode: BDD (6 cm^2) Cathode: CF (60 cm^2) j_{cat}: 1.7–7.5 mA cm^{-2} *Q*: MS T: 25 °C pH: 2.9–4.0 $[TDI]_0$ (pyrite): 0.5–2 g L^{-1}	95/2.2	[115]
Acid Orange 7 azo dye	1.4–18 mg Acid Orange 7 L^{-1} in 7.0–14 g Na_2SO_4 L^{-1} or 6.1–12 g $NaClO_4$ L^{-1} or 2.9 g NaCl L^{-1}	EF	UC	0.2	Anode: Pt (1 cm^2) Cathode: Graphite felt (3.8–7.6 cm^2) *E*: −0.5 to −1.0 V *Q*: MS T: Amb. pH: 3.0 $[TDI]_0$: 5.6 mg L^{-1}	75	[130]
Acid Orange 7 azo dye metabolites: sulphanilic acid (SA), 1-amino-2-naphthol (AN)	20–60 mg SA or AN L^1 in 5.0 g Na_2SO_4 L^{-1} or 5.8 g NaCl L^{-1} 300 mg Acid Orange 7 L^{-1} in a simulated effluent	AO	UC or FP with plug-flow cell	0.2	Anode: UC: BDD (20 cm^2) FP: BDD (8 cm^2) Cathode: UC: SS (20 cm^2) FP: SS (8 cm^2) j_{cat}: 1.3–30 mA cm^{-2} *Q* (UC): MS *Q* (FP): MS T: 25 °C pH: Neutral	41	[129]
Acid Orange 7 monoazo dye Acid Red 151 diazo dye Direct Blue 71 triazo dye	6.3–350 mg Acid Orange 7 L^{-1} or 8.2–454 mg Acid Red 151 L^{-1} or 19–1030 mg Direct Blue 71 L^{-1} in 7.0 g Na_2SO_4 L^{-1}	AO-H_2O_2 EF	UC	0.1	Anode: Pt or BDD (3 cm^2) Cathode: C-PTFE A-D or Graphite (3 cm^2) j_{cat}: 8.3–100 mA cm^{-2} *Q*: MS T: 35 °C pH: 3.0 $[TDI]_0$ (EF): 28 mg L^{-1}	n.a.	[166]
Acid Red 1 azo dye	236 mg Acid Red 1 L^{-1} in 7.0 g Na_2SO_4 L^{-1}	AO-H_2O_2 EF PEF-UVA	UC	0.1	Anode: Pt or BDD (3 cm^2) Cathode: C-PTFE A-D (3 cm^2) j_{cat}: 17–100 mA cm^{-2} *Q*: MS T: 35 °C pH: 3.0 $[TDI]_0$ (EF, PEF-UVA): 28 mg L^{-1}	PEF-UVA: ≈100	[171]
Acid Red 29 azo dye	244 mg Acid Red 29 L^{-1} in 7.0 g Na_2SO_4 L^{-1}	EF PEF-UVA	UC	0.1	Anode: BDD (3 cm^2) Cathode: C-PTFE A-D (3 cm^2) j_{cat}: 17–100 mA cm^{-2} *Q*: MS T: 35 °C pH: 2.0–6.0 $[TDI]_0$: 11–279 mg L^{-1}	PEF-UVA: >92/n.a.	[97]
Acid Red 88, Acid Yellow 9 azo dyes	119 mg Acid Red 88 L^{-1} or 127–508 mg Acid Yellow 9 L^{-1} in 7.0 or 14 g Na_2SO_4 L^{-1}	EF SPEF	FP with undivided FPC and planar photoreactor	2.5	Anode: BDD (20 cm^2) Cathode: C-PTFE A-D (20 cm^2) j_{cat}: 25–150 mA cm^{-2} *Q*: 3.3 L min^{-1} T: 35 °C pH: 3.0 $[TDI]_0$: 5.6–45 mg L^{-1}	SPEF: 93/1	[170]
Acid Yellow 23 azo dye	278 mg Acid Yellow 23 L^{-1} in 7.0 g Na_2SO_4 L^{-1} or 2.9 g NaCl L^{-1}	EC + AO, AO-H_2O_2, EF or PEF-UVA	UC	0.13	Anode: Pt or BDD (3 cm^2) Cathode: AO: SS (3 cm^2) AO-H_2O_2, EF, PEF-UVA: C-PTFE A-D (3 cm^2) j_{cat}: 33–100 mA cm^{-2} *Q*: MS T: 25 °C pH: 3.0 $[TDI]_0$ (EAOPs as a single stage): 28 mg L^{-1} $[TDI]_0$ (EAOPs after EC): 34 mg L^{-1}	EC + PEF-UVA: 100/n.a.	[23]

Table 3 (*Continued*)

Pollutant	Wastewater characteristics	Process	Electrochemical reactor		Electrodes/ Operational parameters	Maximum DOC decay (%)/ EC_{DOC} (kWh (g DOC)$^{-1}$)[a]	Refs.
			Configuration	*V* (L)			
Acid Yellow 36 azo dye	20 mg Acid Yellow 36 L^{-1} + 5 mg kaolin L^{-1} in 1.1 g KCl L^{-1}	AO + MF	FP with tubular ceramic membrane with imbedded electrodes	2	Anode: BDD (9.4 cm^2) Cathode: SS tube j_{cat}: 30 mA cm^{-2} *Q*: n.s. T: Amb. pH: 3.0	n.a./n.a.	[172]
Allura Red AC azo dye	115–460 mg Allura Red AC L^{-1} in 3.5–43 g Na_2SO_4 L^{-1} or 5.3 g $LiClO_4$ L^{-1} or 4.2 g $NaNO_3$ L^{-1} or 1.5–8.8 g NaCl L^{-1}	AO-H_2O_2 EF PEF-UVA	UC	0.13	Anode: Pt or BDD (3 cm^2) Cathode: C-PTFE A-D (3 cm^2) j_{cat}: 33–150 mA cm^{-2} *Q*: MS T: 25 °C pH: 3.0 $[TDI]_0$ (EF, PEF-UVA): 28 mg L^{-1}	PEF-UVA: 100/n.a.	[131]
Azure B dye	31 mg Azure B L^{-1} in 7.0 g Na_2SO_4 L^{-1}	AO-H_2O_2 EF	UC	0.2	Anode: Pt mesh or BDD (25 cm^2) Cathode: CF *I*: 50–500 mA *Q*: MS T: Amb. pH: 3.0 $[TDI]_0$ (EF): 5.6 mg L^{-1}	EF: 90/n.a.	[232]
Basic Red 46 azo dye	2–20 mg Basic Red 46 L^{-1} in 7.0 g Na_2SO_4 L^{-1}	EF PEF-Vis PEF-Vis/oxalate	UC	0.8	Anode: Pt (1 cm^2) Cathode: Multi walled CNT-PTFE (5.4 cm^2) j_{cat}: 19 mA cm^{-2} *Q*: MS T: Amb. pH: 3.0 $[TDI]_0$: 5.6–28 mg L^{-1}	n.a./n.a.	[156]
Basic Yellow 28 dye	10–40 mg Basic Yellow 28 L^{-1} in 7.0 g Na_2SO_4 L^{-1}	EF PEF-UVC PEF-UVA or PEF-UVB or PEF-UVC catalyzed by ZnO nanoparticles	UC	2	Anode: Pt (11.5 cm^2) Cathode: Multi walled CNT-PTFE (5.4 cm^2) j_{cat}: 9.2–93 mA cm^{-2} *Q*: MS T: Amb. pH: 2.0–6.0 $[TDI]_0$: 5.6 mg L^{-1}	PEF-UVC-ZnO: 95/n.a.	[116]
Cibacron Marine FG azo dye	30–70 mg Cibacron Marine FG L^{-1} in ultrapure water	AO	FP with undivided FPC	1	Anode: Sb-SnO_2 (40 cm^2) Cathode: SS (40 cm^2) j_{cat}: 10–30 mA cm^{-2} *Q*: 0.36–0.67 T: 24 °C pH: 5.8	≈100/0.32	[121]
Congo Red azo dye	45–362 mg Congo Red L^{-1} in 7.0 g Na_2SO_4 L^{-1}	AO-H_2O_2 EF PEF-UVA SPEF	AO-H_2O_2, EF, PEF-UVA: UC SPEF: FP with undivided FPC and planar photoreactor	AO-H_2O_2, EF, PEF-UVA: 0.1 SPEF: 2.5	Anode: AO-H_2O_2, EF, PEF-UVA: BDD (3 cm^2) SPEF: BDD (20 cm^2) Cathode: AO-H_2O_2, EF, PEF-UVA: C-PTFE A-D (3 cm^2) SPEF: C-PTFE A-D (20 cm^2) j_{cat}: 50–150 mA cm^{-2} *Q* (SPEF): 3.3 L min^{-1} *Q* (others): MS T: 35 °C pH: 3.0 $[TDI]_0$ (EF, PEF-UVA, SPEF): 14–112 mg L^{-1}	SPEF: 100/0.4	[168]
Direct Orange 61 azo dye	44–175 mg Direct Orange 61 L^{-1} in 7.0 g Na_2SO_4 L^{-1}	EF	UC	–	Anode: Pt (5.5 cm^2) Cathode: CF (60 cm^2) j_{cat}: 0.5–1.7 mA cm^{-2} *Q*: MS T: Amb. pH: 3.0 $[TDI]_0$: 5.6–28 mg L^{-1}	98/n.a.	[112]

Table 3 (*Continued*)

Pollutant	Wastewater characteristics	Process	Electrochemical reactor		Electrodes/ Operational parameters	Maximum DOC decay (%)/ EC_{DOC} (kWh (g DOC)$^{-1}$)[a]	Refs.
			Configuration	*V* (L)			
Direct Red 23 azo dye	10–50 mg Direct Red 23 L^{-1} in 7.0 g Na_2SO_4 L^{-1}	EF PEF-Vis PEF-Vis/citrate	UC	2	Anode: Pt (11.5 cm^2) Cathode: Multi walled CNT-PTFE (5.4 cm^2) j_{cat}: 19–93 mA cm^{-2} *Q*: MS T: Amb. pH: 2.0–9.0 $[TDI]_0$: 5.6–45 mg L^{-1}	n.a./n.a.	[118]
Direct Yellow 4 azo dye	50–200 mg Direct Yellow 4 L^{-1} in 7.0 g Na_2SO_4 L^{-1}	SPEF	FP with undivided FPC and photoreactor	10	Anode: Pt or BDD (90.2 cm^2) Cathode: C-PTFE A-D (90.2 cm^2) j_{cat}: 33–55 mA cm^{-2} *Q*: 3.3 L min^{-1} T: 35 °C pH: 3.0 $[TDI]_0$: 14–279 mg L^{-1}	97/n.a.	[123]
Disperse Red 1, Disperse Yellow 3 azo dyes	82–327 mg Disperse Red 1 L^{-1} or 150 mg Disperse Yellow 3 L^{-1} in 14.0 g Na_2SO_4 L^{-1}	EF SPEF	FP with undivided FPC and planar photoreactor	2.5	Anode: BDD (20 cm^2) Cathode: C-PTFE A-D (20 cm^2) j_{cat}: 15–80 mA cm^{-2} *Q*: 3.3 L min^{-1} T: 35 °C pH: 2.0–6.0 $[TDI]_0$: 28 mg L^{-1}	SPEF: ≈90/0.15	[96]
E122 (Azorubine), E124 (Ponceau 4R), E129 (Allura Red AC) azo dyes	7.0 or 70 mg E122 L^{-1}, 8.5 or 85 mg E124 L^{-1}, 7.2 or 72 mg E129 L^{-1} (mixture) in 7.0 g Na_2SO_4 L^{-1} or 5.3 g $LiClO_4$ L^{-1} or 4.2 g $NaNO_3$ L^{-1} or 2.9 g NaCl L^1 or simulated wastewater or real WWTP secondary effluent	EF PEF-UVA SPEF	EF, PEF-UVA: UC SPEF: FP with undivided FPC and photoreactor	EF, PEF-UVA: 0.13 SPEF: 2.5	Anode: EF, PEF-UVA: Pt or BDD (3 cm^2) SPEF: BDD (20 cm^2) Cathode: EF, PEF-UVA: Pt or BDD (3 cm^2) SPEF: BDD (20 cm^2) j_{cat} (EF, PEF-UVA): 33 mA cm^{-2} j_{cat} (SPEF): 50–150 mA cm^{-2} *Q* (SPEF): 3.3 L min^{-1} *Q* (others): MS T: 35 °C pH: 3.0 $[TDI]_0$: 28 mg L^{-1}	SPEF: 100/0.25	[99]
Evans Blue azo dye	235 mg Evans Blue L^{-1} in 7.0 g Na_2SO_4 L^{-1}	EF PEF-UVA SPEF	LS: UC PS: FP with undivided FPC and photoreactor	LS: 0.1 PS: 10	Anode: LS: BDD (3 cm^2); PS: Pt (90.3 cm^2) Cathode: C-PTFE A-D LS: 3 cm^2; PS: 90.3 cm^2 j_{cat}: 17–100 mA cm^{-2} *Q*: LS: MS; PS: 3.3 L min^{-1} T: 35 °C pH: 3.0 $[TDI]_0$: 28 mg L^{-1}	SPEF: 88/0.22	[138]
Indigo Carmine dye	112–881 mg Indigo Carmine L^{-1} in 7.0 g Na_2SO_4 L^{-1}	EF PEF-UVA PEF/UVA catalyzed by Cu^{2+}	UC	0.1	Anode: Pt or BDD (3 cm^2) Cathode: C-PTFE A-D (3 cm^2) j_{cat}: 33–150 mA cm^{-2} *Q*: MS T: 35 °C pH: 2.0–6.0 $[TDI]_0$: 11–279 mg L^{-1} (alone or + 16 mg Cu^{2+} L^{-1})	PEF-UVA-Cu^{2+}: ≈100/n.a.	[105]
Indigo dye	315 mg Indigo L^{-1} in 2.9 g NaCl L^{-1}	AO	FP with undivided FPC	1	Anode: 2D (plate) BDD (64 cm^2) or 3D (mesh) BDD (444 cm^2) Cathode: Pt j_{cat}: 5.6 or 15 mA cm^{-2} *Q*: 0.10–1.1 L min^{-1} T: 25 °C pH: 6.3	n.a./n.a.	[174]
Lissamine Green B, Methyl Orange azo, Reactive Black 5 azo, Fuchsin Acid dyes	8.5 mg Lissamine Green B L^{-1}, 1.5 mg Methyl Orange L^{-1}, 70 mg Reactive Black 5 L^{-1}, 15 mg Fuchsin Acid L^{-1} in 1.4 g Na_2SO_4 L^{-1} for solutions with one dye or in 5.7 g Na_2SO_4 L^{-1} for a mixture of all dyes	EF	Flow bubble reactor with UC	0.675	Anode: Graphite (1.27 cm^2) Cathode: Graphite (1.27 cm^2) E_{cell}: 15 V *Q*: n.s. T: Amb. pH: 2.0–5.0 $[TDI]_0$ (single solutions): 150 mg L^{-1} TDI]$_0$ (mixture): 600 mg L^{-1}	46/n.a.	[162]

Table 3 (*Continued*)

Pollutant	Wastewater characteristics	Process	Electrochemical reactor		Electrodes/ Operational parameters	Maximum DOC decay (%)/ EC_{DOC} (kWh (g DOC)$^{-1}$)[a]	Refs.
			Configuration	V (L)			
Lissamine Green B, Azure B dyes	8.5 mg Lissamine Green L^{-1} or 4.83 mg Azure B L^{-1} in 1.4 g Na_2SO_4 L^{-1}	EF catalyzed by Fe alginate gel beads	UC or flow bubble reactor with UC	UC: n.s. Flow bubble reactor with UC: 0.15	Anode: Graphite (1.27 cm^2) Cathode: Graphite (1.27 cm^2) E_{cell}: 14 V Q (UC): MS Q (Flow bubble reactor): n.s. T: Amb. pH: 2.0–8.0 $[TDI]_0$ (Fe alginate gel beads): 58 g L^{-1}	93/n.a.	[175]
Methyl Red, Orange II, Biebrich Scarlett azo dyes	100 mg L^{-1} in pure water for each dye solution	EF	DC	n.s.	Anode: Pt (31.4 cm^2) Cathode: CF (42 or 378 cm^2) E: −0.5 V Q: MS T: 30 °C pH: 1.0 or 3.0 $[TDI]_0$: 56 mg L^{-1}	11/n.a.	[173]
Methyl Violet 2B dye	69–548 mg Methyl Violet 2B L^{-1} in 7.0 g Na_2SO_4 L^{-1}	AO	UC	0.1	Anode: BDD or Pt (3 cm^2) Cathode: SS (3 cm^2) j_{cat}: 33–150 mA cm^{-2} Q: MS T: 35 °C pH: 3.0 or 7.4	74/0.51	[119]
Orange G azo dye	294–3580 mg Orange G L^{-1} in 7.0 g Na_2SO_4 L^{-1}	AO	UC or DC	0.1	Anode: BDD (3 cm^2) Cathode: SS (3 cm^2) j_{cat}: 33–150 mA cm^{-2} Q: MS T: 35 °C pH: 2.0–6.0	100/n.a.	[145]
Orange II azo dye	50 mg Orange II L^{-1} in 7.0 g Na_2SO_4 L^{-1}	AO-H_2O_2 EF PEF-UVA	FP with concentric annular cell	0.4	Anode: Graphite cloth (200 cm^2) Cathode: Graphite cloth (164 cm^2) j_{cat}: 300 mA cm^{-2} Q: 0.1 L min^{-1} T: Amb. pH: 3.0 $[TDI]_0$ (EF, PEF-UVA): 11–28 mg L^{-1}	PEF-UVA: 80/n.a.	[169]
Ponceau S azo dye	34–202 mg Ponceau S L^{-1} in 7.0–14 g Na_2SO_4 L^{-1} or 5.8 g NaCl L^{-1} or 7.5 g KCl L^{-1}	EF	UC	0.45	Anode: Pt (3.8 cm^2) Cathode: RVC (35 cm^2) E: −0.5 to 1.0 V Q: MS T: Amb. pH: 2.5–4.5 $[TDI]_0$: 2.8–56 mg L^{-1}	98/n.a.	[67]
Reactive Blue 4 dye	100 mg Reactive Blue 4 L^{-1} in 7.0 g Na_2SO_4 L^{-1}	EF	UC	0.2	Anode: Pt (6 cm^2) Cathode: CF (50 cm^2) j_{cat}: 1.2–4 mA cm^{-2} Q: MS T: Amb. pH: 3.0 $[TDI]_0$: 11 mg L^{-1}	78/n.a.	[163]
Rhodamine B azo dye	5 mg Rhodamine B L^{-1} in 7.0 g Na_2SO_4 L^{-1} or 5.3 mg Na_2CO_3 L^{-1} or 4.2 g $NaNO_3$ L^{-1}	EF	UC	n.s.	Anode: Pt (2 cm^2) Cathode: Sandwich film cathode: ACF + Fe^{2+}-chitosan deposited on Ni (6 cm^2) j_{cat}: 0.08–3.3 mA cm^{-2} Q: MS T: Amb. pH: 2.5–9.8 Electrogenerated iron	n.a./n.a.	[132]
Sunset Yellow FCF azo dye	90 mg Sunset Yellow FCF L^{-1} in 7.0 g Na_2SO_4 L^{-1} or 5.8 g NaCl L^{-1} or 7.5 g KCl L^{-1}	EF	UC	0.45	Anode: Pt (3.8 cm^2) Cathode: RVC (35 cm^2) E: −0.5 to 1.0 V Q: MS T: 25 °C pH: 3.0–5.0 $[TDI]_0$: 0.56–28 mg L^{-1}	n.a./n.a.	[68]

Table 3 (*Continued*)

Pollutant	Wastewater characteristics	Process	Electrochemical reactor		Electrodes/ Operational parameters	Maximum DOC decay (%)/ EC_{DOC} (kWh (g DOC)$^{-1}$)[a]	Refs.
			Configuration	*V* (L)			
Sunset Yellow FCF azo dye	290 mg Sunset Yellow FCF in 7.0 g Na_2SO_4 L^{-1}	AO-H_2O_2 EF PEF-UVA SPEF	LS: UC PS: FP with undivided FPC and photoreactor	LS: 0.1 PS: 10	Anode: LS: BDD (3 cm^2); PS: Pt (90.2 cm^2) Cathode: C-PTFE A-D LS: 3 cm^2; PS: 90.2 cm^2 j_{cat}: LS: 17–100 mA cm^{-2}; PS: 33–78 mA cm^{-2} *Q*: LS: MS; PS: 3.3 L min^{-1} T: 35 °C pH: 3.0 $[TDI]_0$ (EF, PEF-UVA, SPEF): 28 mg L^{-1}	SPEF: 92/0.77	[167]

Amb. – Ambient;
C-PTFE A-D – Carbon-PTFE air-diffusion;
DC – Divided cell;
FP – Flow plant;
FPC – Filter-press cell;
LS – Lab-scale;
MS – Magnetic stirring;
n.a. – not assessed;
n.s. – not specified;
PS – Pilot-scale;
Q – Liquid flow rate;
UC – Undivided cell.

[a] Under the best experimental conditions, when applicable.

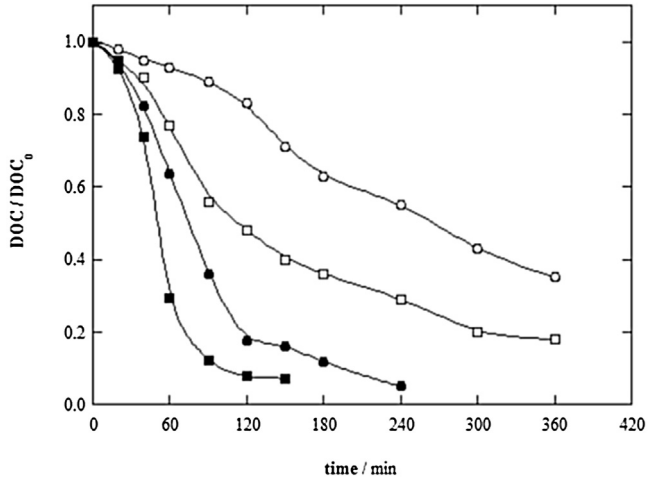

Fig. 4. Normalized DOC removal as a function of time for the treatment of 100 mL of 290 mg Sunset Yellow FCF azo dye L^{-1} in 7.0 g Na_2SO_4 L^{-1} using BDD anode, carbon-PTFE air-diffusion cathode, 35 °C, pH 3.0, $[TDI]_0$ of 28 mg L^{-1} for Fenton's reaction assisted processes and *j* of 33.3 mA m^{-2}. Process: (○) AO-H_2O_2, (□) EF, (●) PEF-UVA and (■) SPEF. Reprinted (adapted) from Moreira et al. [167], Copyright © (2013), with permission from Elsevier.

colored by-products that react more hardly with generated •OH are generated during the degradation process. For example, Solano et al. [168] found total dye decay and total color removal after 60 and 150 min of SPEF, respectively.

Thiam et al. [23] presented the only research study comparing AO with other processes. Similar mineralization and decolorization were attained for AO and AO-H_2O_2 processes, which revealed a negligible role of H_2O_2 on the dye degradation.

Khataee et al. [66,118] executed PEF processes using visible light, alone and in combination with Fe(III)-oxalate and Fe(III)-citrate complexes, and achieved processes decolorization ability in the following order: PEF-Vis/oxalate or citrate > PEF-Vis > EF. As aforementioned, the Fe(III)-carboxylate complexes are able to be photodecarboxylated under UV–vis radiation via Eq. (29) with higher quantum yields for Fe^{2+} generation than that of Fe(III)-hydroxy complexes, among other advantages. The improvement of PEF process was also accomplished by Flox et al. [105] and Iranifam et al. [116] by adding Cu^{2+} and ZnO nanoparticles, respectively. Cu^{2+} can form complexes with carboxylic acids that are more rapidly destroyed than Fe(III)-carboxylate complexes and acids alone and, in addition, greater amounts of •OH can be produced in the medium from the Cu^{2+}/Cu^{+} catalytic system. ZnO is a semiconductor that forms an electron-hole pair under UV radiation and the hole has a so high oxidative potential that allows the direct oxidation of organics and also the generation of •OH by water decomposition.

The combination of EAOPs with other technologies for dyes removal has been only slightly explored. Juang et al. [172] used a microfiltration (MF)/AO system to remove a mixture of an azo dye and kaolin particles. The MF was able to remove particles but the performance of AO alone was not discussed. Thiam et al. [23] proved the suitability of applying EC prior to a PEF-UVA process. In this study, EC was used as source of $Fe(OH)_2$ or $Fe(OH)_3$ coagulant to provide color removal and separation of a large fraction of organic matter and also as source of Fe^{3+}/Fe^{2+} catalyst to the subsequent EAOP, in which the remaining persistent organic matter was degraded.

3.1.3. Electrochemical reactor

Most of the studies have been performed in undivided electrochemical reactors, typically employing solution volumes of 100–200 mL, although volumes of 1 and 2 L were occasionally used [116,118,172]. Fig. 5 shows a schematic representation of a thermostated undivided electrochemical reactor with around 100 mL capacity equipped with a carbon-PTFE O_2-diffusion cathode. This equipment can also be used upon direct injection of an air flow to the cathode. Divided cells use a separator between the anolyte and the catholyte that makes the treatment process more expensive and demanding by the penalty overvoltage of the separator and, consequently, their use was very sparse, with only two studies displayed in Table 3 [145,173]. El-Ghenymy et al. [145] compared the applica-

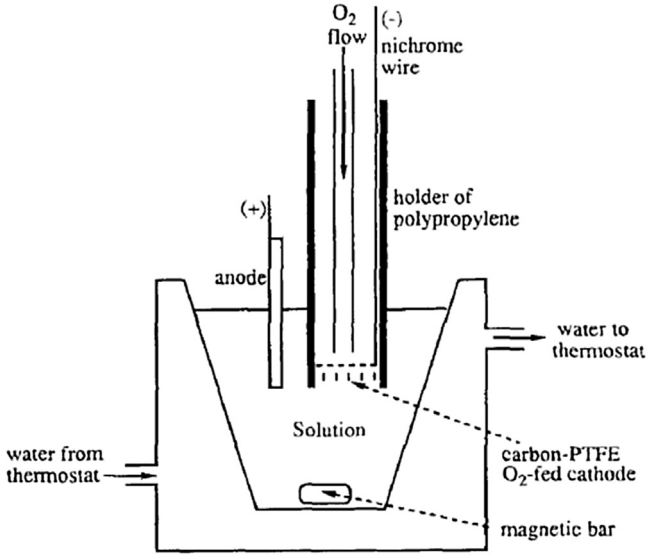

Fig. 5. Sketch of a thermostated undivided cell of around 100 mL capacity equipped with a carbon-PTFE O_2-diffusion cathode. Reprinted (adapted) from Brillas et al. [57], Copyright © (1995), with permission from The Electrochemical Society.

tion of both undivided and divided cells and revealed the need for a higher supporting electrolyte concentration in the divided cell due to a large E_{cell} increase. The decolorization was faster in the divided cell, which can be attributed to the interaction of organics with an electric field of higher magnitude because of the higher E_{cell}. This is responsible for the enhancement of the mass transport toward the anode, thus promoting a quicker reaction between organics and M(•OH).

Filter-press cells have shown quite popularity and they have been used in simple reactors by coupling to a pump and a reservoir (volume of solution of 1 L) [121,174]. An example is presented in Fig. 6. More complex flow plants with a structure for radiation capture have been described like a planar 2.5 L photoreactor with a mirror at the bottom [96,99,168,170], schematized in Fig. 7, a 10 L photoreactor composed of borosilicate tubes mounted in an aluminum plane sheet [123,138,167], illustrated in Fig. 8, or a 2.2 L photoreactor composed of CPCs [167], schematized in Fig. 9. Antonin et al. [138] reached total Evans Blue diazo dye removal after 60 and 5 min and 88% and more than 95% mineralization after 300 min of SPEF reaction at the pilot-scale plant of Fig. 8 and the 100 mL undivided cell of Fig. 5, respectively. This difference was attributed to the distinct electrode area/solution volume ratio of both reactors, among other factors. Other kinds of flow plants equipped with a plug-flow cell [129], a tubular ceramic membrane with imbedded electrodes [172] or a concentric annular cell [169] were occasionally used.

Moreira et al. [167] made a scale-up for SPEF process from a 100 mL undivided cell to a 10 L pilot-scale flow plant with filter-press cell and a photoreactor. The viability of using a pilot-scale plant was demonstrated but direct comparison between both units cannot be executed in view of the different experimental conditions such as anode nature, electrodes area/solution volume ratio, irradiated volume/total volume ratio and solar radiation capture system.

EAOPs mainly used BDD or Pt as anode, with the exception of the employment of SnO_2 doped with antimony (Sb) in AO [121], graphite cloth in AO-H_2O_2, EF and PEF-UVA [169] and graphite bar in EF [162,175]. Some studies performed a comparison between BDD and Pt anodes and, in general, BDD exhibited superiority over Pt, both in terms of decolorization and mineralization [23,105,119,131,171], since BDD shows a much higher potential

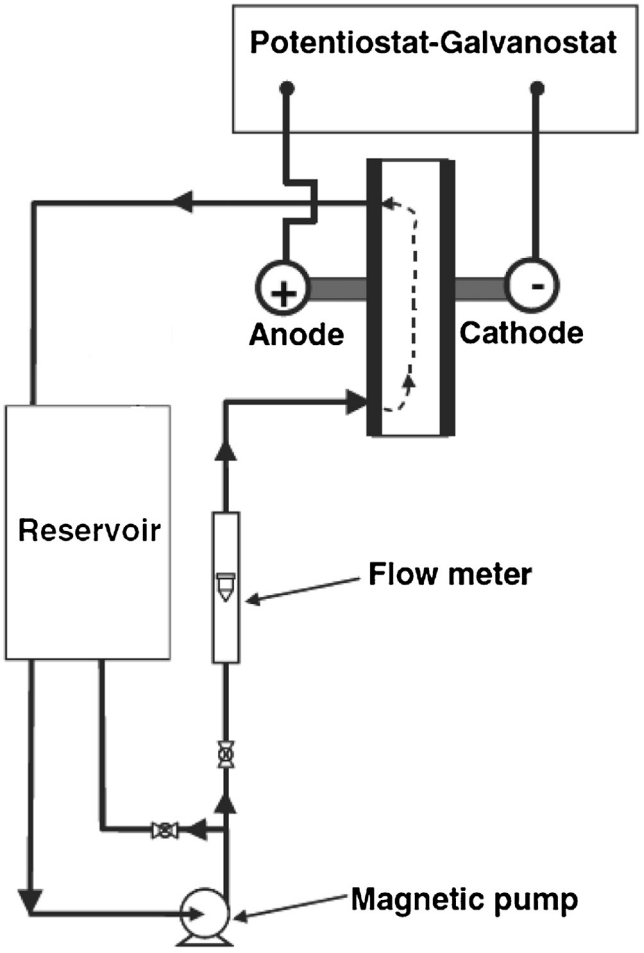

Fig. 6. Sketch of a simple reactor equipped with an electrochemical cell, a pump and a reservoir. Reprinted (adapted) from Nava et al. [174], Copyright © (2014), with permission from Springer-Verlag Berlin Heidelberg.

for O_2 evolution, producing larger amounts of M(•OH) to degrade organics. Surprisingly, in Garcia-Segura et al. [166] both AO-H_2O_2 and EF processes achieved quite similar decolorization by applying BDD or Pt anodes, pointing to very slow reaction of both BDD(•OH) and Pt(•OH) with the Acid Orange 7 monoazo dye. In turn, Thiam et al. [23] achieved similar mineralization by applying Pt and BDD in a PEF-UVA process, contrasting to what was found for AO, AO-H_2O_2 and EF, which can be related to the improvement of Acid Yellow 23 removal by light-induced mechanisms. Nava et al. [174] determined superiority of 2D (plate) BDD anode over 3D (mesh) BDD in terms of chemical oxygen demand (COD) removal.

All AO processes of Table 3 used steel cathodes, apart from Nava et al. [174] in which a Pt cathode was applied. The most popular cathode for AO-H_2O_2, EF, PEF and SPEF techniques has been carbon-PTFE air-diffusion electrodes, widely used by Brillas' research team. Some EF applications, chiefly carried out by Oturan's group, employed CF as cathode. Few investigations have operated with other cathodes like RVC [67], CNT [116,118,156], graphite cloth [169] and graphite bar [162,166,175]. Garcia-Segura et al. [166] compared the decolorization ability of azo dyes by AO-H_2O_2 either using carbon-PTFE air-diffusion electrode or graphite bar as cathode. Results showed a superiority of graphite over carbon-PTFE air-diffusion, which was related to the parallel direct reduction of the azo dye on the graphite cathode. This did not take place on the GDE cathode as it mostly comprised the two-electron reduction of oxygen to H_2O_2 via Eq. (16).

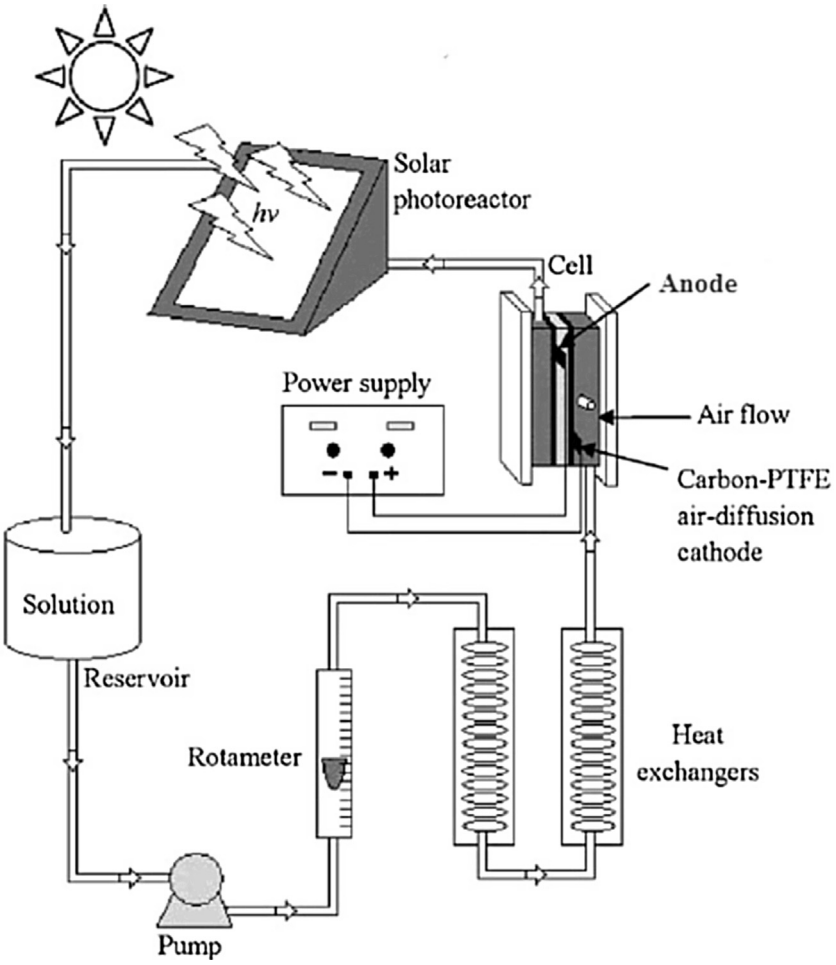

Fig. 7. Sketch of a 2.5 L pre-pilot-scale flow plant equipped with a filter-press electrochemical cell, a planar photoreactor with a mirror at the bottom, a reservoir, a pump and heat exchangers. Reprinted (adapted) from Salazar et al. [96], Copyright © (2011), with permission from Elsevier.

Commonly, undivided cells with working volumes of 100–200 mL employed electrodes with active areas of 3 cm^2, although areas up to 20 cm^2 were used. Undivided cells with superior solution volumes up to 2 L and flow plants with a filter-press cell using 1 L of solution applied larger electrodes areas from 11.5 to 90 cm^2. The 2.5 L flow plant with planar photoreactor used electrodes of 20 cm^2 of active area (see Fig. 7) and the 10 L flow plant equipped with borosilicate tubes used ca. 90 cm^2 electrodes (see Fig. 8). While steel and carbon-PTFE air-diffusion cathodes usually presented the same active area as the anode, graphite felts were always much larger, thus favoring the reduction of Fe^{3+} to Fe^{2+}.

3.1.4. Operational parameters

The majority of studies assessed the influence of *j* on decolorization, dye removal and mineralization and the results corroborate with Section 2.4.3. For initial DOC contents of around 100 mg L^{-1}, j_{cat} of 30–150 mA cm^{-2} were mostly employed, excluding when applying CF cathodes, for which j_{cat} below 10 mA cm^{-2} were used due to the larger active areas of these electrodes.

Only Nava et al. [174] evaluated the effect of liquid flow rate on the process efficiency. It was found a very low influence of this parameter on COD decay using AO process in a flow plant with an undivided filter-press cell with continuous solution recirculation.

All studies employed ambient temperature or a temperature of 35 °C to avoid water evaporation and H_2O_2 decomposition.

As referred in the general Section 2.4.6, the influence of pH on AO process achieved controversial results [119,145] and a best pH around 3.0 has been achieved for EF, PEF-UVA, PEF-UVC-ZnO and PEF-Vis/citrate processes [67,68,97,116,118], although with some variations [96,105,162,175].

Studies on the influence of $[TDI]_0$ revealed best results for contents of 5.6–28 mg L^{-1} in EF, PEF-UVA, PEF-Vis/oxalate, PEF-Vis/citrate and SPEF treatments of wastewaters with DOC up to 50 mg L^{-1} [68,112,118,123,156,169,170]. For dye wastewaters with DOC contents around 100 mg L^{-1}, larger $[TDI]_0$ of 28–56 mg L^{-1} were needed for PEF-UVA and SPEF processes [97,168], excluding the work of Flox et al. [105] where similar and best mineralization was attained for $[TDI]_0$ of 11–279 mg L^{-1}, indicating a very important role of BDD(•OH) on the dye degradation. In general, the $[TDI]_0$ values here presented are slightly above than those used by Oturan's group in the degradation of dyes [115] and other pollutants [60,146,176–178], typically between 5.6 and 11 mg L^{-1}.

Although most of the investigations have employed iron salts like $FeSO_4{\cdot}7H_2O$ and $FeCl_3{\cdot}6H_2O$ as iron source, some studies resorted to distinct sources. Rosales et al. [175] used Fe alginate gel beads in a concentration of 58 g L^{-1} for EF process, which attained higher decolorization than the classical EF using $[TDI]_0$ of 150 mg L^{-1}. This heterogeneous catalyst can avoid iron precipitation in virtue of the formation of ionic cross-links between the carboxyl group on alginate chains. In turn, Labiadh et al. [115] employed 0.5–2 g L^{-1} of pyrite as iron source for EF treatment, which allowed to get [TDI] of 50–130 mg L^{-1}. Faster dye removals

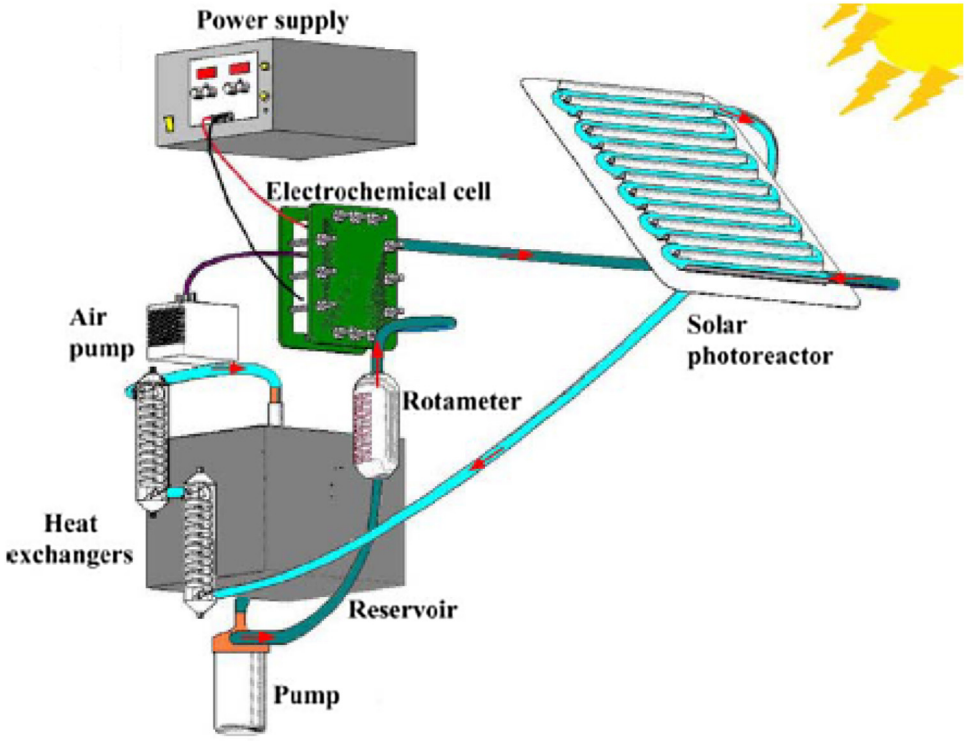

Fig. 8. Sketch of a 10 L pilot-scale flow plant equipped with a filter-press electrochemical cell, a photoreactor with borosilicate tubes and an aluminum reflector, a reservoir, a pump and heat exchangers. Reprinted (adapted) from Garcia-Segura et al. [151], Copyright © (2011), with permission from Elsevier.

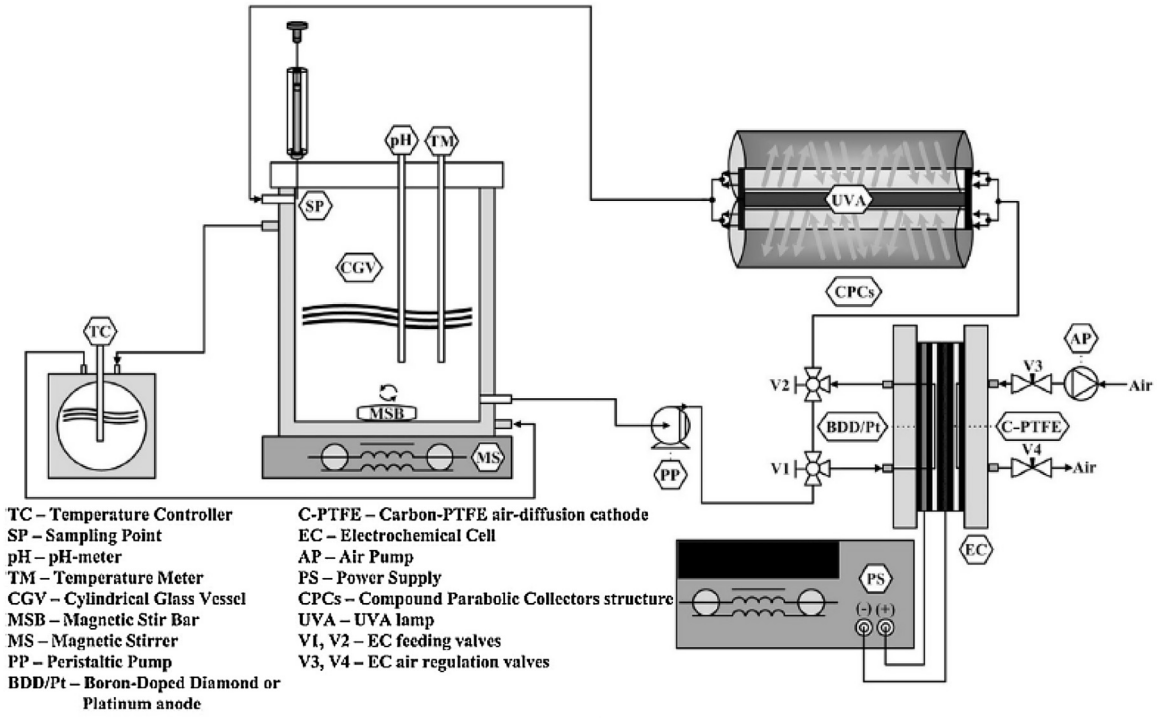

Fig. 9. Sketch of a 2.2 L lab-scale flow plant equipped with a filter-press electrochemical cell, a photoreactor composed of CPCs, a cylindrical glass vessel, a pump and a heat exchanger. Reprinted (adapted) from Moreira et al. [133], Copyright © (2014), with permission from Elsevier.

were reached at higher pyrite contents and the employment of 2 g pyrite L^{-1} led to faster degradation than using $[TDI]_0$ of 25 mg L^{-1}. Moreover, the addition of pyrite drove to pH self-regulation from neutral to 2.9–4.0. On the other hand, a sandwich film cathode composed of an active carbon fiber and Fe^{2+}-chitosan deposited on Ni was used by Fan et al. [132], allowing the release of iron into the solution and operation with similar efficiency at pH range of 2.5–6.2. The application of an EC step prior to EAOP stage in Thiam et al. [23] permitted to attain a [TDI] of 34 mg L^{-1}.

3.2. Wastewaters containing pesticides

The term pesticide refers to herbicides, insecticides, bactericides, fungicides, antimicrobials, rodenticides and various other substances used to control pests. Pollution of aqueous media by these compounds, mainly resulting from agriculture activities and pesticide manufacturing plants, constitutes a very serious environmental problem for human health and ecosystems due to their potential toxicity and resistance toward biological and chemical degradation [4]. Information of nineteen articles about decontamination of synthetic wastewaters with pesticides by EAOPs is summarized in Table 4.

3.2.1. Pesticide content

A look of Table 4 highlights that most of the articles refer to the treatment of herbicides, excluding the works of Skoumal et al. [139] and Vargas et al. [124], which regarded the degradation of antimicrobial and insecticide agents, respectively. Only a small number of investigations used mixtures of pesticides or compared the degradation of various pesticides [58,146,176], with almost all surveys using a single model compound. Abdessalem et al. [146,176] found pesticides removal readiness in the order chlorotoluron > carbofuran > bentazon for AO-H_2O_2 and EF processes.

Oturan and Oturan [179] appraised the degradation of three commercial formulations of pesticides used in viticulture, namely Mistel GD, Cuprofix CZ and Lannate 20L, which included many active ingredients and additives such as cymoxanil, mancozeb, zinebe, $CuSO_4$ and surfactants. The •OH radicals produced by EF process were consumed not only by the active ingredients but also by the additives.

Initial pesticide contents from 4.0 to 634 mg L^{-1} were applied. Some publications assessed the influence of initial pesticide concentration on EAOPs efficiency, always attaining lower percentages of mineralization and/or pollutant removal for larger initial pesticide amounts, as pointed out above.

3.2.2. Process

Most of the works of Table 4 embraced EF technique. A lot of works regarding AO treatment were also reported, although some works regarding AO treatment are not included in it. Only few studies assessed the application of SPEF. Predominantly, the mineralization ability of EAOPs followed the order SPEF > PEF-UVA > EF > AO-H_2O_2 ≈ AO. As can be seen in Fig. 10, Boye et al. [135] achieved 98%, 60%, 28% and 25% of DOC removal after 180 min of treatment by PEF-UVA, EF, AO-H_2O_2 and AO processes, respectively, using 194 mg 4-chlorophenoxyacetic acid (4-CPA) pesticide L^{-1}. Flox et al. [111] found a mineralization of 80% and 67% after 100 min of SPEF and PEF-UVA processes, respectively, for the treatment of 2.5 L of 100 mg mecoprop pesticide L^{-1} using a BDD anode, a carbon-PTFE air-diffusion cathode, pH 3.0, 25 °C, $[TDI]_0$ of 28 mg L^{-1} and j_{cat} of 50 mA cm^{-2}. Only Brillas et al. [161] and Skoumal et al. [139] attained different mineralization abilities from what mentioned above. In the former study, similar DOC removals were reached for PEF-UVA and EF technologies, indicating a large participation of •OH in the bulk from Fenton's reaction (21) on the degradation of 2-(2,4-dichlorophenoxy)-propionic acid (2,4-D) pesticide and its by-products. In the second study, AO gained superiority over EF for longer reaction times, suggesting that BDD(•OH) were able to oxidize more quickly the final carboxylic acids than their Fe(III) complexes.

With respect to pesticide removal, SPEF, PEF-UVA and EF processes usually attained similar results and better than AO-H_2O_2 and AO, pointing to effective degradation of parent compound by •OH in the bulk. On opposite, Borràs et al. [106], Dhaouadi and Adhoum [180] and Garza-Campos et al. [181] observed superiority of light-assisted EAOPs over EF in terms of pesticide abatement,

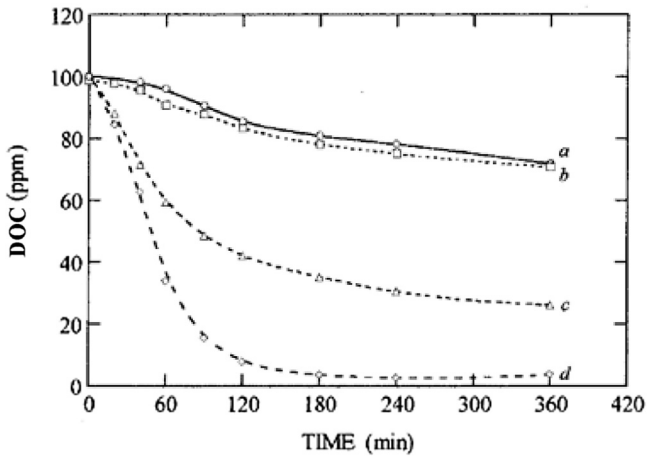

Fig. 10. DOC removal as a function of time for the treatment of 194 mg 4-CPA L^{-1} in 7.0 g Na_2SO_4 L^{-1} by various EAOPs using Pt anode, carbon-PTFE air-diffusion cathode, pH 3.0, 35 °C, $[TDI]_0$ of 56 mg L^{-1} for EF, PEF-UVA and SPEF and j of 32 mA cm^{-2}. EAOP: (a-○) AO, (b-□) AO-H_2O_2, (c-△) EF and (d-◊) PEF-UVA. Reprinted (adapted) from Boye et al. [135], Copyright © (2002), with permission from American Chemical Society.

proposing contribution of photoreduction reactions (28) and (29) under the applied conditions. Regarding AO and AO-H_2O_2 efficiencies in terms of pesticide removal, tendencies are not clear since Boye et al. [135] determined superiority of AO-H_2O_2 over AO, but in Boye et al. [94] both processes yielded similar herbicide decay. This may be related to the oxidation ability of H_2O_2 on the initial molecule, although more research is required for confirmation.

Abdessalem et al. [176] accomplished a direct comparison between EF and PF-UVC using an initial $[H_2O_2]$ of 340 mg L^{-1}. The PF-UVC process attained faster mineralization than EF, which was attributed to the initial addition of H_2O_2 and Fe^{3+} to form •OH in the bulk from Fenton's reaction (21) in the former in contrast with the gradual formation of •OH in the latter. Certainly, the generation of additional •OH in the presence of H_2O_2 and UVC radiation via Eq. (30) and photoreduction reactions (28) and (29) also had a large contribution to the faster mineralization by PF-UVC. Moreover, costs of reagents and electrical energy consumption were evaluated to be 4 times lower for EF, which then results clearly beneficial for application. In turn, Dhaouadi and Adhoum [180] observed superiority of PF-UVA over PEF-UVA in terms of COD and pesticide removals for the first times of reaction, followed by very poor decays with superiority of the electrochemical process over the chemical one. While the initial superiority of PF-UVA over PEF-UVA can be associated with the presence of higher contents of reactants at the beginning of the reaction, parasitic reactions such as Eqs. (24) and (25) probably occurred in large extent in both processes for longer reaction times.

Comparison between PC, EF and EC technologies for several chlorophenoxy and chlorobenzoic herbicides was performed by Brillas et al. [58]. The authors achieved the following mineralization ability: PC > EF » EC. These results pointed to a small retention of pesticide into $Fe(OH)_3$ precipitate in EC method and a larger production of •OH in the bulk in PC technique due to the generation of Fe^{2+} at the anode via Eq. (27), simultaneously with the coagulation of oxidation by-products. Despite the superiority of PC over EF, the latter is more economically viable because it avoids the further treatment of the large sludge produced in the former.

Garza-Campos et al. [181] performed an innovative SPEF process combined with solar heterogeneous photocatalysis (SPEF-SPC) using TiO_2 nanoparticles synthetized by sol-gel and supported on glass spheres by dip-coating as catalyst. This combined process attained higher degradation ability in terms of atrazine decay and

Table 4
Examples on the treatment of synthetic wastewaters contaminated with pesticides by EAOPs.

Pollutant	Wastewater characteristics	Process	Electrochemical reactor		Electrodes/ Operational parameters	Maximum DOC decay (%)/ EC_{DOC} (kWh (g DOC)$^{-1}$)[a]	Refs.
			Configuration	*V* (L)			
2-(2,4-dichlorophenoxy)-propionic acid (2,4-D) pesticide	217 mg 2,4-D L^{-1} in 7.0 g Na_2SO_4 L^{-1}	AO EF PEF-UVA	UC	0.1	Anode: Pt (10 cm^2) or BDD (3 cm^2) Cathode: AO: Graphite (3 cm^2) EF, PEF-UVA: C-PTFE O-D (3 cm^2) j_{cat}: 33–150 mA cm^{-2} *Q*: MS T: 35 °C pH: 3.0 $[TDI]_0$ (EF, PEF-UVA): 112 mg L^{-1}	PEF-UVA: 83/n.a.	[161]
2,4,5-trichlorophenoxyacetic acid (2,4,5-T) pesticide	53–266 mg 2,4,5-T L^{-1} in 7.0 g Na_2SO_4 L^{-1}	AO AO-H_2O_2 EF PEF-UVA	UC	0.1	Anode: Pt (10 cm^2) Cathode: AO: Graphite (3 cm^2) AO-H_2O_2, EF, PEF-UVA: C-PTFE O-D (3.1 cm^2) j_{cat}: 32–145 mA cm^{-2} *Q*: MS T: 35 °C pH: 2.0–6.0 $[TDI]_0$ (EF, PEF-UVA): 28–112 mg L^{-1}	PEF-UVA: 100/n.a.	[94]
2,4-dichlorophenoxyacetic acid (2,4-D) pesticide	60 mg 2,4-D L^{-1} in 7.0 g Na_2SO_4 L^{-1}	AO EF	FP with undivided FPC	3	Anode: BDD (64 cm^2) Cathode: BDD (64 cm^2) (with or without air bubbling for EF or AO, respectively) j_{cat}: 7.8–31 mA cm^{-2} *Q*: 4–10 L min^{-1} T: Amb. pH: 3.0 $[TDI]_0$ (EF): 17 or 39 mg L^{-1}	EF: 83/0.095	[70]
4-chloro-2-methylphenoxyacetic acid (MCPA) pesticide	186 mg MCPA L^{-1} in 7.0 g Na_2SO_4 L^{-1}	SPEF	FP with undivided FPC and photoreactor	10	Anode: Pt (90.3 cm^2) Cathode: C-PTFE A-D (90.3 cm^2) j_{cat}: 18–93 mA cm^{-2} *Q*: 3 L min^{-1} T: 35 °C pH: 3.0 $[TDI]_0$: 23–117 mg L^{-1}	75/0.0877	[151]
4-chlorophenoxyacetic acid (4-CPA) pesticide	40–387 mg 4-CPA L^{-1} in 7.0 g Na_2SO_4 L^{-1}	AO AO-H_2O_2 EF PEF-UVA	UC	0.1	Anode: Pt (10 cm^2) Cathode: AO: Graphite (3 cm^2) AO-H_2O_2, EF, PEF-UVA: C-PTFE O-D (3.1 cm^2) j_{cat}: 32–145 mA cm^{-2} *Q*: MS T: 25–45 °C pH: 2.0–6.0 $[TDI]_0$ (EF, PEF-UVA): 28–112 mg L^{-1}	PEF-UVA: 100/n.a.	[135]
4-chlorophenoxyacetic acid (4-CPA), 4-chloro-2-methylphenoxyacetic acid (MCPA), 2,4-dichlorophenoxyacetic acid (2,4-D), 2,4,5-trichlorophenoxyacetic acid (2,4,5-T), 3,6-dichloro-2-methoxybenzoic acid (dicamba) pesticides	200 mg 4-CPC L^{-1} or 194 mg MCPA L^{-1} or 230 mg 2,4-D L^{-1} or 269 mg 2,4,5-T L^{-1} or 230 mg dicamba L^{-1} in 7.0 g Na_2SO_4 L^{-1}	PC EC EF	UC	0.1	Anode: PC, EC: Fe (10 cm^2) EF: Pt (10 cm^2) Cathode: PC, EF: C-PTFE O-D (3.1 cm^2) EC: Graphite (3 cm^2) j_{cat}: 33–150 mA cm^{-2} *Q*: MS T: 35 °C pH: 3.0 $[TDI]_0$ (EF): 56 mg L^{-1}	PC: 94/n.a.	[58]
Amitrole pesticide	350 mg amitrole L^{-1} in 7.0 g Na_2SO_4 L^{-1}	AO EF	UC	0.1	Anode: AO: Pt or BDD (3 cm^2) EF: Pt (3 cm^2) Cathode: AO: SS (3 cm^2) EF: C-PTFE O-D (3.1 cm^2) j_{cat}: 32–145 mA cm^{-2} *Q*: MS T: 35 °C pH: 3.0 $[TDI]_0$ (EF): 56 mg L^{-1}	EF: 80/n.a.	[184]

Table 4 (*Continued*)

Pollutant	Wastewater characteristics	Process	Electrochemical reactor		Electrodes/ Operational parameters	Maximum DOC decay (%)/ EC_{DOC} (kWh (g DOC)$^{-1}$)[a]	Refs.
			Configuration	*V* (L)			
Atrazine pesticide	20 mg atrazine L^{-1} in 7.0 g Na_2SO_4 L^{-1}	AO EF SPEF SPC SPEF-SPC	UC	0.2	Anode: BDD (7.5 cm^2) Cathode: AO: Pt mesh (7.5 cm^2) EF, SPEF, SPEF-SPC: BDD (7.5 cm^2) (with air bubbling) j_{cat}: 13 mA cm^{-2} *Q*: MS T: Amb. pH: 3.0 $[TDI]_0$ (EF, SPEF, SPEF-SPC): 5.6 mg L^{-1}	SPEF-SPC: 80/2	[181]
Atrazine pesticide	22 mg atrazine L^{-1} in 14 g Na_2SO_4 L^{-1}	AO-H_2O_2 EF	UC	0.22	Anode: AO-H_2O_2, EF: BDD (25 cm^2) EF: Pt mesh (4.5 cm^2) Cathode: CF (60 cm^2) j_{cat}: 0.83–17 mA cm^{-2} *Q*: MS T: Amb. pH (AO-H_2O_2): 6.3 pH (EF): 3.0 $[TDI]_0$ (EF): 5.6 mg L^{-1}	EF: 97/n.a.	[178]
Chloroxylenol pesticide	100 mg chloroxylenol L^{-1} in 7.0 g Na_2SO_4 L^{-1}	AO EF PEF-UVA	UC	0.1	Anode: Pt or BDD (3 cm^2) Cathode: AO: SS (3 cm^2) EF, PEF-UVA: C-PTFE O-D (3 cm^2) j_{cat}: 33–150 mA cm^{-2} *Q*: MS T: 25 °C pH: 3.0 $[TDI]_0$ (EF, PEF-UVA): 11–279 mg L^{-1}	PEF-UVA: ≈100/n.a.	[139]
Chlortoluron, carbofuran, bentazon pesticides	27 mg chlortoluron L^{-1}, 28 mg carbofuran L^{-1}, 30 mg bentazon L^{-1} (mixture) in 7.0 g Na_2SO_4 L^{-1}	AO-H_2O_2 EF	UC	0.25	Anode: BDD (14 cm^2) Cathode: CF (60 cm^2) j_{cat}: 5.0 mA cm^{-2} *Q*: MS T: 23 °C. pH (AO-H_2O_2): 3.0–12 pH (EF): 3.0 $[TDI]_0$ (EF): 5.6 mg L^{-1}	EF: 90/n.a.	[146]
Chlortoluron, carbofuran, bentazon pesticides	27 mg chlortoluron L^{-1}, 28 mg carbofuran L^{-1}, 30 mg bentazon L^{-1} (mixture) in 7.0 g Na_2SO_4 L^{-1}	EF PF-UVC	UC	0.25	Anode: Pt grid Cathode: CF (60 cm^2) j_{cat}: 5.0 mA cm^{-2} *Q*: MS T: Amb. pH: 3.0 $[TDI]_0$: 5.6 mg L^{-1}	EF: 82/n.a.	[176]
Cyanazine pesticide	55–145 mg cyanazine L^{-1} in 7.0 g Na_2SO_4 L^{-1}	AO-H_2O_2 EF PEF-UVA	UC	0.1	Anode: BDD (3 cm^2) Cathode: C-PTFE A-D (3 cm^2) j_{cat}: 33–150 mA cm^{-2} *Q*: MS T: 35 °C pH: 3.0 $[TDI]_0$ (EF, PEF-UVA): 28 mg L^{-1}	PEF-UVA: 98/n.a.	[106]
Dichlorvos pesticide	4.0–87 mg dichlorvos L^{-1} in 14 g Na_2SO_4 L^{-1}	AO	DC	n.s.	Anode: SnO_2-Sb_2O_5 (1 cm^2) Cathode: Pt gauze *E*: 1.8–2.7 V *Q*: MS T: Amb. pH: Neutral	n.a./n.a.	[124]
Diuron pesticide	40 mg diuron L^{-1} in 7.0 g Na_2SO_4 L^{-1}	EF PF-UVC Fenton	EF: UC PF-UVC, Fenton: FP with an interior quartz tube that can allocate a lamp	0.25	Anode: n.s. Cathode: CF (40 cm^2) j_{cat}: 1.5–7.5 mA cm^{-2} *Q*: 3 L min^{-1} T: Amb. pH: 3.0 $[TDI]_0$ (PEF-UVC): 14–140 mg L^{-1} $[TDI]_0$ (Fenton): 11–56 mg L^{-1} $[TDI]_0$ (EF): 11 mg L^{-1}	EF: 96/n.a.	[60]

Table 4 (*Continued*)

Pollutant	Wastewater characteristics	Process	Electrochemical reactor		Electrodes/ Operational parameters	Maximum DOC decay (%)/ EC_{DOC} (kWh (g DOC)$^{-1}$)[a]	Refs.
			Configuration	*V* (L)			
Diuron pesticide	43 mg diuron L^{-1} in 7.0 g Na_2SO_4 L^{-1}	AO-H_2O_2 EF PEF-UVA SPEF	LS: UC PS: FP with undivided FPC and planar photoreactor	LS: 0.1 PS: 2.5	Anode: LS: Pt or BDD (3 cm^2); PS: BDD (20 cm^2) Cathode: C-PTFE A-D LS: 3 cm^2; PS: 20 cm^2 j_{cat}: 33–150 mA cm^{-2} *Q*: LS: MS; PS: 3.3 L min^{-1} T: 25 °C pH: 3.0 $[TDI]_0$ (EF, PEF-UVA, SPEF): 28 mg L^{-1}	SPEF: 70/3.7	[183]
Mecoprop pesticide	100–634 mg mecoprop L^{-1} in 7.0 g Na_2SO_4 L^{-1}	AO-H_2O_2 EF PEF-UVA SPEF	FP with undivided FPC and planar photoreactor	2.5	Anode: BDD (20 cm^2) Cathode: C-PTFE O-D (20 cm^2) j_{cat}: 25–150 mA cm^{-2} *Q*: 3 L min^{-1} T: 25 °C pH: 3.0 $[TDI]_0$ (EF, PEF-UVA): 28 mg L^{-1} $[TDI]_0$ (SPEF): 14–279 mg L^{-1}	SPEF: >97/n.a.	[111]
Mistel GD (Cymoxanil + Mancozeb + additives), Cuprofix CZ (Cymoxanil + Zineb + $CuSO_4$ + additives), Lannate 20L (Metomyl + ethanol + other additives) pesticides	Mistel GD or Cuprofix CZ or Lannate 20L in ultrapure water	EF	UC	0.15	Anode: Pt Cathode: CF *I*: 60–300 mA *Q*: MS T: Amb. pH: 3.0 $[TDI]_0$: 5.6 mg L^{-1} (or 6.4–7944 mg Cu^{2+} L^{-1})	n.a./n.a.	[179]
Paraquat pesticide	10–50 mg paraquat L^{-1} in 7.0 g Na_2SO_4 L^{-1}	AO EF PEF-UVA PF-UVA	UC	0.1	Anode: Pt net (5 cm^2) Cathode: CF (15 cm^2) (with or without O_2 bubbling for PEF-UVA/EF or AO, respectively) j_{cat}: 3.3–13 mA cm^{-2} *Q*: MS T: 25 °C pH: 3.0 $[TDI]_0$ (EF): 5.6–112 mg L^{-1} or Co^{2+} or Ag^+ $[TDI]_0$ (PEF-UVA): 11 mg L^{-1}	PEF-UVA: 97/n.a.	[180]
Picloram pesticide	30–242 mg picloram L^{-1} in 7.0 g Na_2SO_4 L^{-1}	EF	UC	0.15	Anode: Pt gauze Cathode: CF (50 cm^2) j_{cat}: 0.6–10 mA cm^{-2} *Q*: MS T: Amb. pH: 3.0 $[TDI]_0$: 1.1–56 mg L^{-1}	≈100/n.a.	[233]

Amb. – Ambient;
C-PTFE A-D – Carbon-PTFE air-diffusion;
C-PTFE O-D – Carbon-PTFE O_2-diffusion;
DC – Divided cell;
FP – Flow plant;
FPC – Filter-press cell;
LS – Lab-scale;
MS – Magnetic stirring;
n.a. – not assessed;
n.s. – not specified;
PS – Pilot-scale;
Q – Liquid flow rate;
UC – Undivided cell.

[a] Under the best experimental conditions, when applicable.

DOC removal compared to traditional SPEF, with 10% larger mineralization after 300 min of reaction.

Most studies assessed the generation of aromatic by-products during pesticides oxidation by EAOPs. For example, the degradation of 2,4-dichlorophenoxyacetic acid by AO, EF and PEF processes led to the production of dichlorophenol, 4,6-dichlororesorcinol, chlorohydroquinone and chloro-*p*-benzoquinone [70,161]. While these by-products were accumulated in AO, more potent processes as EF and PEF processes allowed their fast removal. For atrazine pesticide, Garza-Campos et al. [181] found an inhibition of its mineralization by the formation of cyanuric acid, achieving a maximum mineralization of 65% by SPEF-SPC. In contrast, the use of EF-BDD to degrade cyanuric acid at high current led to 90% mineralization after 10 h of reaction [178]. The degradation of cyanazine pesti-

cide by AO-H_2O_2, EF and PEF-UVA also induced the formation of cyanuric acid, in addition to deisopropylatrazine, desethyldeisopropylatrazine and ammeline intermediates, with total removal of this compound after 240–360 min of electrolysis [106].

Oturan et al. [182] measured the toxicity of diuron aqueous solutions during EF treatment by using the bacteria *Vibrio fischeri* (Microtox) and the green alga *Scenedesmus obliquus*. It was observed a strong increase of the solution toxicity at the beginning of electrolysis due to the formation of more biorecalcitrant by-products, being necessary to apply EF for a long time (several hours) and at relatively high current (250 mA) to reach an almost complete mineralization of the herbicide.

3.2.3. Electrochemical reactor

Undivided cells have been by far the most popular electrochemical reactors for wastewaters contaminated with pesticides, commonly applying volumes from 100 to 250 mL and electrodes with active areas up to 25 cm^2, except for CF cathode, which were larger. Few investigations used other reactors like a divided cell [124], a simple 3 L flow plant with a filter-press cell [70], the 2.5 L flow plant with a filter-press cell and a planar photoreactor of Fig. 7 [111,183] and the 10 L pilot-scale flow plant with a filter-press cell and a photoreactor made-up of borosilicate tubes of Fig. 8 [151]. Pipi et al. [183] reported faster pesticide degradation by SPEF using a 100 mL undivided cell than the above 2.5 L flow plant, which was mainly attributed to the distinct electrode area/solution volume ratio.

Pt and BDD have been mainly and equally used as anode. Only Vargas et al. [124] employed a different anode material like SnO_2-SbO_5. In general, the BDD anode showed superiority over Pt both in terms of mineralization and pesticide removal for all EAOPs due to its higher potential for O_2 evolution [161,178,183–185]. Exceptionally, Skoumal et al. [139] found similar pesticide abatement using BDD and Pt for EF and PEF-UVA processes, meaning that the main oxidant for chloroxylenol pesticide was •OH generated from Fenton's reaction (21). Da Pozzo et al. [184] found an unusual fast DOC removal of amitrole pesticide in aqueous solution using an AO-Pt system, which could be due to the release of volatile species that are not mineralized.

Various cathodes have been used in AO treatment, including graphite [94,135,161,185], stainless steel (SS) [139,184], Pt [124,181], BDD without air bubbling [70] and CF without oxygen bubbling [180]. AO-H_2O_2, EF and PEF-UVA mostly applied carbon-PTFE air-diffusion electrodes and CF as cathodes, with the exception of García et al. [70], which employed BDD with air injection as cathode in EF process. SPEF mainly resorted to carbon-PTFE air-diffusion cathodes, apart from Garza-Campos et al. [181] that used BDD with air injection. None of the presented studies performed a comparison between efficiencies with different cathodes, which seems necessary to build-up the best electrolytic cell for use in practice.

3.2.4. Operational parameters

Almost all studies assessed the effect of j on pesticides degradation, mainly in terms of DOC removal, and the results are in agreement with Section 2.4.3, with exception for Pipi et al. [183], which attained quite similar mineralization with the increment of j for PEF-UVA and SPEF systems at lab-scale and pilot-scale, respectively, pointing to mineralization control by photoreduction reactions (28) and (29). In general, pesticide solutions with DOC contents of 50–100 mg L^{-1} were tested at j_{cat} of 25–150 mA cm^{-2}, apart from when employing CF as cathode, where j_{cat} below 17 mA cm^{-2} were used. Brillas et al. [58] determined higher treatment efficiency for PC process using low j_{cat} and short electrolysis times. At low j_{cat}, mineralization and coagulation were in competition, whereas at high j_{cat} the coagulation process was predominant, impeding further mineralization.

García et al. [70] assessed the influence of liquid flow rate from 4 to 10 L min^{-1} for 2,4-dichlorophenoxyacetic acid mineralization by AO using a flow plant with an undivided filter-press cell. A faster mineralization was reached for higher liquid flow rate due to the improvement of mass transfer of pesticide and its oxidation products to anode surface to react with BDD(•OH).

The effect of temperature on pesticide degradation was checked by Boye et al. [135]. A temperature increase from 25 to 35 °C enhanced the mineralization ability mainly for PEF-UVA process, with very poor improvement for AO-H_2O_2 and EF processes. From 35 to 45 °C, the degradation improvement was null and it was related to a significant increase of water evaporation and oxygen release with electrolysis time. Based on this study, most subsequent research used 35 °C as the best temperature, although many works preferred the use of ambient temperature.

As mentioned in the general Section 2.4.6, the influence of pH on AO and AO-H_2O_2 processes achieved controversial results [135,146], while a pH near 3.0 was the best for EF, PEF-UVA and SPEF processes [94,151].

Best results for the degradation of synthetic wastewaters contaminated with pesticides were achieved employing $[TDI]_0$ of 1–56 mg L^{-1} for EF, PEF-UVA and SPEF processes using wastewaters with around 100 mg DOC L^{-1} [94,135,151,161,185]. For EF applied to wastewaters up to 50 mg DOC L^{-1}, best $[TDI]_0$ of 11–39 mg L^{-1} were found [70,180,184]. Flox et al. [111] and Skoumal et al. [139] observed a small influence of $[TDI]_0$ on DOC removal using a wide $[TDI]_0$ range of 14–279 and 28–112 mg L^{-1} in SPEF and PEF-UVA processes, respectively, to degrade solutions with around 50 mg DOC L^{-1}. These results indicate that a small amount of this catalyst was sufficient to yield the maximum generation of oxidant •OH from Fenton's reaction (21) under the experimental conditions used. Other catalysts such as Ag^+ and Co^{2+} were tested by Dhaouadi and Adhoum [180] in EF process, reaching a degradation ability in the order $Ag^+ > Fe^{2+} > Co^{2+}$. Despite these achievements, it seems more reasonable to choose Fe^{2+} as the best catalyst due to the higher cost and toxicity of Ag^+. Oturan and Oturan [179] achieved higher mineralization of commercial formulations of pesticides by applying Fe^{3+} in comparison with Cu^{2+}.

3.3. Wastewaters containing pharmaceuticals

Pharmaceuticals include various compounds such as antibiotics, antipyretics, analgesics, anti-inflammatories, antimicrobials and hormones. These compounds and their bioactive metabolites are continuously introduced into the aquatic systems at ng L^{-1} or μg L^{-1} levels by several routes including emission from production sites, direct disposal of overplus drugs in households and hospitals, excretion after drug administration to humans and animals and water treatments in fish farms [186]. Their presence constitutes a serious environmental problem since they are toxic and cause other negative effects to humans and other living organisms even at trace concentrations and, furthermore, they are resistant to biological degradation processes, escaping almost intact from conventional WWTPs [3,187]. Twenty-three studies regarding the treatment of synthetic wastewaters polluted with pharmaceuticals by the application of EAOPs are displayed in Table 5.

3.3.1. Pharmaceutical content

The decontamination of wastewaters with antibiotics or antimicrobial drugs was more expressive, although many other pharmaceuticals were considered such as anti-inflammatories, beta-blockers and endocrine disrupting agents. All investigations were performed with synthetic solutions of just one pharmaceutical.

Table 5
Examples on the treatment of synthetic wastewaters contaminated with pharmaceuticals by EAOPs.

Pollutant	Wastewater characteristics	Process	Electrochemical reactor		Electrodes/ Operational parameters	Maximum DOC decay (%)/ EC_{DOC} (kWh (g DOC)$^{-1}$)[a]	Refs.
			Configuration	*V* (L)			
Amoxicillin antibiotic	36 mg amoxicillin L^{-1} in 7.0 g Na_2SO_4 L^{-1}	AO	UC	0.25	Anode: CF, carbon fiber, carbon graphite, Pt, PbO_2, DSA (Ti/RuO_2–IrO_2) or BDD (24 cm^2) Cathode: SS (24 cm^2) j_{cat}: 2.1–42 mA cm^{-2} *Q*: MS T: 20 °C pH: 5.3	≈100/n.a.	[35]
Atenolol, metoprolol, propranolol beta-blockers	158 mg atenolol L^{-1} or 66 mg metoprolol L^{-1} or 135 mg propranolol L^{-1} in 14 g Na_2SO_4 L^{-1}	EF SPEF	FP with undivided FPC and photoreactor	10	Anode: Pt or BDD (90.3 cm^2) Cathode: C-PTFE A-D or CF (90.3 cm^2) j_{cat} (C-PTFE A-D): 17–55 mA cm^{-2} j_{cat} (CF):4.4 mA cm^{-2} *Q*: 4.2 L min^{-1} T: 35 °C pH: 3.0 $[TDI]_0$: 28 mg L^{-1}	SPEF: 97/0.08	[191]
Chloramphenicol antibiotic	25–245 mg chloramphenicol L^{-1} in 7.0 g Na_2SO_4 L^{-1}	AO-H_2O_2 EF PEF-UVA SPEF	LS: UC PS: FP with undivided FPC and photoreactor	LS: 0.1 PS: 10	Anode: LS: Pt or BDD (3 cm^2); PS: Pt (90.2 cm^2) Cathode: C-PTFE A-D LS: 3 cm^2; PS: 90.2 cm^2 j_{cat}: 33–100 mA cm^{-2} *Q*: LS: MS; PS: 3.3 L min^{-1} T: 35 °C pH: 3.0 $[TDI]_0$: 28 mg L^{-1}	SPEF: ≈100/n.a.	[98]
Chlorophene antimicrobial drug	84 mg chlorophene L^{-1} in 7.0 g Na_2SO_4 L^{-1}	AO-H_2O_2 EF	UC	0.2	Anode: Pt or BDD (3 cm^2) or Pt mesh (4.5 cm^2) Cathode: C-PTFE O-D (3 cm^2) or CF (70 cm^2) j_{cat} (C-PTFE A-D): 20–100 mA cm^{-2} j_{cat} (CF): 0.86–4.3 mA cm^{-2} *Q*: MS T: Amb. pH: 3.0 $[TDI]_0$ (EF): 11–447 mg L^{-1}	EF: ≈100/n.a.	[84]
Clofibric acid	89–557 mg clofibric L^{-1} in 7.0 g Na_2SO_4 L^{-1}	AO-H_2O_2 EF PEF-UVA	UC	0.1	Anode: BDD (3 cm^2) Cathode: C-PTFE O-D (3 cm^2) j_{cat}: 33–150 mA cm^{-2} *Q*: MS T: 35 °C pH: 3.0 $[TDI]_0$ (EF. PEF-UVA): 56 mg L^{-1}	PEF-UVA: ≈100/n.a.	[188]
Diclofenac anti-inflammatory	175 mg diclofenac L^{-1} in 7.0 g Na_2SO_4 L^{-1} or neutral buffer solution of 7.0 g Na_2SO_4 L^{-1} + 20 g KH_2PO_4 L^{-1} + NaOH	AO	UC	0.1	Anode: Pt or BDD (3 cm^2) Cathode: SS (3 cm^2) j_{cat}: 17–150 mA cm^{-2} *Q*: MS T: 35 °C pH: 6.5	100/n.a.	[195]
Ibuprofen anti-inflammatory drug	41 mg ibuprofen L^{-1} in 7.0 g Na_2SO_4 L^{-1}	EF PEF-UVA SPEF	UC	0.1	Anode: Pt or BDD (3 cm^2) Cathode: C-PTFE O-D (3 cm^2) j_{cat}: 3.3–100 mA cm^{-2} *Q*: MS T: 25 °C pH: 2.0–6.0 $[TDI]_0$: 5.6–112 mg L^{-1}	SPEF: 92/n.a.	[148]
Ketoprofen endocrine disrupting drug	50 mg ketoprofen L^{-1} in 7.0–70 g Na_2SO_4 L^{-1}	AO	FP with undivided FPC	n.s.	Anode: BDD (12.5 cm^2) Cathode: BDD (12.5 cm^2) j_{cat}: 40–320 mA cm^{-2} *Q*: 0.00142–0.00834 L min^{-1} T: 25 °C pH: 3.0–11	n.a./n.a.	[69]

Table 5 (*Continued*)

Pollutant	Wastewater characteristics	Process	Electrochemical reactor		Electrodes/ Operational parameters	Maximum DOC decay (%)/ EC_{DOC} (kWh (g DOC)$^{-1}$)[a]	Refs.
			Configuration	*V* (L)			
Omeprazole gastrointestinal drug	17–169 mg omeprazole L^{-1} in neutral buffer solution of 18 g NaH_2PO_4 L^{-1} + 2.5 g H_3PO_4 L^{-1}	AO-H_2O_2	UC	0.1	Anode: Pt or BDD (3 cm^2) Cathode: C-PTFE A-D (3 cm^2) j_{cat}: 33–150 mA cm^{-2} *Q*: MS T: 35 °C pH: 7.0	78/n.a.	[120]
Paracetamol analgesic, antipyretic	157 mg paracetamol L^{-1} in 7.0 g Na_2SO_4 L^{-1}	SPEF	FP with undivided FPC and photoreactor	10	Anode: Pt (90.2 cm^2) Cathode: C-PTFE A-D (90.2 cm^2) j_{cat}: 39–94 mA cm^{-2} *Q*: 3 L min^{-1} T: 35 °C pH: 1.4–4.4 $[TDI]_0$: 18–65 mg L^{-1}	75/0.093	[150]
Propranolol beta-blocker	77–616 mg propranolol L^{-1} in 7.0 g Na_2SO_4 L^{-1}	EF PEF-UVA	UC	0.1	Anode: Pt or BDD (3 cm^2) Cathode: C-PTFE A-D or CF (3 cm^2) j_{cat} (C-PTFE A-D): 10–80 mA cm^{-2} j_{cat} (CF): 4 mA cm^{-2} *Q*: MS T: 35 °C pH: 2.0–6.0 $[TDI]_0$: 5.6–279 mg L^{-1}	PEF-UVA: ≈100/n.a.	[113]
Ranitidine H_2 receptor antagonist	34–113 mg ranitidine L^{-1} in 7.0 g Na_2SO_4 L^{-1}	EF SPEF	FP with undivided FPC and planar photoreactor	2.5	Anode: Pt (20 cm^2) Cathode: C-PTFE A-D (20 cm^2) j_{cat}: 25–100 mA cm^{-2} *Q*: 3.3 L min^{-1} T: 35 °C pH: 3.0 $[TDI]_0$: 11–112 mg L^{-1}	SPEF: 70/n.a.	[193]
Salicylic acid	164 mg salicylic acid L^{-1} in 7.0 g Na_2SO_4 L^{-1}	AO AO-H_2O_2 EF PEF-UVA SPEF	UC	0.1	Anode: Pt or BDD (3 cm^2) Cathode: AO: Graphite (3 cm^2) Others: C-PTFE A-D (3 cm^2) j_{cat}: 33–150 mA cm^{-2} *Q*: MS T: 35 °C pH: 2.0–6.0 $[TDI]_0$: 11–112 mg L^{-1}	SPEF: >82/n.a.	[155]
Sulfamethazine antimicrobial veterinary drug	193–1930 mg sulfamethazine L^{-1} in 7.0 g Na_2SO_4 L^{-1}	EF PEF-UVA	UC	0.1	Anode: BDD (3 cm^2) Cathode: C-PTFE A-D (3 cm^2) j_{cat}: 33–100 mA cm^{-2} *Q*: MS T: 35 °C pH: 2.0–6.0 $[TDI]_0$: 11–84 mg L^{-1}	PEF-UVA: ≈100/n.a.	[114]
Sulfamethazine antimicrobial veterinary drug	25–198 mg sulfamethazine L^{-1} in 7.0 g Na_2SO_4 L^{-1}	AO-H_2O_2 EF	FP with UC	1	Anode: Pt (38 cm^2) Cathode: CF (208 cm^2) j_{cat}: 0.24–2.9 mA cm^{-2} *Q*: 2 L min^{-1} T: 18–45 °C pH: 3.0 $[TDI]_0$ (EF): 2.8–56 mg L^{-1}	n.a./n.a.	[142]
Sulfamethazine antimicrobial veterinary drug	29 mg sulfamethazine L^{-1} in 7.0 g Na_2SO_4 L^{-1}	AO EF	UC	0.3	Anode: Pt, BDD, DSA, (Ti/RuO_2-IrO_2) or graphite felt (24 cm^2) Cathode: Graphite felt (87.5 cm^2) j_{cat}: 2.1–42 mA cm^{-2} *Q*: MS T: Amb. pH: 3.0 $[TDI]_0$ (EF): 11 mg L^{-1}	EF: ≈100/≈2	[194]

Table 5 (*Continued*)

Pollutant	Wastewater characteristics	Process	Electrochemical reactor		Electrodes/ Operational parameters	Maximum DOC decay (%)/ EC_{DOC} (kWh (g DOC)$^{-1}$)[a]	Refs.
			Configuration	*V* (L)			
Sulfamethoxazole antibiotic	21–329 mg sulfamethoxazole L^{-1} in 7.0 g Na_2SO_4 L^{-1}	AO-H_2O_2 EF	UC	0.22	Anode: AO: Pt mesh EF: Pt mesh or BDD (25 cm^2) Cathode: CF (60 cm^2) j_{cat}: 1.0–7.5 mA cm^{-2} *Q*: MS T: Amb. pH: 3.0 $[TDI]_0$ (EF): 11 mg L^{-1} (+/or 13 mg Cu^{2+} L^{-1})	EF: 96/n.a.	[189]
Sulfamethoxazole antibiotic	50–300 mg sulfamethoxazole L^{-1} in 7.0 g Na_2SO_4 L^{-1}	AO AO-H_2O_2 EF PEF-UVA	UC	0.125	Anode: RuO_2 mesh (16 cm^2) Cathode: AO: RuO_2 mesh (16 cm^2) Others: ACF (16 cm^2) j_{cat}: 7.5–31 mA cm^{-2} *Q*: MS T: Amb. pH: 3.0 $[TDI]_0$ (EF, PEF-UVA): 28–112 mg L^{-1}	PEF-UVA: 80/n.a.	[64]
Sulfanilamide antimicrobial drug	239–2390 mg sulfanilamide L^{-1} in 7.0 g Na_2SO_4 L^{-1} (UC) or 70 g Na_2SO_4 L^{-1} (DC)	AO	UC or DC	0.1	Anode: BDD (3 cm^2) Cathode: SS (3 cm^2) j_{cat}: 33–150 mA cm^{-2} *Q*: MS T: 35 °C pH: 2.0–6.0	≈100/n.a.	[144]
Sulfanilamide antimicrobial drug	239–1195 mg sulfanilamide L^{-1} in 7.0 g Na_2SO_4 L^{-1}	EF SPEF	FP with undivided FPC and planar photoreactor	2.5	Anode: Pt (20 cm^2) Cathode: C-PTFE A-D (20 cm^2) j_{cat}: 50–150 mA cm^{-2} *Q*: 3.3 L min^{-1} T: 35 °C pH: 3.0 $[TDI]_0$: 14–279 mg L^{-1}	SPEF: 91/0.12	[192]
Tetracycline antibiotic	25–150 mg tetracycline L^{-1} in 7.0 g Na_2SO_4 L^{-1}	EF + Biological treatment	UC	0.8	Anode: Pt (17 cm^2) Cathode: CF (78 cm^2) j_{cat}: 0.64–5.1 mA cm^{-2} *Q*: MS T: Amb. pH: 3.0 $[TDI]_0$: 2.8–11 mg L^{-1}	86/n.a.	[190]
Tetracycline antibiotic	100–300 mg tetracycline L^{-1} in 14 g Na_2SO_4 L^{-1}	AO-H_2O_2	UC	0.4	Anode: RuO_2-IrO_2 Cathode: CF (240 cm^2) j_{cat}: 2.1–6.3 mA cm^{-2} *Q*: MS T: Amb. pH: 3.0–9.0	n.a./n.a.	[117]
Trimethoprim antibiotic	50 mg trimethoprim L^{-1} in 0–70 g Na_2SO_4 L^{-1}	AO	FP with undivided FPC	n.s.	Anode: BDD (12.5 cm^2) Cathode: BDD (12.5 cm^2) j_{cat}: 0–320 mA cm^{-2} *Q*: 0.00125–0.0108 L min^{-1} T: 25 °C pH: 3.0–11	51/n.a.	[134]
Trimethoprim antibiotic	20 mg trimethoprim in 7.0 g Na_2SO_4 L^{-1} or secondary MWWTP effluent with the following characteristics: DOC (mg L^{-1}) = 12 COD (mg O_2 L^{-1}) = 55 C (μS cm^{-1}) = 890 TSS (mg L^{-1}) = 11 pH = 6.8 [TDI] (mg L^{-1}) = <0.1 [SO_4^{2-}] (mg L^{-1}) = 60 [Cl^-] (mg L^{-1}) = 110 [NH_4^+] (mg L^{-1}) = 5.5 [NO_2^-] (mg L^{-1}) = 3.4 [NO_3^-] (mg L^{-1}) = 30 [PO_4^{3-}] (mg L^{-1}) = 15	AO-H_2O_2 EF PEF-UVA SPEF Fenton PF-UVA	FP with undivided FPC and CPCs	1.25	Anode: BDD or Pt (10 cm^2) Cathode: C-PTFE A-D (10 cm^2) j_{cat}: 2.5–150 mA cm^{-2} *Q*: MS + 0.67 L min^{-1} T: 20 °C pH: 3.0–4.5 $[TDI]_0$ (EF, PEF-UVA, SPEF): 2.0–8.0 mg L^{-1}	SPEF: Synthetic: 73/n.a. Real: 57/n.a.	[133]

Table 5 (*Continued*)

Pollutant	Wastewater characteristics	Process	Electrochemical reactor		Electrodes/ Operational parameters	Maximum DOC decay (%)/ EC_{DOC} (kWh (g DOC)$^{-1}$)[a]	Refs.
			Configuration	*V* (L)			
Trimethoprim antibiotic	2.0–20 mg trimethoprim in 7.0 g Na_2SO_4 L^{-1}	PEF-UVA/oxalate PEF-UVA/citrate PEF-UVA/tartrate PEF-UVA/malate	FP with undivided FPC and CPCs	1.25	Anode: BDD (10 cm^2) Cathode: C-PTFE A-D (10 cm^2) j_{cat}: 5.0 mA cm^{-2} *Q*: MS + 0.67 L min^{-1} T: 10–40 °C pH: 4.5–5.5 $[TDI]_0$: 2.0 mg L^{-1}	PEF-UVA/oxalate PEF-UVA/citrate: ≈40/n.a.	[108]

Amb. – Ambient;
C-PTFE A-D – Carbon-PTFE air-diffusion;
C-PTFE O-D – Carbon-PTFE O_2-diffusion;
DC – Divided cell;
FP – Flow plant;
FPC – Filter-press cell;
LS – Lab-scale;
MS – Magnetic stirring;
n.a. – not assessed;
n.s. – not specified;
PS – Pilot-scale;
Q – Liquid flow rate;
UC – Undivided cell.

[a] Under the best experimental conditions, when applicable.

A vast range of drug contents from 2.0 to 2390 mg L^{-1} have been used. Approximately half of the studies evaluated the effect of initial drug content on the process efficiency, conquering greater DOC and/or pollutants removal rates with increasing initial drug contents for AO, AO-H_2O_2, EF, PEF-UVA, PEF-UVA/citrate and SPEF.

Moreira et al. [133] found slow and partial mineralization of trimethoprim antibiotic by AO-H_2O_2, EF, PEF-UVA and SPEF processes, mainly related to the formation of a high content of hardly oxidizable *N*-derivatives. Wu et al. [117] also observed the generation of hardly mineralized intermediates during the degradation of tetracycline antibiotic by AO-H_2O_2, along with the increase of acute toxicity, attributed to the formation of highly toxic quinone intermediates.

3.3.2. Process

The majority of works of Table 5 embraced EF process, however a large number of investigations on AO treatment are not included. Some studies on AO-H_2O_2, PEF-UVA and SPEF processes are also reported. In general, processes ability to remove drugs and oxidize their by-products could be arranged in the order SPEF > PEF-UVA > EF > AO-H_2O_2 ≈ AO. Fig. 11 illustrates this tendency in terms of mineralization of 164 mg salicylic acid L^{-1} in 7.0 g Na_2SO_4 L^{-1}, and the corresponding MCE values of Fig. 11b are given in Fig. 12. For total mineralization, the SPEF-BDD process at j_{cat} of 33 mA cm^{-2} showed a MCE of 45%. Moreira et al. [133] determined a MCE of 30% to reach 77% mineralization of a 20.0 mg trimethoprim L^{-1} solution in 7.0 g Na_2SO_4 L^{-1} subjected to a SPEF-BDD process at j_{cat} of 5.0 mA cm^{-2}, together with an EC_V of 0.9 kWh m^{-3} and an UV energy accumulation of 37 kJ L^{-1}. On the other hand, some studies reached similarity between EF and PEF-UVA [64,148,155,188] and between EF and SPEF [98] in terms of drug decay, indicating that drug molecules were mainly degraded by •OH in the bulk. Furthermore, Wang et al. [64] attained superiority of AO-H_2O_2 over AO in terms of sulfamethoxazole antibiotic removal.

PEF-UVA process mediated by various Fe(III)-carboxylate complexes such as Fe(III)-oxalate, Fe(III)-citrate, Fe(III)-tartrate and Fe(III)-malate was assessed by Moreira et al. [108]. Besides

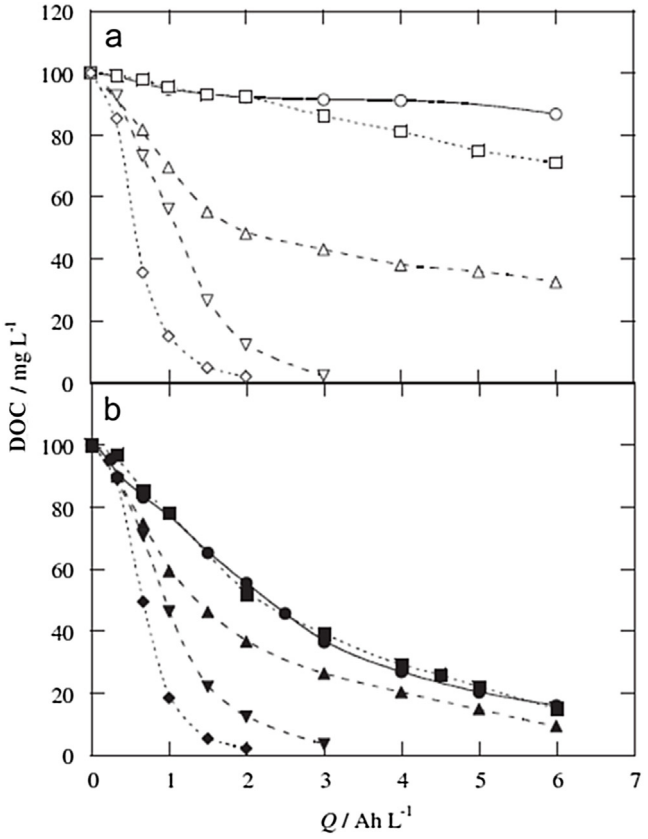

Fig. 11. DOC removal as a function of consumed specific charge for the treatment of 164 mg salicylic acid L^{-1} in 7.0 g Na_2SO_4 L^{-1} by various EAOPs using (a) Pt or (b) BDD anode, carbon-PTFE air-diffusion cathode, pH 3.0, 35 °C, $[TDI]_0$ of 28 mg L^{-1} for EF, PEF-UVA and SPEF and *j* of 33 mA cm^{-2}. EAOP: (○,●) AO, (□,■) AO-H_2O_2, (△,▲) EF, (▽,▼) PEF-UVA and (◇,◆) SPEF. Reprinted (adapted) from Guinea et al. [155], Copyright © (2008), with permission from Elsevier.

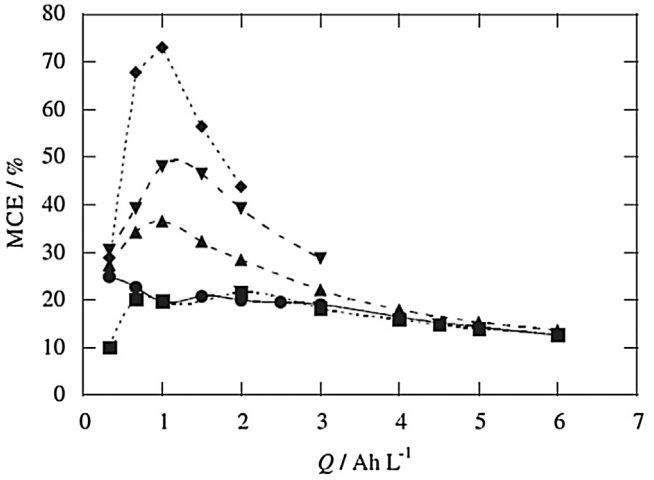

Fig. 12. Mineralization current efficiency as a function of consumed specific charge for experiments reported in Fig. 11b. Reprinted from Guinea et al. [155], Copyright © (2008), with permission from Elsevier.

the appraisal of the influence of Fe(III)-carboxylate complexes nature on process degradation ability, the effect of initial Fe(III)-to-carboxylate molar ratio and pH was also evaluated. PEF-UVA/oxalate, PEF-UVA/citrate and PEF-UVA/tartrate processes revealed quite similar ability to degrade trimethoprim antibiotic at pH 4.5 with the employment of 1:3, 1:1 and 1:1 Fe(III)-to-carboxylate molar ratios, respectively. Their efficiency was even higher than traditional PEF-UVA process at pH 3.5 (best pH). The PEF process mediated by Fe(III)-malate complexes was much less effective than the other combined systems. At pH 5.0 and 5.5, 1:6 and 1:9 Fe(III)-to-oxalate molar ratios were required to yield similar drug decay kinetics than at pH 4.5 with 1:3 Fe(III)-to-oxalate molar ratio, respectively.

Dirany et al. [189] tested the EF process catalyzed by Cu^{2+} instead of Fe^{2+} and simultaneously by Fe^{2+} and Cu^{2+} to degrade sulfamethoxazole antibiotic, noticing lower drug decay and mineralization using Cu^{2+} alone and in combination with Fe^{2+} compared to Fe^{2+} alone. The beneficial effect of Cu^{2+} has been mainly attributed to the formation of Cu(II)-carboxylate complexes that can be more quickly destroyed than Fe(III)-carboxylate complexes. Consequently, one can infer that carboxylic acids with the ability to form complexes with Cu^{2+} were not produced during the degradation of sulfamethoxazole.

Classical Fenton and PF-UVA processes were compared to their electrochemical analogous, i.e., EF and PEF-UVA, respectively, in the degradation of trimethoprim antibiotic by Moreira et al. [133]. The authors achieved superiority of Fenton and PF-UVA processes in terms of drug removal over their electrochemical analogous during the first 2 min of reaction because of the availability of high amounts of H_2O_2 from the first instant of the chemical processes, contrasting with the absence of H_2O_2 at the reaction beginning and its continuously generation during the electrochemical methods. In terms of mineralization, the chemical processes were less efficient, demonstrating that electrochemical contributions, such as BDD(•OH) formation and Fe^{2+} regeneration from cathodic reduction of Fe^{3+}, played an important role in the mineralization enhancement of intermediates.

Ferrag-Siagh et al. [190] degraded tetracycline antibiotic solutions by coupling an EF pre-treatment with a further biological process. The 5-day biochemical oxygen demand (BOD_5)/COD ratio increased from 0.02 to 0.56 after 6 h of EF and, as a result, tests using activated sludge reached mineralization enhancement from 28% for the non-pretreated solution to 68% and 86% after 2 and 4 h of EF, respectively.

3.3.3. Electrochemical reactor

The majority of studies presented in Table 5 used undivided cells with a wastewater volume of 100 mL and electrodes of 3 cm^2 of active area, although solution volumes up to 800 mL, anodes up to 25 cm^2 and CF cathodes up to 78 cm^2 were employed as well. The flow plants of Figs. 7–9 were also employed for the decontamination of synthetic pharmaceutical wastewaters [98,108,133,150,191–193]. Beyond that, other reactors have been utilized such as a divided cell [144] and simple flow plants with a filter-press cell [69,134]. El-Ghenymy et al. [144] achieved higher mineralization of sulfanilamide antimicrobial drug by AO using a divided cell instead of an undivided one, mainly because of the action of the BDD electrode over half of the volume in the divided cell compared to the undivided one. Garcia-Segura et al. [98] found faster mineralization under SPEF conditions using the 100 mL undivided cell of Fig. 5 instead of the 10 L pilot-scale flow plant of Fig. 8, along with greater persistence of Fe(III)-carboxylate complexes at the flow plant, probably mainly due to a low irradiated volume/total volume ratio.

Pt and BDD electrodes have been chiefly employed as anode in the degradation of synthetic pharmaceutical wastewaters. Many surveys compared the performance of these two anode and, for the major part of them, BDD showed superiority over Pt both in terms of oxidation ability and drug decay, independently on the EAOP checked. However, some studies found only slight or even null superiority of BDD over Pt for PEF-UVA and SPEF processes, indicating an important role of light-induced mechanisms on some pharmaceuticals removal. This is illustrated in Fig. 11 for the remediation of salicylic acid by Thiam et al. [23] and a similar behavior was also checked for trimethoprim, ibuprofen and chloramphenicol by Moreira et al. [133], Skoumal et al. [148] and Garcia-Segura et al. [98], respectively. Surprisingly, Sirés et al. [84] attained higher rates for chlorophene antimicrobial drug decay and mineralization using Pt instead of BDD anode for EF systems employing either a carbon-PTFE O_2-diffusion electrode or a CF as cathode. This was ascribed to a quicker oxidation of Fe^{2+} to Fe^{3+} at the BDD anode together with Fe^{2+} destruction with persulfate ion to get Fe^{3+} and sulfate at this anode, diminishing the amount of Fe^{2+} to produce •OH by Fenton's reaction (21). Note that the superiority of Pt over BDD using CF as cathode in terms of mineralization was only verified for the first 2 h of EF. For longer reaction times, the BDD achieved larger mineralization due to the faster destruction of final recalcitrant by-products such as carboxylic acids by BDD(•OH) compared to Pt(•OH).

Sopaj et al. [35] compared the performance of various types of anodes for the oxidation of amoxicillin antibiotic by AO, achieving an increasing efficiency of anodes in terms of apparent rate constants of amoxicillin oxidation at j_{cat} of 21 mA cm^{-2} in the order: BDD > CF > PbO_2 > Pt > carbon fiber > carbon graphite > DSA (Ti/RuO_2-IrO_2). However, the oxidation rate constants proved to be strongly dependent on j for all anode materials. Carbon graphite showed robustness against incineration in the range of low j, on opposite to CF and carbon fiber. More recently, Sopaj et al. [194] found almost similar efficiency for sulfamethazine oxidation by EF at j_{cat} of 21 mA cm^{-2} by using BDD, Pt, graphite felt and DSA (Ti/RuO_2-IrO_2) anodes. Considering the drug mineralization, the anodes performance could be arranged in the order: BDD > Pt > DSA. The graphite felt burned for j_{cat} above 4.2 mA cm^{-2}.

From Table 5, one can infer that AO process used various cathodes such as SS [144,195], graphite [155], RuO_2 [64] and BDD [69,134], whereas AO-H_2O_2, EF, PEF-UVA and SPEF processes have been mainly resorting to carbon-PTFE air-diffusion electrodes as cathode, followed by CF. Sirés et al. [84] compared the ability of carbon-PTFE air-diffusion and CF cathodes to electrogenerate H_2O_2 by Eq. (16), regenerate Fe^{3+} to Fe^{2+} via Eq. (26) and oxidize chlorophene antimicrobial drug and its by-products. The

carbon-PTFE air-diffusion cathode showed higher ability for H_2O_2 electrogeneration, but the CF demonstrated larger ability to regenerate Fe^{3+} to Fe^{2+}, leading to generation of more •OH from Fenton's reaction (21) and then faster mineralization. Isarain-Chávez et al. [113,191] employed a novel electrochemical cell composed of two pairs of electrodes. One pair comprising a Pt or a BDD anode and a carbon-PTFE air-diffusion cathode and the other equipped with a Pt anode and a CF cathode. These systems were compared to Pt/carbon-PTFE air-diffusion and BDD/carbon-PTFE air-diffusion single systems. EF and PEF-UVA degradations of beta-blockers such as atenolol, metoprolol and propranolol revealed higher efficiency for combined systems in terms of drugs removal and mineralization in comparison to the single systems because of the larger production of •OH from Fenton's reaction (21) by the quicker Fe^{2+} regeneration from Fe^{3+} reduction via Eq. (26) at the CF cathode.

3.3.4. Operational parameters

The majority of studies assessed the influence of j on the degradation of pharmaceuticals both in terms of parent compound removal and mineralization, achieving results in corroboration with Section 2.4.3. Typically and for treatments not using CF, pharmaceutical solutions with DOC around 100 mg L^{-1} were degraded with j_{cat} of 17–150 mA cm^{-2}, whereas solutions with lower DOC employed j_{cat} with a minimum value of 3.3 mA cm^{-2}. When using CF, j_{cat} values from 0.24 to 7.5 mA cm^{-2} were applied.

Domínguez et al. [69] and González et al. [134] applied RSM to determine the optimum liquid flow rate for AO treatments in a system composed of a flow plant with an undivided filter-press cell. The obtained efficiencies corresponds to a single-pass of the solution through the cell (continuous mode). Slightly larger drug removals were reached for the lowest liquid flow rate as long as this parameter was inversely proportional to the residence time of molecules inside the reactor, providing more contact between reactants and pollutant. Moreira et al. [108,133] ensured proper mass transfer of pollutants toward electrodes, catalyst and illuminated zone in the flow plant of Fig. 9 by using a high liquid flow rate supplied by a peristaltic pump in combination with magnetic stirring into the glass vessel.

Mansour et al. [142] found higher drug removal in EF from 18 to 35 °C and a lower gain from 35 to 45 °C. This slight efficiency enhancement in the latter range was attributed to lower concentration of dissolved oxygen and also to self-decomposition of H_2O_2, although the last reaction occurs in large extent only for temperatures above 50 °C [143]. In turn, Moreira et al. [108] achieved similar drug and DOC removals for 20 and 30 °C and only slightly higher degradation for 40 °C by applying a PEF-UVA/oxalate process to trimethoprim antibiotic, suggesting that the regeneration of Fe^{2+} through thermal reactions (22), (23) and (44) played a poor role in this process. Besides that, theoretical calculations within the same framework indicated that temperature affects not only the rate of Fe^{2+} regeneration by thermal reactions but also the amounts of $Fe(OH)_3$ precipitate, and, for light-induced EAOPs, photoactive species.

Once again, the influence of pH on AO and AO-H_2O_2 processes achieved distinct results. While the application of RSM determined optimum pH values of 3.0 or 4.0 [69,117,134], El-Ghenymy et al. [144] found quite similar mineralization for pH values from 2.0 to 6.0 for AO of sulfanilamide. In general, EF, PEF-UVA and SPEF attained faster degradations at pH close to 3.0 [114,148,150,192], although similar efficiencies were also reported for pH 2.0, 3.5 and 4.0 [113,133,155].

The remediation of synthetic pharmaceutical wastewaters with 100 mg DOC L^{-1} has been achieving better performance using $[TDI]_0$ contents of 11–56 mg L^{-1} for EF, PEF-UVA and SPEF treatments [64,113,114,150,155,192]. Solutions with DOC amounts below 60 mg L^{-1} mainly used $[TDI]_0$ from 5.6 to 28 mg L^{-1} for EF and PEF-UVA treatments [84,142,148,190,193]. Some reports attained similar and best degradations for a large range of $[TDI]_0$, namely for 11–56 mg L^{-1} in Guinea et al. [155], 5.6–28 mg L^{-1} in Isarain-Chávez et al. [113] and 5.6–56 mg L^{-1} in Mansour et al. [142], suggesting the enhancement of Fenton's reaction (21) in similar extent than parasitic reactions and, for PEF-UVA, inner filter effects and light attenuation along the photoreactor. Despite the achievement of faster trimethoprim removal from 2.0 to 8.0 mg $[TDI]_0$ L^{-1} in a PEF-UVA process, Moreira et al. [133] chose 2.0 mg L^{-1} as the best $[TDI]_0$ mainly because this is the limit imposed by current Portuguese legislation for discharge of treated effluents, thus avoiding the need for iron removal.

3.4. Other synthetic wastewaters

Beyond the application of EAOPs to synthetic wastewaters containing dyes, pesticides and pharmaceuticals, many other wastewaters contaminated with pollutants such as anilines, phenols and low-molecular-weight carboxylic acids (LMCA) have been degraded by EAOPs. Examples of these studies are collected in Table 6.

Aniline and its derivatives are commonly produced as by-products of petroleum, pulp and paper, coal, perfume and rubber industries. These compounds are highly toxic because they react easily in the blood to convert hemoglobin into methahemoglobin, thereby preventing oxygen uptake [196]. Brillas et al. [57] degraded 100 mg L^{-1} of aniline and 4-chloroaniline solutions by AO and AO-H_2O_2 techniques at alkaline pH in a 100 mL undivided cell using a PbO_2 anode and a graphite (for AO) or a carbon-PTFE O_2-diffusion (for AO-H_2O_2) cathode. Various supporting electrolytes were tested such as NaOH, Na_2CO_3 and Na_2CO_3 in combination with $NaHCO_3$, all leading to quite similar compounds removal. In turn, Brillas et al. [197] degraded 100 mg L^{-1} of aniline in Na_2SO_4 aqueous solution by AO-H_2O_2, EF and PEF-UVA processes at pH 3.0, resorting to a Pt anode and a carbon-PTFE O_2-diffusion cathode. The mineralization rates decreased with the increment of $[TDI]_0$ from 14 to 167 mg L^{-1} in PEF-UVA process and a gradual increase in DOC removal rate was achieved for growing initial aniline concentration, but with decreasing percentage of DOC removal. Taking into consideration the achievements of both aforementioned frameworks, processes for anilines mineralization can be arranged in the order PEF-UVA > EF > AO-H_2O_2 > AO. Furthermore, faster degradations were achieved for higher j in AO-H_2O_2 and PEF-UVA. Brillas et al. [57] proposed two parallel decomposition pathways for aniline and 4-chloroaniline that occur via degradation of either the corresponding nitrobenzene derivative or benzoquinone imine. Benzoquinone, hydroquinone, nitrobenzene, phenol and 1,2,4-benzenetriol were detected as intermediates [197].

Phenols are widely used in pharmaceutical plants, oil refineries, coke plants, pulp and food-processing industries, constituting a serious hazardous for the environment since they are highly toxic for aquatic fauna and flora and also for human beings [198]. Pimentel et al. [199] assessed the degradation of 31 or 99 mg L^{-1} of phenol solutions by EF process at pH 3.0 in an undivided cell equipped with a Pt grid as anode and a CF as cathode. Distinct catalysts like Fe^{2+}, Co^{2+}, Mn^{2+} and Cu^{2+} were tested. While 5.6 mg Fe^{2+} L^{-1} led to the best degradation in terms of pollutant removal and mineralization, 5.9 mg Co^{2+} L^{-1} led to equal compound abatement but with lower mineralization. Mn^{2+} and Cu^{2+} induced to highly poorer degradation, which was mainly ascribed to changes in catalyst content due to the formation of metal deposits. Larger cathode surface area and smaller solution volumes managed higher oxidation ability. The main reaction intermediates were hydroquinone, *p*-benzoquinone and catechol.

Cresols are very popular phenols that have a methyl group linked to the ring of phenol. Flox et al. [200] appraised the degra-

dation of the three *o*-, *m*- and *p*- cresol isomers by AO process at pH 4.0 in a 1 L flow plant with an undivided filter-press cell composed of a BDD or a PbO_2 anode and a zirconium (Zr) cathode. While cresols mineralization was faster using BDD instead of PbO_2, their concentration decay was similar using both anodes. Aromatic intermediates such as 2-methylhydroquinone and 2-methyl-*p*-benzoquinone were identified.

LMCA have been detected as final and recalcitrant by-products of various aromatics, being hardly destroyed by •OH and largely prolonging the mineralization time with consequent efficiency loss and/or greater operation cost of the treatment. Although their

Table 6
Examples on the treatment of synthetic wastewaters polluted with other contaminants by EAOPs.

Pollutant	Wastewater characteristics	Process	Electrochemical reactor		Electrodes/ Operational parameters	Maximum DOC decay (%)/ EC_{DOC} (kWh (g DOC)$^{-1}$)[a]	Refs.
			Configuration	*V* (L)			
Aniline	100–550 mg aniline L^{-1} in 7.0 g Na_2SO_4 L^{-1}	AO-H_2O_2 EF PEF-UVA	UC	0.1	Anode: Pt (10 cm^2) Cathode: C-PTFE O-D or graphite (3.1 cm^2) j_{cat}: 32–97 mA cm^{-2} *Q*: MS T: 25 °C pH: 3.0 $[TDI]_0$ (EF): 56 mg L^{-1} $[TDI]_0$ (PEF-UVA): 14–167 mg L^{-1}	PEF-UVA: 92/n.a.	[197]
Aniline, 4-chloroaniline	100 mg aniline L^{-1} or 100 mg 4-chloroaniline L^{-1} in 2.0 g NaOH L^{-1} or 11 g Na_2CO_3 L^{-1} or 11 g Na_2CO_3 L^{-1} + 8.4 g $NaHCO_3$ L^{-1}	AO AO-H_2O_2	UC	0.1	Anode: PbO_2 (10 cm^2) Cathode: AO: Graphite (3.1 cm^2) AO-H_2O_2: C-PTFE O-D or grafite (3.1 cm^2) j_{cat}: 32–194 mA cm^{-2} *Q*: MS T: 25 °C pH: 10–13	AO-H_2O_2: 100/n.a.	[57]
Phenol	31 or 99 mg phenol L^{-1} in 7.0 g Na_2SO_4 L^{-1}	EF	UC	0.15–0.4	Anode: Pt grid Cathode: CF (48 or 102 cm^2) j_{cat} (CF-48 cm^2): 2.1 mA cm^{-2} j_{cat} (CF-102 cm^2): 0.98 mA cm^{-2} *Q*: MS T: Amb. pH: 3.0 $[TDI]_0$: 2.8–56 mg L^{-1} or 2.9–59 Co^{2+} or 5.5–55 mg Mn^{2+} L^{-1} or 64–635 mg Cu^{2+} L^{-1}	100/n.a.	[199]
o-, *m*-, *p*-Cresols	541 mg *o*-, *m*- or *p*-cresol L^{-1} in 7.0 g Na_2SO_4 L^{-1}	AO	FP with undivided FPC	1	Anode: BDD or PbO_2 (63 cm^2) Cathode: Zr (63 cm^2) j_{cat}: 40 mA cm^{-2} *Q*: 2.1 L min^{-1} T: 25 °C pH: 4.0	100/n.a.	[200]
Formic, glyoxylic, oxalic, acetic, glycolic, pyruvic, malonic, maleic, fumaric, succinic, malic acids	4.6–23 mg formic L^{-1}, 7.4–37 mg glyoxylic L^{-1}, 9.0–45 mg oxalic L^{-1}, 6.0–30 mg acetic L^{-1}, 7.6–38 mg glycolic L^{-1}, 8.8–44 mg pyruvic L^{-1}, 10–52 mg malonic L^{-1}, 12–58 mg maleic L^{-1}, 12-58 mg fumaric L^{-1}, 12–59 mg succinic L^{-1} or 13–67 mg malic L^{-1} in 5.6 g KCl L^{-1}	EF	UC	0.2	Anode: Pt mesh (4.5 cm^2) Cathode: CF (56 or 112 cm^2) j_{cat} (CF-56 cm^2): 1.1–5.4 mA cm^{-2} j_{cat} (CF-112 cm^2): 1.8–2.7 mA cm^{-2} *Q*: MS T: Amb. pH: 3.0 $[TDI]_0$: 5.6 mg L^{-1}	100/n.a.	[177]
Formic, oxalic, acetic, pyruvic or maleic acids	192 mg formic L^{-1}, 188 mg oxalic L^{-1}, 125 mg acetic L^{-1}, 122 mg pyruvic L^{-1} or 121 mg maleic L^{-1} in 14 g Na_2SO_4 L^{-1}	UVA-Vis H_2O_2 H_2O_2-UVA-Vis Fenton (Fe^{3+}) SPF (Fe^{3+}) AO AO-UVA-Vis AO-Fe^{3+} AO-Fe^{3+}-UVA-Vis	FP with FPC and planar photoreactor	2.5	Anode: BDD (20 cm^2) Cathode: SS (20 cm^2) j_{cat}: 50 mA cm^{-2} *Q*: 3.3 L min^{-1} T: 35 °C pH: 3.0 $[TDI]_0$ (Fenton, SPF, AO-Fe^{3+}, AO-Fe^{3+}-UVA-Vis): 56 mg L^{-1}	100/n.a.	[201]

Table 6 (*Continued*)

Pollutant	Wastewater characteristics	Process	Electrochemical reactor		Electrodes/ Operational parameters	Maximum DOC decay (%)/ EC_{DOC} (kWh (g DOC)$^{-1}$)[a]	Refs.
			Configuration	*V* (L)			
Oxalic, oxamic acids	188 mg oxalic L^{-1} or 185 mg oxamic L^{-1} in 7.0 g Na_2SO_4 L^{-1}	UVA Fe^{2+}-UVA Fe^{3+}-UVA AO AO-Fe^{2+} AO-Fe^{2+}-UVA EF	UC	0.1	Anode: BDD (3 cm^2) Cathode: AO, AO-Fe^{2+}, AO-Fe^{2+}-UVA: SS (3 cm^2) EF: C-PTFE A-D (3 cm^2) j_{cat}: 33 mA cm^{-2} *Q*: MS T: 35 °C pH: 3.0 $[TDI]_0$ (Fe^{2+}-UVA, Fe^{3+}-UVA, AO-Fe^{2+}, AO-Fe^{2+}-UVA, EF): 28 mg L^{-1}	100/n.a.	[202]

Amb. – Ambient;
C-PTFE A-D – Carbon-PTFE air-diffusion;
C-PTFE O-D – Carbon-PTFE O_2-diffusion;
FP – Flow plant;
FPC – Filter-press cell;
MS – Magnetic stirring;
Q – Liquid flow rate;
UC – Undivided cell.
[a] Under the best experimental conditions, when applicable.

intrinsic toxicity is low, they have a potential environmental impact due to their tendency to form complexes with heavy metals like Fe^{3+}. Oxalic, oxamic, formic, acetic, pyruvic, maleic, malic, fumaric, glyoxylic, glycolic, malonic and succinic acids are some of the main LMCA identified during the degradation of aromatics by EAOPs and their removal was extensively studied by Oturan et al. [177], Guinea et al. [201] and Garcia-Segura and Brillas [202]. According to Oturan et al. [177], the ability of some acids to be degraded by EF process using a Pt mesh anode and a CF cathode decreased in the following order: fumaric ≈ maleic > glyoxylic > malic > glycolic > pyruvic > succinic > formic > malonic ≈ acetic. These results represent the ability of free acids and/or their Fe(III)-carboxylate complexes to be mainly degraded by •OH in the bulk and Pt(•OH). In Guinea et al. [201], the individual effect of •OH in the bulk, BDD(•OH), H_2O_2 and UVA-vis radiation on the removal of either free carboxylic acids or their Fe(III)-carboxylate complexes was assessed by applying distinct processes such as UVA-vis, Fenton, solar photo-Fenton (SPF), H_2O_2, H_2O_2-UVA-Vis and electrochemical AO, AO-UVA-Vis, AO-Fe^{3+} and AO-Fe^{3+}-UVA-vis processes using a BDD anode and a SS cathode. Formic and maleic free acids as well as their Fe(III)-carboxylate complexes proved to be mainly degraded by •OH in the bulk and BDD(•OH). Acetic acid, either free or complexed with Fe^{3+}, was predominantly degraded by BDD(•OH), even though at a slow rate, showing a very high recalcitrant character. In turn, oxalic free acid was only degraded by BDD(•OH) and at very slow rate, whereas Fe(III)-oxalate complexes were highly photodecarboxylated and only slightly degraded by BDD(•OH). Pyruvic free acid was rapidly degraded by •OH in the bulk, BDD(•OH) and H_2O_2, but with null abatement upon UVA-Vis radiation, whereas Fe(III)-pyruvate complexes were rapidly removed by all these agents. Moreover, cyclic voltammetry analyses carried out by Garcia-Segura and Brillas [202] indicated that the ultimate oxalic acid is not degraded by BDD(•OH) but rather by direct anodic oxidation at the BDD surface. These results were extended to the ultimate oxamic acid. On the other hand, cyclic voltammograms of Fe(III)-oxalate and Fe(III)-oxamate complexes suggested that these compounds react with BDD(•OH) at the anode surface. Further application of UVA, Fe^{2+}-UVA, Fe^{3+}-UVA and electrochemical AO, AO-Fe^{2+}, AO-Fe^{2+}-UVA and EF processes employing BDD as anode and SS (for AO and AO based processes) or carbon-PTFE air-diffusion electrode (for EF) as cathode allowed concluding about the participation of •OH in the bulk, BDD(•OH) and UVA radiation on the direct mineralization of oxalic and oxamic acids either free or complexed with Fe^{3+}. While both free acids showed null ability to be destroyed by UVA light, Fe(III)-oxamate complexes were slowly photolyzed and Fe(III)-oxalate complexes proved to be much more rapidly photodecarboxylated. Free acids and their Fe(III) complexes were poorly oxidized by •OH in the bulk. Furthermore, Fe(III)-oxamate complexes were oxidized more quickly with BDD(•OH) than Fe(III)-oxalate ones. These findings are of interest because can help to understand the performance of EAOPs. Contrary to what has been achieved for aromatic dyes, pesticides and pharmaceuticals, Oturan et al. [177] reached lower carboxylic acids removal rates when using rising organics content during the first treatment stages. The authors explained these results by the higher resistance to oxidation of carboxylic acids compared to aromatics, which can enhance parasitic reactions such as Eqs. (24) and (25) in detriment of the mineralization reaction.

4. Degradation of real wastewaters by EAOPs

A review on many studies regarding the remediation of real textile effluents, pharmaceutical effluents, wastewaters from secondary treatment of WWTPs, landfill leachates, among others, by EAOPs is presented.

4.1. Textile wastewaters

Textile wastewaters result from several different activities involved in the dyeing process, such as pre-treatment, dyeing, printing and finishing of the textile material. They are composed by various dyes with a complex organic structure, surfactants, detergents and inorganic salts, which constitutes a risk for the environment and ecosystems when they are improperly released into the environment [203].

Table 7
Examples on the treatment of real textile wastewaters by EAOPs.

Pollutant	Wastewater characteristics			Process	Electrochemical reactor		Electrochemical reactor / Operational parameters	Maximum DOC decay (%) / EC_{DOC} (kWh (g DOC)$^{-1}$) [a]	Ref.
					Configuration	V (L)			
Real or synthetic textile wastewater		Real	Synthetic	AO	UC	0.12	Anode: BDD (15 cm^2) Cathode: Zr j_{cat} (synthetic): 4–50 mA cm^{-2} j_{cat} (real): 8 mA cm^{-2} *Q*: MS T (synthetic): 22–43 °C T (real): 22 °C pH (synthetic): 1.0–12 pH (real): 1	70 / n.a.	[140]
	DOC (mg L^{-1})	120	82						
	COD (mg O_2 L^{-1})	470	300						
	C (μS cm^{-1})	7200	8400						
	TSS (mg L^{-1})	68	0						
	pH	8.8	11						
	[Total iron] (mg L^{-1})	0.1	0						
	in 10–50 g $HClO_4$ L^{-1} (synthetic) or 25 g $HClO_4$ L^{-1} (real)								
	Filtered before trials								
Textile wastewater		Raw	1:2 diluted	AO	FP with undivided FPC	n.s.	Anode: DSA (50 cm^2) Cathode: SS (88 cm^2) j_{cat}: 10–100 mA cm^{-2} *Q*: 0.0005–0.015 L min^{-1} T: Amb. pH: 2.8–12	n.a. / n.a.	[204]
	COD (mg O_2 L^{-1})	5957	2978						
	C (μS cm^{-1})	n.m.	135000						
	pH	7.3	8.1						
Textile wastewater	DOC (mg L^{-1}) = 395 COD (mg O_2 L^{-1}) = 1224 BOD_5 (mg O_2 L^{-1}) = 324 C (μS cm^{-1}) = 2914 pH = 4.8 [SO_4^{2-}] (mg L^{-1}) = 38 [Cl^-] (mg L^{-1}) = 234 Filtered before trials			EF	UC	0.5	Anode: Pt wire Cathode: PAN based-ACF (63 cm^2) j_{cat}: 0.8–4.8 mA cm^{-2} *Q*: MS T: 20–40 °C pH: 2.0–5.0 $[TDI]_0$: 18–147 mg L^{-1}	n.a. / n.a.	[149]

Amb. – Ambient;
FP – Flow plant;
FPC – Filter-press cell;
MS – Magnetic stirring;
n.a. – not assessed;
n.m. – not measured;
n.s. – not specified;
Q – Liquid flow rate;
UC – Undivided cell.
[a] Under the best experimental conditions, when applicable.

Three examples of textile wastewaters treatments by EAOPs are given in Table 7. While Wang et al. [149] treated the effluent as collected, both Tsantaki et al. [140] and Vaghela et al. [204] filtered the wastewater prior to treatment in order to remove any suspended particle. Furthermore, Tsantaki et al. [140] added perchloric acid ($HClO_4$) as supporting electrolyte, an undesirable practice in view of the high toxicity of ClO_4^- to increase effluent conductivity and decrease the electrical consumption, although the conductivity of this effluent was already high (7200 $\mu S\,cm^{-1}$). In fact, the three effluents exhibited high conductivity, above 2900 $\mu S\,cm^{-1}$. Vaghela et al. [204] performed trials not only using the original effluent after filtration but also subjecting it to dilutions of 25% and 50%. The organic load of the three raw effluents embraced distinct COD values from 470 to 5957 mg O_2 L^{-1}. Only Wang et al. [149] determined the BOD_5 content, attaining a BOD_5/COD ratio of 0.26 that reveals a low biodegradability. Divergent pH values of 8.8, 7.3 and 4.8 were utilized by Tsantaki et al. [140], Vaghela et al. [204] and Wang et al. [149], respectively. The amount of some ions was only assessed by Wang et al. [149], pointing out a moderate chloride content of 234 mg L^{-1} and a low sulfate content of 38 mg L^{-1}.

Tsantaki et al. [140] and Vaghela et al. [204] applied AO treatments, the first using a BDD anode and a Zr cathode and the second employing a dimensionally stable anode (DSA) and a SS cathode. In turn, Wang et al. [149] assessed the effluent treatment by EF technique using a Pt anode and a polyacrylonitrile (PAN) based ACF. Undivided cells or simple flow plants with a filter-press cell were employed with volumes up to 0.5 L. Trials were performed under galvanostatic conditions, with low j_{cat} values of 8.0 and 3.2 mA cm^{-2} indicated as the best ones by Tsantaki et al. [140] and Wang et al. [149], respectively. For AO process, the effect of temperature proved to be negligible [140], whereas higher COD decay was achieved for increasing temperature in EF [149]. Distinct best pH values for AO were pointed out. Tsantaki et al. [140] indicated pH 1 as the best one, attributing this to a change in electrode surface properties under alkaline conditions, whereas Vaghela et al. [204] achieved highest and similar color removal at pH 2.8 and 8.1 and highest COD removal at pH 8.1. The best attained pH for EF was 3.0, along with a best $[TDI]_0$ of 112 mg L^{-1}.

70% of DOC removal and 53% of COD removal were achieved for AO treatments of raw filtered effluent with 25 g $HClO_4$ L^{-1} or raw effluent by Tsantaki et al. [140] and Vaghela et al. [204], respectively, after 180 or 20 min of electrolysis using pH 1 or 7.3, ambient temperature and j_{cat} of 8 or 100 mA cm^{-2}, respectively. The EF process reached 74% of COD removal after 240 min of reaction using pH 3.0, 20 °C, $[TDI]_0$ of 112 mg L^{-1} and j_{cat} of 3.2 mA cm^{-2} [149].

Moreover, Tsantaki et al. [140] also employed a simulated textile effluent, reaching a quite similar DOC removal for simulated and real effluents and faster COD decay and lower energy consumption for the real one. All these results confirm the best viability of EF than AO for textile wastewater treatment.

4.2. Pharmaceutical wastewaters and urban wastewaters after secondary treatment

The application of an AO process to the treatment of a wastewater from a pharmaceutical industry plant using a BDD anode and a SS cathode under galvanostatic conditions was carried out by Domínguez et al. [205] (see Table 8). The real effluent exhibited a high organic content, with DOC of 1600 mg L^{-1} and COD of 12,000 mg L^{-1}, composed of high amounts of pharmaceuticals (aromatic and aliphatic compounds) and also solvents such as methanol and ethanol. Its pH was alkaline and it exhibited a high conductivity of 7000 $\mu S\,cm^{-1}$. A RSM was performed to optimize j and liquid flow rate, using ambient temperature and original pH. Higher mineralization was achieved for greater j from 26 to 179 mA cm^{-2}. The reactor operated in continuous mode and, as a consequence, the increment of liquid flow rate led to shorter residence times in the filter-press cell, diminishing the mineralization.

Conventional WWTPs are not able to entirely remove micropollutants at ng L^{-1} and $\mu g\,L^{-1}$ levels, such as pharmaceuticals, personal care products, pesticides, detergents and various industrial additives [206]. As a result, these undesirable compounds end up in the environment and may cause a multitude of risks to all living organisms. Table 8 collects some studies on the treatment of effluents collected after the secondary treatment in WWTPs, mostly MWWTPs, by EAOPs. The treatment was directly applied to the secondary effluent [147] or a membrane separation process like MF, ultrafiltration (UF) and/or reverse osmosis (RO) was firstly employed to concentrate pollutants and treat only the concentrate by EAOPs [22,61,207–209]. After membrane filtration processes, micropollutants concentrations from 0.005 to 24 $\mu g\,L^{-1}$ were reported [22,208]. In some cases, the effluent was spiked with micropollutants contents of 7.8–100 $\mu g\,L^{-1}$ to allow their determination in the analytical equipment throughout EAOPs [147,209]. The total organic content of effluents was very low, mainly from 10–24 mg DOC L^{-1} for both unchanged and concentrated effluents, but Radjenovic et al. [209] presented a higher DOC of 57 mg L^{-1}. The pH was near neutral for all wastewaters to comply with regulatory limits for the discharge of wastewaters from WWTPs into the environment. Chloride ions were available in moderate/high concentrations of 302–1500 mg L^{-1} and the amounts of sulfate and ammonium were low (25–584 and 18–208 mg L^{-1}, respectively), which led a low/moderate conductivity of 1700–4800 $\mu S\,cm^{-1}$.

All studies referred to the treatment of secondary effluents by AO process at ambient temperature using 2–10 L flow plants equipped with an undivided or a divided filter-press cell. The most widely employed anode was BDD, with only Radjenovic et al. [209] using another anode, i.e., $Ru_{0.7}Ir_{0.3}O_2$. Both BDD and SS were used as cathodes.

Most of the degradations were performed in galvanostatic mode. Exceptionally, Dialynas et al. [207] mentioned the employment of two j, 51 and 254 mA cm^{-2}, by using the effluent after RO without changes and by adding sulfuric acid to increase its conductivity, respectively. Besides the use of a single j value along the experiment in batch mode, Radjenovic et al. [209] also applied AO with increasing j values from 0.1 to 25 mA cm^{-2} in continuous mode, achieving higher micropollutants removal efficiency when operating in batch mode. DOC and COD removals were faster with increasing j in Garcia-Segura et al. [147] and Pérez et al. [208], but micropollutants removal was not significantly influenced by j in Pérez et al. [208]. In this case, the rate-limiting step of the reaction was the diffusion of pollutants from the bulk solution to the anode surface The majority of micropollutants was completely removed after 1–2 h of AO using 2–20 mA cm^{-2}. Nevertheless, some recalcitrant micropollutants required longer times of 24 h to be totally degraded and few could not be removed even after long times of electrolysis [22,147,208,209]. Since AO is unable to remove some micropollutants, more basic research is necessary to know the applicability of this EAOP. In addition, Pérez et al. [208] detected faster ammonium conversion to nitrate at larger j together with the production of increasing amounts of ClO_3^-, free chlorine and trihalomethanes. Garcia-Segura et al. [147] detected the formation of active chlorine species, ClO_3^- and ClO_4^- ions and organochloride and organobromide derivatives. The formation of noxius ClO_3^- and ClO_4^- ions is detrimental for the application of this technology and their formation can be avoided operating a low j values.

Contrasting to all the other studies, which performed AO with the original neutral pH of the effluent, Garcia-Segura et al. [147] tested both pH 7.0 and 3.0. Faster DOC and COD removals were attained at acidic pH, which was ascribed to the electrogeneration of higher amounts of active chlorine species with higher standard redox potential, predominantly HClO, in parallel with the formation

Table 8
Examples on the treatment of real pharmaceutical and secondary WWTPs effluents by AO.

Pollutant	Wastewater characteristics				Electrochemical reactor		Electrochemical reactor/ Operational parameters	Maximum DOC decay (%)/ EC_{DOC} (kWh (g DOC)$^{-1}$)[a]	Refs.
					Configuration	V (L)			
Pharmaceutical wastewater	DOC (mg L^{-1}) = 1600 COD (mg O_2 L^{-1}) = 12000 C (μS cm^{-1}) = 7000 TSS (mg L^{-1}) = 5000 pH = 8.5				FP with undivided FPC	0.6	Anode: BDD (78 cm^2) Cathode: SS (78 cm^2) j_{cat}: 26–179 mA cm^{-2} Q: 0.10-0.56 L min^{-1} T: 20 °C pH: 8.5	≈100/n.a.	[205]
Mixture of secondary MWWTP and textile wastewaters after RO	COD (mg O_2 L^{-1}) = 158 C (μS cm^{-1}) = 3990 pH = 8.2 [Cl^-] (mg L^{-1}) = 592				FP with undivided FPC	1	Anode: BDD (60 cm^2) Cathode: Ti (60 cm^2) j_{cat}: 17 mA cm^{-2} Q: 0.25 L min^{-1} T: 22 °C pH: 8.2	n.a./n.a.	[210]
		No. 1	No. 2	No. 3			Anode: PbO_2, SnO_2, RuO_2 or BDD (50 cm^2)		
Mixture of secondary MWWTP and textile wastewaters after RO	COD (mg O_2 L^{-1}) C (μS cm^{-1}) pH [Cl^-] (mg L^{-1})	151 5060 8.7 777	218 5290 7.9 804	171 3990 8.1 595	FP with undivided FPC	1	Cathode: Ti (50 cm^2) j_{cat}: 10–30 mA cm^{-2} Q: 0.25 L min^{-1} T: 22 °C pH: 8.7/7.9/8.0	n.a./n.a.	[211]
		No. 1	No. 2				Anode: $Ru_{0.7}Ir_{0.3}O_2$ (24 cm^2)		
Mixture of secondary WWTP wastewaters after MF + RO spiked with 28 micropollutants at 7.8–37 μg L^{-1} each	DOC (mg L^{-1}) C (μS cm^{-1}) pH [Fe^{2+}] (mg L^{-1}) [SO_4^{2-}] (mg L^{-1}) [Cl^-] (mg L^{-1})	57 4250 7.5 0.22 242 1500	57 3970 7.7 0.35 239 1200		FP with divided FPC	10	Cathode: SS mesh (24 cm^2) j_{cat} (continuous mode): 0.1–25 mA cm^{-2} j_{cat} (batch mode): 25 mA cm^{-2} Q: 0.16 L min^{-1} T: Amb. pH: 7.5/7.7 $[Fe^{2+}]_0$: 0.22/0.35 mg L^{-1}	31/0.350	[209]
Primary MWWTP wastewater after MBR + RO	DOC (mg L^{-1}) = 10				FP with undivided FPC	8	BDD-70 cm^2 Anode: BDD (70 cm^2) Cathode: BDD (70 cm^2) Operated in potentiostatic mode Q: 20 L min^{-1} T: Amb. pH: 8.5	36/n.a.	[207]
Secondary MWWTP wastewater spiked with 29 micropollutants at ≈ 100 μg L^{-1} each	DOC (mg L^{-1}) = 23 COD (mg O_2 L^{-1}) = 21 pH = 7.0 [SO_4^{2-}] (mg L^{-1}) = 25 [Cl^-] (mg L^{-1}) = 309				FP with divided FPC	10	Anode: BDD (41 cm^2) Cathode: SS (41 cm^2) j_{cat}: 9.8 or 20 mA cm^{-2} Q: 0.16 L min^{-1} pH: 3.0 or 7.0	100/n.a.	[147]
Secondary MWWTP wastewater after UF + RO	DOC (mg L^{-1}) = 17 C (μS cm^{-1}) = 2665 TSS (mg L^{-1}) = 5.7 pH = 7.5 [SO_4^{2-}] (mg L^{-1}) = 537 [Cl^-] (mg L^{-1}) = 655 [NH_4^+] (mg L^{-1}) = 120 [NO_3^-] (mg L^{-1}) = 114 [PO_4^{3-}] (mg L^{-1}) = n.d.				FP with undivided FPC	2	Anode: BDD (70 cm^2) Cathode: BDD (70 cm^2) j_{cat}: 10 mA cm^{-2} Q: 10 L min^{-1} T: 20 °C pH: 7.5	n.a./n.a.	[22]
		No. 1	No. 2				Anode: BDD (70 cm^2)		
Secondary WWTP wastewater after UF + RO	DOC (mg L^{-1}) COD (mg O_2 L^{-1}) C (μS cm^{-1}) TSS (mg L^{-1}) pH [SO_4^{2-}] (mg L^{-1}) [Cl^-] (mg L^{-1}) [NH_4^+] (mg L^{-1}) [NO_2^-] (mg L^{-1}) [NO_3^-] (mg L^{-1})	20 n.m. 1700 0 7.6 302 328 18 n.d. n.d.	27 133 4800 0 7.9 584 630 208 n.d. 12		FP with undivided FPC	2	Cathode: BDD (70 cm^2) j_{cat}: 2–20 mA cm^{-2} Q: 10 L min^{-1} T: 20 °C pH: 7.6/7.9	n.a./n.a.	[208]

Amb. – Ambient;
FP – Flow plant;
FPC – Filter-press cell;
MBR – Membrane bioreactor;
n.a. – not assessed;
n.d. – not detected;
n.m. – not measured;
Q – Liquid flow rate.
[a] Under the best experimental conditions, when applicable.

of lower amounts of BDD(•OH) and higher contents of less oxidizing species such as $O_2^{\bullet-}$ at the BDD anode at neutral and alkaline medium.

Van Hege et al. [210,211] degraded RO concentrates from mixtures of secondary MWWTP effluents and textile wastewaters by AO using a 1 L flow plant with an undivided filter-press cell, 22 °C and alkaline pH. These mixtures were characterized by COD values of 151–218 mg O_2 L^{-1}, high conductivities of 3990–5290 μS cm^{-1}, alkaline pH and moderate chloride content of 592–804 mg L^{-1}. Ti was employed as cathode in both studies and Van Hege et al. [211]

found that the ability of different anodes for COD removal could be arranged in the order BDD > $SnO_2 \approx PbO_2$ > RuO_2. For PbO_2 and SnO_2, salts precipitation and electrode scaling were experienced due to pH increase, whereas *j* values in a range of 10–30 mA cm^{-2} proved to have a low influence on COD removal both using BDD and RuO_2 anodes. In addition, it was observed increasing accumulation of ClO_3^- using both anodes, with a greater accumulation for BDD. Active chlorine species were also accumulated, but only at the end of electrolysis and, once again, in larger extent for BDD.

4.3. Landfill leachates

The deposition of municipal and industrial solid wastes into landfills leads to the production of a highly contaminated liquid called leachate by means of percolation of rainfall in combination with the decomposition of the solid wastes [212]. Landfill leachates can reach the adjacent surface and groundwater, causing potentially serious hazards on the surrounding environment and public health [213]. Characteristics of landfill leachates vary with the amount, composition and moisture of solid wastes, age of the landfill, hydrogeology and climate of the site, seasonal weather variations, among other factors [214]. Table 9 displays twelve surveys regarding the treatment of municipal landfill leachates and one investigation on the remediation of an industrial landfill leachate by EAOPs.

4.3.1. Landfill leachate characteristics and pre-treatments

Raw municipal landfill leachates are characterized by: (i) high amounts of organic matter, with DOC of 1341–3100 mg L^{-1} and COD of 3385–5000 mg O_2 L^{-1}, including recalcitrant compounds like humic and fulvic acids and xenobiotic organic compounds such as aromatic hydrocarbons, phenols, chlorinated aliphatics, pesticides, plastizers, among others; (ii) low amounts of biodegradable compounds (BOD_5/COD ratios of 0.07–0.27); (iii) high contents of inorganic ions like chloride (2124–6200 mg L^{-1}) and ammonium (1125–3200 mg L^{-1}), leading to very high conductivities of 12770–25000 μS cm^{-1}; (iv) alkaline pH; and (v) the presence of heavy metals like cadmium, chromium, copper, lead, nickel and zinc [24,48,49,215–217]. The raw industrial landfill leachate displayed much larger COD and chloride contents of 17100–18400 mg O_2 L^{-1} and 52300–54280 mg L^{-1}, respectively [218]. Some authors directly applied EAOPs to the remediation of raw landfill leachates [209,215,217–219], while others subjected the raw municipal landfill leachate to the following treatments before EAOPs application: (i) biological treatment [137,220,221], (ii) biological treatment followed by physico-chemical treatment [215], (iii) biological treatment followed by coagulation and aeration [24,152], (iv) biological treatment followed by Fenton process [216] or (v) filtration [222]. Biological pre-treatments led to the removal of biodegradable organic matter, which culminated in only slightly lower DOC and COD values since it only represents a low fraction of organic compounds. For Urtiaga et al. [216] and Moreira et al. [24], a conversion of ammonium into nitrite and/or nitrate along with alkalinity consumption was observed. The biological/physico-chemical pre-treatment carried out by Cabeza et al. [215] was not specified but it led to high DOC, COD and BOD_5 abatements of 66%, 74% and 81%, respectively, simultaneously with the removal of 56% of ammonium and 52% of chloride. The coagulation of the bio-treated landfill leachate performed by Moreira et al. [24] aimed to remove humic acids, suspended solids and colloidal particles that are able to act as photons absorbers in EAOPs and also to provoke the electrochemical cell clogging. After coagulation and subsequent clarification, it was attained 63–65% DOC removal, 44–51% COD removal, 57–67% total suspended solids (TSS) abatement, 40–54% volatile suspended solids (VSS) removal, partial oxidation of nitrite to nitrate and color changing from very dark brown to moderate yellowish brown associated with the presence of fulvic acids and absence of humic acids. An additional aeration step was implemented in this study to completely convert nitrite into nitrate since the presence of nitrite demonstrated to lead to pH decay and extra consumption of H_2O_2 in the subsequent EAOP stage. The application of a Fenton process to the bio-treated landfill leachate by Urtiaga et al. [216] intended to degrade non-biodegradable organic matter, achieving 85% COD removal. Panizza and Martinez-Huitle [222] proceeded with the filtration of raw leachate in order to remove suspended solids that can influence the electrochemical process.

4.3.2. Process

Most of the studies presented in Table 9 refer to the application of AO process. This EAOP was performed with two purposes: (i) ammonium oxidation through mediated oxidation by active chlorine species, and (ii) organics oxidation via reaction at the anode surface with electrogenerated M(•OH) and mediated oxidation. Cabeza et al. [215] and Chiang et al. [48] demonstrated that faster ammonium oxidation and COD removal were achieved by adding larger chloride contents from around 1400 to 10,000 mg L^{-1} to the effluent, which was associated with the production of higher amounts of Cl_2/ClO^-. To take advantage of high chloride content benefits, Anglada et al. [49] increased the concentration of chloride up to 4500 mg L^{-1} by adding NaCl before starting AO.

Fernandes et al. [137] diluted the bio-treated landfill leachate to be subjected to AO and added Na_2SO_4 to compensate the greater ohmic drop attained by diluting samples. Slower organics removal in terms of absolute value and higher energy consumption were attained for higher dilutions. Moreover, the authors also established that electrolysis was controlled by *j* for small dilutions and by mass transport for high dilutions. Note that Chiang et al. [48] detected that the addition of Na_2SO_4 caused a negative effect on both ammonium oxidation and COD removal due to the suppression of Cl_2/ClO^- formation.

On the other hand, Oturan et al. [219] applied AO-H_2O_2 and EF processes to the treatment of a mixture of 8 municipal landfill leachates, aiming the degradation of recalcitrant organic compounds, including the removal yield of organic micropollutants such as 36 polycyclic aromatic hydrocarbons, 15 volatile organic compounds, 7 alkylphenols, 7 polychlorobiphenyls, 5 organochlorine pesticides and 2 polybrominated diphenyl ethers. 91% and 93% of DOC removal were achieved after 18 h of AO-H_2O_2 and EF treatments, respectively. Both EAOPs led to a quasi-complete removal (about 98%) of the organic micropollutants under examination.

Moreira et al. [24,152] employed other EAOPs like AO, EF, PEF and SPEF, only targeting the degradation of organics since ammonium was previously removed by biological treatment/aeration. Based on both studies, the oxidation ability of EAOPs followed the order SPEF ≈ PEF-UVA ≈ PEF-UVC > PEF-UVA-Vis > EF with 60 mg $[TDI]_0$ L^{-1} ≈ AO > EF with 12 mg $[TDI]_0$ L^{-1}, showing DOC removals of 78%, 72%, 71%, 49%, 42%, 45% and 34%, respectively, after 300 min and an EC_V of around 85 kWh m^{-3}. Regarding light-induced EAOPs, these achievements indicated that: (i) the photonic flux in the PEF-UVA process was able to induce almost maximum photoreduction via Eqs. (28) and (29); (ii) the •OH production in PEF-UVC from the H_2O_2 photolysis through Eq. (30) allowed to attain similar results than under UVA and solar radiation; and (iii) the $FeOH^{2+}$ photoreduction by Eq. (28) was slower under UVA-Vis radiation compared to UVA and solar radiation due to its poor light emission below 400 nm. The superiority of EF with 60 mg $[TDI]_0$ L^{-1} over EF with 12 mg $[TDI]_0$ L^{-1} (original [TDI] of the pre-treated leachate) was not very emphasized, pointing to a slight mineralization improvement carried out by the additional •OH formed from Fenton's reaction (21) in the presence of more 48 mg $[TDI]_0$ L^{-1}. The AO process led to slower DOC removal than EF with 12 mg $[TDI]_0$ L^{-1} during the

Table 9
Examples on the treatment of real landfill leachates by EAOPs.

Pollutant	Wastewater characteristics	Process	Electrochemical reactor		Electrochemical reactor/ Operational parameters	Maximum DOC decay (%)/ EC_{DOC} (kWh (g DOC)$^{-1}$)[a]	Refs.
			Configuration	V (L)			
Municipal sanitary landfill leachate	Raw COD (mg O_2 L^{-1}) = 3385 BOD_5 (mg O_2 L^{-1}) = 500 C (μS cm^{-1}) = 22600 pH = 8.4 [SO_4^{2-}] (mg L^{-1}) = 11 [Cl^-] (mg L^{-1}) = 2574 [NH_4^+] (mg L^{-1}) = 1591 [NO_2^-] (mg L^{-1}) = <2 [NO_3^-] (mg L^{-1}) = 1.9 [PO_4^{3-}] (mg L^{-1}) = 31 in 0–3.1 g NaCl L^{-1} ([Cl^-]$_0$ = 2574–4476 mg L^{-1})	AO	FP with undivided FPC	10	Anode: BDD (70 cm^2) Cathode: BDD (70 cm^2) j_{cat}: 90–257 mA cm^{-2} Q: 10 L min^{-1} pH: 5.0–8.3	n.a./n.a.	[49]
Municipal sanitary landfill leachate	Raw COD (mg O_2 L^{-1}) = 4100–5000 BOD_5 (mg O_2 L^{-1}) = <1000 C (μS cm^{-1}) = 25000 pH = 8 [Cl^-] (mg L^{-1}) = 2500 [NH_4^+] (mg L^{-1}) = 2100–3000 in 0–12 g NaCl L^{-1} ([Cl^-]$_0$ = 2500–10000 mg L^{-1}) without or with addition of 5.3 g Na_2SO_4 L^{-1} (5000 mg SO_4^{2-} L^{-1})	AO	UC	n.s.	Anode: Graphite, PbO_2, DSA (Ti/RuO_2-TiO_2) or Ti/SnO_2-PdO_2-RuO_2 (40 cm^2) Cathode: Steel (40 cm^2) j_{cat}: 25–100 mA cm^{-2} Q: MS pH: 4.0–10	n.a./n.a	[48]
Municipal sanitary landfill leachate	Raw COD (mg O_2 L^{-1}) = 3782 BOD_5 (mg O_2 L^{-1}) = 560 pH = 8.4 [Cl^-] (mg L^{-1}) = 3702 [NH_4^+] (mg L^{-1}) = 3143	AO	FP with three-dimensional granular AC bed reactor	0.8	Anode: RuO_2-IrO_2 (300 cm^2) Cathode: SS (300 cm^2) j_{cat}: 30–90 mA cm^{-2} Q: Air diffusion, recirculation at n.s. flow T: Amb. pH: 8.4	n.a./n.a	[217]
Industrial landfill leachate	Raw COD (mg O_2 L^{-1}) = 17100–18400 pH = 8.9 [Total iron] (mg L^{-1}) = 20 [Cl^-] (mg L^{-1}) = 52300–54280 [NH_4^+] (mg L^{-1}) = 1200–1320	AO	UC with three-dimensional granular AC bed reactor	1.1	Anode: Carbon plate Cathode: 2 SS (140 cm^2 × 2) I: 1–3 A Q: Air diffusion T: Amb. pH: 8.9	83/0.00369	[218]
Municipal sanitary landfill leachate	Filtrated COD (mg O_2 L^{-1}) = 780 BOD_5 (mg O_2 L^{-1}) = <78 C (μS cm^{-1}) = 9770 pH = 8.2 [Cl^-] (mg L^{-1}) = 1800 [NH_4^+] (mg L^{-1}) = 343	AO	FP with UC	0.35	Anode: Ti-Ru-SnO_2, PbO_2 or BDD (50 cm^2) Cathode: SS (50 cm^2) j_{cat}: 40 mA cm^{-2} Q: 7.0 L min^{-1} T: 25 °C pH: 8.2	n.a./n.a	[222]
Municipal sanitary landfill leachate	Biologically pretreated COD (mg O_2 L^{-1}) = 920–1448 C (μS cm^{-1}) = 10000–10900 pH = 8.1–9.4 [SO_4^{2-}] (mg L^{-1}) = 140–199 [Cl^-] (mg L^{-1}) = 1615–1819 [NH_4^+] (mg L^{-1}) = 896–980 [NO_2^-] (mg L^{-1}) = n.d.–163 [NO_3^-] (mg L^{-1}) = 5–1207	AO	LS, PS: FP with undivided FPC	LS: 1 PS: 250	Anode: BDD LS: 70 cm^2; 10500 cm^2 Cathode: SS LS: 70 cm^2; PS: 10500 cm^2 j_{cat}: 45 mA cm^{-2} Q: LS: 3.8–12 L min^{-1}; PS: 5.6–18.3 L min^{-1} T: LS: 20–40 °C; PS: 20 °C pH: 8.1–9.4	n.a./n.a	[220]

Municipal sanitary landfill leachate	Biologically pre-treated DOC ($mg\,L^{-1}$) = 830 COD ($mg\,O_2\,L^{-1}$) = 5800 C ($\mu S\,cm^{-1}$) = 22100 TSS ($mg\,L^{-1}$) = 1770 pH = 8.4 $[Cl^-]$ ($mg\,L^{-1}$) = 4400 $[NH_4^+]$ ($mg\,L^{-1}$) = 1210 without dilution or 1:2-1:16 diluted in 4.3 g $Na_2SO_4\,L^{-1}$			AO	UC	0.2	Anode: BDD (10 cm^2) Cathode: SS (10 cm^2) j_{cat}: 5–70 $mA\,cm^{-2}$ *Q*: MS T: 25 °C pH: 8.4	1:1 dil.: 37/n.a	[137]
Municipal sanitary landfill leachate	Biologically pre-treated DOC ($mg\,L^{-1}$) = 2060 COD ($mg\,O_2\,L^{-1}$) = 6200 BOD_5 ($mg\,O_2\,L^{-1}$) = 800 C ($\mu S\,cm^{-1}$) = 22000 pH = 9.0 $[Cl^-]$ ($mg\,L^{-1}$) = 4700 $[NH_4^+]$ ($mg\,L^{-1}$) = 480 $[NO_2^-]$ ($mg\,L^{-1}$) = 300 $[NO_3^-]$ ($mg\,L^{-1}$) = 80			AO	UC	0.2	Anode: Ti/Pt/PbO_2, Ti/Pt/SnO_2-Sb_2O_4 or BDD (10 cm^2) Cathode: SS (10 cm^2) j_{cat}: 30 $mA\,cm^{-2}$ *Q*: MS T: Amb. pH: 8.4	32/n.a	[221]
Municipal sanitary landfill leachate		Raw	Bio/physicochemically pretreated	AO	FP with undivided FPC	n.s.	Anode: BDD (70 cm^2) Cathode: SS (70 cm^2) j_{cat} (raw): 15–90 $mA\,cm^{-2}$ j_{cat} (pre-treated): 30 $mA\,cm^{-2}$ T: 20 °C pH: 8.4/7.5	n.a./n.a	[215]
	DOC ($mg\,L^{-1}$)	2782	949						
	COD ($mg\,O_2\,L^{-1}$)	4434	1134						
	BOD_5 ($mg\,O_2\,L^{-1}$)	640	120						
	C ($\mu S\,cm^{-1}$)	12770	14360						
	TSS ($mg\,L^{-1}$)	317	1449						
	pH	8.4	7.5						
	$[SO_4^{2-}]$ ($mg\,L^{-1}$)	39	172						
	$[Cl^-]$ ($mg\,L^{-1}$)	3235	1420						
	$[NH_4^+]$ ($mg\,L^{-1}$)	2492	1107						
	$[NO_2^-]$ ($mg\,L^{-1}$)	n.d.	n.d.						
	$[NO_3^-]$ ($mg\,L^{-1}$)	n.d.	n.d.						
	$[PO_4^{3-}]$ ($mg\,L^{-1}$)	55	n.d.						
	Raw: without dilution or 1:2 or 1:4 diluted with addition of NaCl to get $[Cl^-]_0 \approx 3235\,mg\,L^{-1}$ Pretreated: in 0–12 g $NaCl\,L^{-1}$ ($[Cl^-]_0$ = 1420–8570 $mg\,L^{-1}$)								
Mixture of 8 municipal sanitary landfill leachate	DOC ($mg\,L^{-1}$) = 1600–3100 TSS ($mg\,L^{-1}$) = 15310–17602 pH = 8.0–9.0 $[SO_4^{2-}]$ ($mg\,L^{-1}$) = 60–240 $[Cl^-]$ ($mg\,L^{-1}$) = 5000–6200 $[NH_4^+]$ ($mg\,L^{-1}$) = 1900–3200 $[NO_2^-]$ ($mg\,L^{-1}$) = 0 $[NO_3^-]$ ($mg\,L^{-1}$) = 0 EF: in 7.0 g $Na_2SO_4\,L^{-1}$; with or without filtration AO-H_2O_2: in 7.0 g $Na_2SO_4\,L^{-1}$ or without Na_2SO_4 addition; without filtration			AO-H_2O_2 EF	UC	0.25	Anode: BDD or Pt (24 cm^2) Cathode: CF (70 cm^2) j_{cat}: 7.1–14 $mA\,cm^{-2}$ *Q*: MS T: Amb. pH (AO-H_2O_2): 8.0 pH (EF): 3.0 $[TDI]_0$: 11 $mg\,L^{-1}$	EF: 93/n.a	[219]

Table 9 (*Continued*)

Pollutant	Wastewater characteristics				Process	Electrochemical reactor		Electrochemical reactor/ Operational parameters	Maximum DOC decay (%)/ EC_{DOC} (kWh (g DOC)$^{-1}$)[a]	Refs.
						Configuration	*V* (L)			
		Raw	Bio-treated	Coagulated/Aerated				Anode: BDD LS: 10 cm^2; PS: 100 cm^2		
Municipal sanitary landfill leachate	DOC (mg L^{-1})	1341	1009	384	Bio-treatment + Coagulation/Aeration + EF, PEF-UVA, SPEF, Fenton, PF-UVA or SPF	FP with undivided FPC and CPCs (LS, PS)	LS: 1.15 PS: 25	Cathode: C-PTFE A-D LS: 10 cm^2; PS: 100 cm^2 j_{cat}: LS: 25–300 mA cm^{-2}; PS: 200 mA cm^{-2} *Q*: LS: MS + 0.67 L min^{-1}; PS: 9.0 L min^{-1} T: 20 °C pH: 2.8 $[TDI]_0$ (EF): 12 or 60 mg L^{-1} $[TDI]_0$ (others): 60 mg L^{-1}	SPEF: 78/0.277	[24]
	COD (mg O_2 L^{-1})	3582	3036	1268						
	BOD_5 (mg O_2 L^{-1})	240	17	6						
	C (μS cm^{-1})	22150	20400	19600						
	TSS (mg L^{-1})	578	511	185						
	pH	8.6	7.5	2.6						
	[TDI] (mg L^{-1})	2.6	2.8	16						
	$[SO_4^{2-}]$ (mg L^{-1})	83	64	1833						
	$[Cl^-]$ (mg L^{-1})	2500	2559	3434						
	$[NH_4^+]$ (mg L^{-1})	1330	13	5.8						
	$[NO_2^-]$ (mg L^{-1})	219	4900	35						
	$[NO_3^-]$ (mg L^{-1})	42	122	4931						
	$[PO_4^{3-}]$ (mg L^{-1})	<0.02	<0.02	<0.02						
Municipal sanitary landfill leachate	After bio-treatment, coagulation/aeration DOC (mg L^{-1}) = 384 COD (mg O_2 L^{-1}) = 1268 BOD_5 (mg O_2 L^{-1}) = 6 C (μS cm^{-1}) = 19600 TSS (mg L^{-1}) = 185 pH = 2.6 [TDI] (mg L^{-1}) = 16 $[SO_4^{2-}]$ (mg L^{-1}) = 1833 $[Cl^-]$ (mg L^{-1}) = 3434 $[NH_4^+]$ (mg L^{-1}) = 5.8 $[NO_2^-]$ (mg L^{-1}) = 35 $[NO_3^-]$ (mg L^{-1}) = 4980 $[PO_4^{3-}]$ (mg L^{-1}) = <0.02				AO EF PEF-UVA SPEF PEF-UVA/oxalate PEF-UVA-Vis PEF-UVC PF-UVA	FP with undivided FPC and CPCs	1.15	Anode: BDD or Pt (10 cm^2) Cathode (AO): Pt (10 cm^2) Cathode (others): C-PTFE A-D (10 cm^2) j_{cat}: 200 mA cm^{-2} *Q*: MS + 0.67 L min^{-1} T: 15–40 °C pH: 2.8–4.0 $[TDI]_0$ (EF): 12 or 60 mg L^{-1} $[TDI]_0$ (others): 60 mg L^{-1}	SPEF: 78/0.277	[152]
		Raw	Bio-treated	After Fenton				Anode: BDD LS: 70 cm^2; PS: 10500 cm^2		
Municipal sanitary landfill leachate	DOC (mg L^{-1})	2780	1300	200	Bio-treatment + Fenton + AO	FP with undivided FPC	LS: 1 PS: n.s.	Cathode: SS LS: 70 cm^2; PS: 10500 cm^2 j_{cat}: LS: 10–45 mA cm^{-2}; PS: 45 mA cm^{-2} *Q*: LS: 11 L min^{-1}; PS: n.s. T: 20 °C pH (Fenton): 3–3.5 pH (AO): 7.5	n.a./n.a	[216]
	COD (mg O_2 L^{-1})	4430	1750	380						
	BOD_5 (mg O_2 L^{-1})	1196	175	n.m.						
	C (μS cm^{-1})	12770	9100	9400						
	pH	8.4	7.7	7.5						
	$[SO_4^{2-}]$ (mg L^{-1})	438	500	3100						
	$[Cl^-]$ (mg L^{-1})	2124	1876	1460						
	$[NH_4^+]$ (mg L^{-1})	1225	750	700						
	$[NO_2^-]$ (mg L^{-1})	n.d.	20	25						
	$[NO_3^-]$ (mg L^{-1})	n.d.	700	660						

Amb. – Ambient
C-PTFE A-D – Carbon-PTFE air-diffusion;
FP – Flow plant
FPC – Filter-press cell;
LS – Lab-scale
MS – Magnetic stirring;
n.a. – not assessed
n.d. – not detected;
n.s. – not specified
PS – Pilot-scale;
Q – Liquid flow rate
UC – Undivided cell.

[a] Under the best experimental conditions, when applicable.

first times of electrolysis, which was related to the production of •OH from Fenton's reaction (21) in the latter process. However, for longer times the mineralization was slightly faster for AO, which can be mainly attributed to the inability of active chlorine species formed via Eqs. (5)–(7) to degrade organics in EF due to their reaction with the electrogenerated H_2O_2 and, besides that, the scavenging of •OH by their reaction with H_2O_2 via Eq. (24) can occur in EF. Moreira et al. [24] also compared EF, PEF-UVA and SPEF techniques with their chemical analogous, i.e., Fenton, PF-UVA and SPF, respectively, in terms of oxidation ability. EF showed a large superiority over Fenton, PEF-UVA attained less pronounced superiority over PF-UVA and SPEF and SPF achieved similar removals. Moreover, Moreira et al. [24] assessed the biodegradability of the treated landfill leachate during SPEF by performing a Zhan-Wellens test. It was found an enhancement of the biodegradability for increasing reaction times, being necessary to reach a DOC content of 163 mg L^{-1} to fulfill the discharge limits into the environment for the application of a further biological process.

Anglada et al. [49] analyzed the formation of organo-chlorinated compounds such as trihalomethanes, haloacetonitriles, haloketons and 1,2-dichloroethane during the application of AO with BDD anode to a municipal landfill leachate. Apart from 1,2-dichloroethane, the amount of these by-products increased with treatment time, reaching values as high as 1.9 mg L^{-1} of trihalomethanes, 753 μg L^{-1} of haloacetonitriles and 431 μg L^{-1} of haloketons. Furthermore, acidic conditions were found to favor the formation of haloacetonitriles and haloketons.

4.3.3. Electrochemical reactor

Reactors with different configurations have been used for landfill leachate treatments such as undivided cells with magnetic stirring [48,137,219,221], an undivided cell with flow circulation [222], undivided cells with three-dimensional granular activated carbon (AC) bed reactor [217,218], flow plants with an undivided filter-press cell [49,215,216,220] and more complex flow plants with an undivided filter-press cell and CPCs [24,152]. Most of the reactors treated solutions up to around 1 L, but much larger solution volumes up to 250 L were employed. The pilot-scale plant with capacity of 250 L achieved more than 90% of COD after 5 h of reaction and total ammonium oxidation to nitrate after 8 h for the remediation of a biologically treated municipal sanitary landfill leachate using a BDD anode and a SS cathode, effluent pH, 20 °C and j_{cat} of 45 mA cm^{-2} [220].

When using three-dimensional electrodes, faster ammonium oxidation and COD removals were obtained for higher surface area of the granular AC [217,218]. Zhang et al. [217] also found superiority of a three-dimensional electrode over a two-dimensional one when ammonia removal was concerned.

Although BDD has been the most popular anode utilized, other anodes have been used and some studies have compared the performance of various anodes. Panizza and Martinez-Huitle [222] reported that AO ability for both ammonium oxidation and COD removal decreased in the order BDD > PbO_2 > Ti-Ru-SnO_2. Besides that, BDD exhibited lower energy consumption and higher current efficiency. In contrast, Fernandes et al. [221] found higher propensity of PbO_2 and SnO_2-Sb_2O_4 (antimony tetroxide) anodes for ammonium oxidation than BDD. Furthermore, metal oxides promoted ammonium oxidation to nitrogen gas, whereas BDD only oxidized ammonium to nitrate, maintaining a high nitrogen content. Quite similar COD removals were reached for the three anodes, although BDD was superior for DOC removal. In addition, metal oxide anodes led to lower energy consumption because of their higher conductivity. The comparison between BDD and Pt anodes was assessed by Moreira et al. [152] for the degradation of a pre-treated municipal landfill leachate by EF, PEF-UVA and SPEF and also by Oturan et al. [219] for the degradation of a mixture of 8 municipal landfill leachates by EF, reaching high superiority of BDD over Pt for all processes. Chiang et al. [48] found increasing Cl_2/ClO^- production in AO for anodes in the following order: graphite < PbO_2 < DSA (Ti/RuO_2-TiO_2) < Ti/SnO_2-PdO_2-RuO_2. These authors correlated the ability for Cl_2/ClO^- production with ammonium oxidation, COD removal and chloramines production. Since ammonium and COD removals occurred simultaneously by the mediated oxidation, it was proposed a competition between them.

SS has been the most widely employed cathode for landfill leachate remediation by AO, although BDD was also used. EF, PEF and SPEF processes resorted to a carbon-PTFE air-diffusion cathode.

4.3.4. Operational parameters

In general, studies of Table 9 employed j_{cat} from 5 to 100 mA cm^{-2} either for raw or pre-treated leachates. Faster organics degradation and ammonium oxidation were always attained for larger j and, beyond that, Chiang et al. [48] also found increasing Cl_2/ClO^- production. PEF-UVA process carried out by Moreira et al. [24] underwent faster DOC removal from 25 to 200 mA cm^{-2} and similar removals were attained thereon.

The mass transfer was enhanced by applying higher liquid flow rates and temperatures from 20 to 40 °C in an AO process performed at a flow plant with an undivided filter-press cell with continuous solution recirculation [220].

Moreira et al. [152] studied the influence of temperature in both PEF-UVA and PF-UVA processes in the treatment of a pre-treated landfill leachate. For PEF-UVA, quite similar DOC removals were accomplished at 20, 30 and 40 °C and a slightly lower efficiency was attained at 15 °C. A very distinct behavior was achieved for PF-UVA, with high mineralization enhancement from 20 to 30 °C.

As described in Section 2.4.6, the effect of pH on AO efficiency achieved controversial results [48,49] and a pH close to 3.0 was the best for PEF-UVA [152]. Initial addition of 1:3 Fe(III)-to-oxalate molar ratio allowed operating at pH 3.5 with even higher efficiency than at pH 2.8 in the absence of this addition and at pH 4.0 with only slightly lower efficiency [152]. In the same study, the PEF-UVA process attained faster DOC decays for higher $[TDI]_0$ up to 60 mg L^{-1}, with similar efficiency thereon.

4.4. Other real wastewaters

Other real effluents arising from the production of wine, pulp, paper, dairy, tannery and other outputs have also been treated by EAOPs, as can be seen in Table 10.

The various activities carried out during processing and cleaning operations in wineries lead to the generation of high amounts of wastewaters mainly composed of organic compounds like organic acids (tartaric, lactic and acetic), sugars (glucose and fructose) and alcohols (ethanol and glycerol) and also recalcitrant high-molecular weight compounds like polyphenols, tannins and lignins [223]. The release of this kind of effluent into natural aquatic environments without proper treatment can cause deficient oxygen balance, bad odors and decrease of natural photoactivity due to color and turbidity. Raw winery wastewaters used by Moreira et al. [224] and Orescanin et al. [125] were characterized by very high COD contents of 10240–12000 mg O_2 L^{-1}, acidic pH and low ions content, with consequent low/moderate conductivity of 1100–3178 μS cm^{-1}. Moreira et al. [224] determined a BOD_5/COD ratio of 0.7, pointing to a high biodegradability. In this context, the authors firstly subjected the effluent to a biological oxidation to mineralize the biodegradable fraction, which in fact removed 97–98% DOC, COD and BOD_5, and afterwards an AO-H_2O_2, EF, PEF-UVA or SPEF process was employed to mineralize the refractory compounds or transform them into simpler ones that can be further biodegraded. EAOPs were performed in the 2.2 L lab-scale flow plant of Fig. 9 with a BDD/carbon-PTFE air-diffusion filter-press

Table 10
Examples on the treatment of other real wastewaters by EAOPs.

Pollutant	Wastewater characteristics			Process	Electrochemical reactor		Electrochemical reactor/ Operational parameters	Maximum DOC decay (%)/ EC_{DOC} (kWh (g DOC)$^{-1}$)[a]	Refs.
					Configuration	V (L)			
		Raw	Bio-treated				Anode: BDD (10 cm^2)		
Winery wastewater	DOC (mg L^{-1})	4298	130	Bio-treatment + AO-H_2O_2, EF, PEF-UVA or SPEF	FP with undivided FPC and CPCs	1.25	Cathode: C-PTFE A-D (10 cm^2) j_{cat}: 10–100 mA cm^{-2} Q: MS + 0.67 L min^{-1} T: 25 °C pH: 2.8 $[TDI]_0$ (EF, PEF-UVA, SPEF): 20–70 mg L^{-1}	SPEF: 86/0.045	[224]
	COD (mg O_2 L^{-1})	12000	380						
	BOD_5 (mg O_2 L^{-1})	7950	150						
	C (μS cm^{-1})	3178	2998						
	TSS (mg L^{-1})	81	72						
	pH	3.7	8.3						
	$[TDI]$ (mg L^{-1})	<0.1	<0.1						
	$[SO_4^{2-}]$ (mg L^{-1})	30	46						
	$[Cl^-]$ (mg L^{-1})	20	19						
	$[NH_4^+]$ (mg L^{-1})	9.9	9.8						
	$[NO_2^-]$ (mg L^{-1})	1.4	1.2						
	$[NO_3^-]$ (mg L^{-1})	0.89	<0.01						
	$[PO_4^{3-}]$ (mg L^{-1})	<0.02	<0.02						
Winery wastewater	Raw COD (mg O_2 L^{-1}) = 10240 C (μS cm^{-1}) = 1100 TSS (mg L^{-1}) = 2860 pH = 3.7 [Total iron] (mg L^{-1}) = 17 $[SO_4^{2-}]$ (mg L^{-1}) = 187 $[NH_4^+]$ (mg L^{-1}) = 5.4 $[PO_4^{3-}]$ (mg L^{-1}) = 7.5 in 2.0 g NaCl L^{-1}			AO + EC (Fe, Al) (3 treatments in parallel with sonication) + Electromagnetization + Clarification + O_3/H_2O_2/UV	UC	8	Anode: SS Cathode: SS Operate in galvanostatic mode Q: Sonication pH: 3.7	n.a./n.a.	[125]
		Acidic	Alkaline						
Cellulose bleaching wastewater	DOC (mg L^{-1})	499	594	Filtration (UF, NF or RO) + AO-H_2O_2	UC	0.2	Anode: DSA (RuO_2) or BDD (4 cm^2) Cathode: C-PTFE A-D (3 cm^2) E_{cell}: 2–12 V Q: MS T: 25 °C pH: 2.5/10.5	NF + AO-H_2O_2, alkaline: 96/n.a.	[225]
	COD (mg O_2 L^{-1})	1250	1500						
	BOD_5 (mg O_2 L^{-1})	563	595						
	C (μS cm^{-1})	5920	4410						
	pH	2.5	10.5						
	$[Cl^-]$ (mg L^{-1})	488	350						

		Raw	Electro-coagulated						
Dairy wastewater or indole derivative	DOC ($mg\,L^{-1}$) COD ($mg\,O_2\,L^{-1}$) BOD_5 ($mg\,O_2\,L^{-1}$) C ($\mu S\,cm^{-1}$) TSS ($mg\,L^{-1}$) pH $[Cl^-]$ ($mg\,L^{-1}$) $[NH_4^+]$ ($mg\,L^{-1}$) $[NO_2^-]$ ($mg\,L^{-1}$) $[NO_3^-]$ ($mg\,L^{-1}$) in 0.5 g NaCl L^{-1} 117 mg indole L^{-1} in 3.6 g Na_2SO_4 L^{-1} + 1.5 g NaCL L^{-1}, 7.0 g Na_2SO_4 L^{-1} or 2.9 g NaCl L^{-1}	1062 3859 1517 2360 >1988 8.3 1131 177 0.4 1.5	198 395 n.m. n.m. n.m. n.m. 890 n.m. n.m. n.m.	EC + AO	UC	0.1	Anode (dairy wastewater): DSA (IrO_2-Ta_2O_5) (6.6 cm^2) Anode (indole solution): DSA (IrO_2-Ta_2O_5) (2.5 cm^2) Cathode: Pt wire j_{cat} (dairy wastewater): 30 $mA\,cm^{-2}$ j_{cat} (indole solution): 4–80 $mA\,cm^{-2}$ Q: MS T: 25 °C pH (dairy wastewater): 8.3 pH (indole solution): 3.0 or 8.0	85/n.a.	[227]
Tannery wastewater	DOC ($mg\,L^{-1}$) = 1800–1950 COD ($mg\,O_2\,L^{-1}$) = 9922–10180 BOD_5 ($mg\,O_2\,L^{-1}$) = 528 C ($\mu S\,cm^{-1}$) = 6300–9100 TSS ($mg\,L^{-1}$) = 445–530 pH = 3.7–4.3 [Total iron] ($mg\,L^{-1}$) = 2.0–2.8 $[Cl^-]$ ($mg\,L^{-1}$) = 1239			EC AO EF PEF-UVA EC + PEF-UVA	UC	0.25	Anode: BDD (7.6 cm^2) Cathode (AO): Iron plate (7.6 cm^2) Cathode (EF, PEF-UVA): BDD with air bubbling (7.6 cm^2) j_{cat}: 65 or 111 $mA\,cm^{-2}$ Q: MS T: Amb. pH (AO): ≈4.0 pH (EF, PEF-UVA): 3.0 $[TDI]_0$ (AO): n.s. $[TDI]_0$ (EF, PEF-UVA): 56 or 167 $mg\,L^{-1}$	EC + PEF-UVA: 90/0.243	[229]

Amb. – Ambient;
C-PTFE A-D – Carbon-PTFE air-diffusion;
FP – Flow plant;
FPC – Filter-press cell;
MS – Magnetic stirring;
n.a. – not assessed;
n.m. – not measured;
n.s. – not specified;
Q – Liquid flow rate;
UC – Undivided cell.

[a] Under the best experimental conditions, when applicable.

cell. Mineralization ability of EAOPs could be arranged in the order SPEF ≥ PEF-UVA > EF > AO-H_2O_2 and the best operational conditions achieved for PEF-UVA and SPEF were j of 25 mA cm^{-2} and $[TDI]_0$ of 35 mg L^{-1}. In turn, Orescanin et al. [125] firstly added NaCl to the raw winery wastewater in order to allow the formation of active chlorine species by indirect anodic oxidation. Afterwards, the authors implemented an innovative treatment system embracing three consecutive electrochemical methods, including AO with SS electrodes, EC with iron electrodes and EC with aluminum electrodes, the three with simultaneous sonication, followed by effluent recirculation through an electromagnet, clarification and ozonation in the presence of added H_2O_2 combined with UV radiation (O_3/H_2O_2/UV). AO aimed the degradation of organics and EC intended to remove suspended solids, heavy metals and phosphates. Sonication led to rapid formation, growth and collapse of cavitation bubbles that allowed additional pyrolytic organics degradation inside the bubbles. Along electrochemical treatments, pH increased from 3.7 to 7.6 probably due to the degradation of the polyphenols into phenols that exhibited an alkaline reaction. After electrochemical processes, it was attained 55% COD decay and more than 92% suspended solids, heavy metals and phosphate removal. The further O_3/H_2O_2/UV treatment intended to promote higher degradation, with 77% COD removal at the end.

Most of the industrial cellulose bleaching processes are based on the use of ClO_2 (elementary chlorine free processes), with consequent production of toxic and poorly biodegradable organochlorinated by-products in bleaching effluents. Two kinds of bleaching effluents can be generated: (i) an acidic stream from the oxidation stages with ClO_2, and (ii) an alkaline one as a result of alkaline extraction enhanced with oxygen and H_2O_2 [225]. Both acidic and alkaline wastewaters were treated by Salazar et al. [225] utilizing a first filtration process like UF, nanofiltration (NF) or RO, followed by an AO-H_2O_2 method with a DSA (RuO_2) or a BDD anode and a carbon-PTFE air-diffusion cathode. The main characteristics of wastewaters were pH 2.5 and 10.5, DOC of 499 and 594 mg L^{-1}, BOD_5/COD ratio of 0.5 and 0.4, chloride concentration of 488 and 350 mg L^{-1} and moderate/high conductivity of 5920 and 4410 μS cm^{-1} for acidic and alkaline effluents, respectively. The best coupling in terms of mineralization was UF/AO-H_2O_2 for the acidic wastewater and NF/AO-H_2O_2 for the alkaline wastewater. Only the NF/H_2O_2 treatment for the alkaline wastewater entailed a real advantage compared to H_2O_2 alone in terms of mineralization. However, regarding energy consumption, the UF/AO-H_2O_2 coupling for the acidic effluent was advantageous as well. Mineralization was faster at low E_{cell} for the acidic wastewater by the participation of active chlorine species and at high E_{cell} for alkaline wastewater since •OH production was favored. The DOC removal of both bleaching effluents by AO-H_2O_2 was faster using the BDD anode due to the higher oxidizing power of BDD(•OH) and fouling of RuO_2 DSA.

Dairy wastewaters are characterized by high contents of recalcitrant organic compounds such as refractory alcohols, carboxylic acids and indole derivatives, which can damage the natural waters in case of improper discharge [226]. Borbón et al. [227] focused on the treatment of a dairy wastewater with 1062 mg L^{-1} of DOC, a BOD_5/COD ratio of 0.4, alkaline pH, high suspended solids content and moderate ions amount, embracing 1131 mg chloride L^{-1} and conveying in a moderate conductivity of 2360 μS cm^{-1}. A sequential two-step treatment was performed, involving (i) EC to remove solids, which employed an aluminum plate and a large surface iron mesh as monopolar anode and cathode, respectively, followed by (ii) AO to remove organics, in which an IrO_2-tantalum pentoxide (Ta_2O_5) DSA anode and a Pt wire cathode were used at j_{cat} of 30 mA cm^{-2}. A concentration of 0.5 g NaCl L^{-1} was added to the wastewater before EC treatment in order to inhibit or slow down the anode passivation, typically observed for aluminum.

Tannery wastewaters are composed of high amounts of organics, which result from hides and skins and from the addition of reagents during the different operations made on these materials, and also by inorganic contaminants such as ammonia, sulfides and heavy metals [228]. Comparison of tannery wastewater treatment by EC, AO, EF, PEF-UVA and combination of EC followed by PEF-UVA was accomplished by Isarain-Chávez et al. [229]. EC employed iron electrodes, AO used a BDD/iron plate cell and EF and PEF-UVA resorted to a BDD/BDD one with air bubbling to produce H_2O_2 at the cathode. The tannery wastewater was characterized by average DOC of 1875 mg L^{-1}, BOD_5/COD ratio of only 0.05, acidic pH, moderate chloride content of 1239 mg L^{-1} and high conductivity of 7700 μS cm^{-1}. The mineralization ability of individual processes dropped in the order PEF-UVA > EF ≈ EC > AO. DOC removal of 74% and 80% were achieved after 180 min of EC and PEF-UVA, respectively, whereas the combined process attained 90% DOC abatement after 180 min of each process.

5. Conclusions and prospects

The technical feasibility of EAOPs to degrade various classes of persistent organic compounds at distinct contents and in different matrices has been proved by the achievement of high degradation rates, very effective removals and low energy consumptions. In general, the ability of EAOPs to oxidize the various types of wastewaters can be arranged in the order: SPEF > PEF-UVA with low energy power lamps > EF > AO-H_2O_2 ≈ AO. The EAOPs can be even more effective than their chemical analogous, showing higher removal rates and greater abatements. However, the availability of higher amounts of H_2O_2 at the reaction beginning in the chemical processes demonstrated to induce faster initial removal rates for some pollutants. In this sense, one of the EAOPs challenges regards their implementation in continuous mode to provide high H_2O_2 amounts from the start.

Predominantly, researchers have been focused on the application of AO and EF processes for the remediation of synthetic wastewaters typically contaminated with a dye, a pesticide or a pharmaceutical at lab-scale using undivided cells and volumes up to 1 L. Nevertheless, the number of PEF and SPEF applications has been increasing as well as the number of studies on real wastewaters and the use of filter-press cells either in simple flow reactors or in more complex plants with structures for radiation capture and capacities in the order of some liters. Despite these efforts, there is a lack of information regarding the improvement of the reactor design to overcome mass and photon transfer limitations, and also with respect to the scaling-up of EAOPs to large-scale and then allow their applicability to industrial level. To our knowledge, there are few large-scale applications of EAOPs, all of them concerning AO process with BDD anodes. Some examples are: (i) the automated disinfection of private and public swimming pool water by Oxineo® and Sysneo® trademarks; (ii) the water disinfection and industrial wastewater treatment by CONDIACELL® and Diamonox® trademarks; and (iii) the treatment of landfill leachates in the pilot-plant described in Anglada et al. [220]. Less expensive hardware and electrodes materials and more versatile systems should be developed to spread the application of AO and launch the industrial application of EF, PEF and SPEF technologies. In the case of light-induced EAOPs, the system should combine both artificial and natural light.

Considering the divergent achievements regarding the effect of the composition of the supporting electrolyte on EAOPs effectiveness and the influence of pH on the efficiency of AO and AO-H_2O_2 processes, additional research should be carried out. Moreover, the application of PEF and SPEF processes to the degradation of a real textile wastewaters can be an interesting approach due to the lack of information on this topic. As regards Fenton's based EAOPs, their

operation at acidic pH and the need for a final polishing step to remove the catalyst from solution up to the legal discharge limits are known drawbacks that need to be solved. This can be done by developing efficient immobilized catalysts.

Another interesting but complex future approach is the assessment of the economic feasibility of EAOPs. To do it, the investment costs, mainly related to electrochemical cells and, for light-assisted EAOPs, UV lamps or photoreactors for natural sunlight capture, and also the operational costs, including electrical energy for electrochemical cell and plant operation, reagents and maintenance, should be considered.

Acknowledgments

This work was financially supported by: (i) Project UID/EQU/50020/2013 – POCI-01-0145-FEDER-006984 – Associate Laboratory LSRE-LCM funded by FEDER (*Fundo Europeu de Desenvolvimento Regional*) funds through COMPETE2020 (*Programa Operacional Competitividade e Internacionalização* – POCI) – and by national funds through FCT (*Fundação para a Ciência e a Tecnologia*), and (ii) Project NORTE-07-0124-FEDER-0000008, cofinanced by QREN (*Quadro de Referência Estratégico Nacional*), ON2 program (*Programa Operacional Regional do Norte*) and FEDER. F.C. Moreira acknowledges her Ph.D. fellowship SFRH/BD/80361/2011 supported by FCT. V.J.P. Vilar acknowledges the FCT Investigator 2013 Programme (IF/00273/2013).

References

[1] H. Zollinger, Color Chemistry: Syntheses, Properties, and Applications of Organic Dyes and Pigments, 3rd revised ed., VHCA and Wiley-VCH, Zurich, Switzerland/Weinheim, Germany, 2003.
[2] K.P. Sharma, S. Sharma, S. Sharma, P.K. Singh, S. Kumar, R. Grover, P.K. Sharma, Chemosphere 69 (2007) 48–54.
[3] K. Kümmerer, J. Environ. Manage. 90 (2009) 2354–2366.
[4] C.A. Damalas, I.G. Eleftherohorinos, Int. J. Env. Res. Public Health 8 (2011) 1402–1419.
[5] M.A. Oturan, J.J. Aaron, Crit. Rev. Environ. Sci. Technol. 44 (2014) 2577–2641.
[6] W.H. Glaze, J.-W. Kang, D.H. Chapin, Ozone Sci. Eng. 9 (1987) 335–352.
[7] W.M. Latimer, Oxidation Potentials, 2nd ed., Prentice-Hall, New York, United States, 1952.
[8] G.V. Buxton, C.L. Greenstock, W.P. Helman, A.B. Ross, J. Phys. Chem. Ref. Data 17 (1988) 513–886.
[9] E.G. Janzen, Y. Kotake, R.D. Hinton, Free Radic. Biol. Med. 12 (1992) 169–173.
[10] H. Suty, C. De Traversay, M. Cost, Water Sci. Technol. 49 (2004) 227–233.
[11] M.N. Chong, A.K. Sharma, S. Burn, C.P. Saint, J. Clean. Prod. 35 (2012) 230–238.
[12] C. Comninellis, A. Kapalka, S. Malato, S.A. Parsons, I. Poulios, D. Mantzavinos, J. Chem. Technol. Biotechnol. 83 (2008) 769–776.
[13] E. Brillas, I. Sireís, M.A. Oturan, Chem. Rev. 109 (2009) 6570–6631.
[14] C. Barrera-Díaz, P. Cañizares, F.J. Fernández, R. Natividad, M.A. Rodrigo, J. Mex. Chem. Soc. 58 (2014) 256–275.
[15] B.P. Chaplin, Environ. Sci. Process. Impacts 16 (2014) 1182–1203.
[16] C.A. Martínez-Huitle, S. Ferro, Chem. Soc. Rev. 35 (2006) 1324–1340.
[17] M. Panizza, G. Cerisola, Chem. Rev. 109 (2009) 6541–6569.
[18] E. Brillas, J.A. Garrido, R.M. Rodríguez, C. Arias, P.L. Cabot, F. Centellas, Port. Electrochim. Acta 26 (2008) 15–46.
[19] O. Ganzenko, D. Huguenot, E.D. van Hullebusch, G. Esposito, M.A. Oturan, Environ. Sci. Pollut. Res. 21 (2014) 8493–8524.
[20] I. Sirés, E. Brillas, M. Oturan, M. Rodrigo, M. Panizza, Environ. Sci. Pollut. Res. 21 (2014) 8336–8367.
[21] E. Brillas, C.A. Martínez-Huitle, Appl. Catal. B: Environ. 166–167 (2015) 603–643.
[22] A.M. Urtiaga, G. Pérez, R. Ibáñez, I. Ortiz, Desalination 331 (2013) 26–34.
[23] A. Thiam, M. Zhou, E. Brillas, I. Sirés, Appl. Catal. B: Environ. 150–151 (2014) 116–125.
[24] F.C. Moreira, J. Soler, A. Fonseca, I. Saraiva, R.A.R. Boaventura, E. Brillas, V.J.P. Vilar, Water Res. 81 (2015) 375–387.
[25] Y. Deng, J.D. Englehardt, Waste Manage. 27 (2007) 380–388.
[26] L. Feng, E.D. van Hullebusch, M.A. Rodrigo, G. Esposito, M.A. Oturan, Chem. Eng. J. 228 (2013) 944–964.
[27] C.A. Martínez-Huitle, M.A. Rodrigo, I. Sirés, O. Scialdone, Chem. Rev. 115 (2015) 13362–13407.
[28] M.A. Rodrigo, N. Oturan, M.A. Oturan, Chem. Rev. 114 (2014) 8720–8745.
[29] S. Vasudevan, M.A. Oturan, Environ. Chem. Lett. 12 (2014) 97–108.
[30] E. Brillas, J. Mex. Chem. Soc. 58 (2014) 239–255.
[31] E. Brillas, J. Braz. Chem. Soc. 25 (2014) 393–417.
[32] I. Sirés, E. Brillas, Environ. Int. 40 (2012) 212–229.
[33] C. Comninellis, Electrochim. Acta 39 (1994) 1857–1862.
[34] B. Marselli, J. Garcia-Gomez, P.A. Michaud, M.A. Rodrigo, C. Comninellis, J. Electrochem. Soc. 150 (2003) D79–D83.
[35] F. Sopaj, M.A. Rodrigo, N. Oturan, F.I. Podvorica, J. Pinson, M.A. Oturan, Chem. Eng. J. 262 (2015) 286–294.
[36] E. Brillas, C.A. Martínez-Huitle, Synthetic Diamond Films: Preparation, Electrochemistry, Characterization, and Applications, John Wiley & Sons, Inc., New Jersey, United States, 2011.
[37] P.C.S. Hayfield, Development of a New Material: Monolithic Ti_4O_7 Ebonex Ceramic, Royal Society of Chemistry, Cambridge, United Kingdom, 2002.
[38] D. Bejan, L.M. Rabson, N.J. Bunce, Can. J. Chem. Eng. 85 (2007) 929–935.
[39] A.M. Zaky, B.P. Chaplin, Environ. Sci. Technol. 47 (2013) 6554–6563.
[40] D. Bejan, E. Guinea, N.J. Bunce, Electrochim. Acta 69 (2012) 275–281.
[41] D.C. Harris, Exploring Chemical Analysis, 4th ed., W.H Freeman and Company, New York, United States, 2009.
[42] C. Boxall, G.H. Kelsall, Hypochlorite Electrogeneration. 2. Thermodynamics and Kinetic-model of the Anode Reaction Layer, Symposium on Electrochemical Engineering and the Environment, Institution of Chemical Engineers, Rugby, United Kingdom, 1992, pp. 59–70.
[43] C.A. Martínez-Huitle, E. Brillas, Appl. Catal. B: Environ. 87 (2009) 105–145.
[44] A. Sánchez-Carretero, C. Sáez, P. Cañizares, M.A. Rodrigo, Chem. Eng. J. 166 (2011) 710–714.
[45] G.M. Brown, B. Gu, in: B. Gu, J.B. Coates (Eds.), Perchlorate. Environmental Occurrence, Interactions and Treatment, Springer, New York, United States, 2006, pp. 17–47 (Chapter 2).
[46] C. Zhang, J. Wang, T. Murakami, A. Fujishima, D. Fu, Z. Gu, J. Electroanal. Chem. 638 (2010) 91–99.
[47] L. Gomes, D.W. Miwa, G.R.P. Malpass, A.J. Motheo, J. Braz. Chem. Soc. 22 (2011) 1299–1306.
[48] L.-C. Chiang, J.-E. Chang, T.-C. Wen, Water Res. 29 (1995) 671–678.
[49] A. Anglada, A. Urtiaga, I. Ortiz, D. Mantzavinos, E. Diamadopoulos, Water Res. 45 (2011) 828–838.
[50] A.Y. Bagastyo, D.J. Batstone, I. Kristiana, W. Gernjak, C. Joll, J. Radjenovic, Water Res. 46 (2012) 6104–6112.
[51] P. Cañizares, C. Sáez, J. Lobato, M.A. Rodrigo, Ind. Eng. Chem. Res. 43 (2004) 6629–6637.
[52] P. Cañizares, A. Gadri, J. Lobato, B. Nasr, R. Paz, M.A. Rodrigo, C. Saez, Ind. Eng. Chem. Res. 45 (2006) 3468–3473.
[53] P.C. Foller, R.T. Bombard, J. Appl. Electrochem. 25 (1995) 613–627.
[54] E. Brillas, A. Maestro, M. Moratalla, J. Casado, J. Appl. Electrochem. 27 (1997) 83–92.
[55] P. Drogui, S. Elmaleh, M. Rumeau, C. Bernard, A. Rambaud, Water Res. 35 (2001) 3235–3241.
[56] A.A. Gallegos, Y.V. García, A. Zamudio, Sol. Energy Mater. Sol. Cells 88 (2005) 157–167.
[57] E. Brillas, R.M. Bastida, E. Llosa, J. Casado, J. Electrochem. Soc. 142 (1995) 1733–1741.
[58] E. Brillas, B. Boye, M. Ángel Baños, J.C. Calpe, J.A. Garrido, Chemosphere 51 (2003) 227–235.
[59] S. Garcia-Segura, R. Salazar, E. Brillas, Electrochim. Acta 113 (2013) 609–619.
[60] M.A. Oturan, N. Oturan, M.C. Edelahi, F.I. Podvorica, K.E. Kacemi, Chem. Eng. J. 171 (2011) 127–135.
[61] M. Zhou, Q. Tan, Q. Wang, Y. Jiao, N. Oturan, M.A. Oturan, J. Hazard. Mater. 215–216 (2012) 287–293.
[62] A. Özcan, Y. Şahin, A. Savaş Koparal, M.A. Oturan, J. Electroanal. Chem. 616 (2008) 71–78.
[63] A. Özcan, Y. Şahin, A.S. Koparal, M.A. Oturan, Appl. Catal. B: Environ. 89 (2009) 620–626.
[64] A. Wang, Y.-Y. Li, A.L. Estrada, Appl. Catal. B: Environ. 102 (2011) 378–386.
[65] M. Zarei, A. Niaei, D. Salari, A. Khataee, J. Hazard. Mater. 173 (2010) 544–551.
[66] A.R. Khataee, M. Zarei, A.R. Khataee, Clean Soil Air Water 39 (2011) 482–490.
[67] H.S. El-Desoky, M.M. Ghoneim, N.M. Zidan, Desalination 264 (2010) 143–150.
[68] M.M. Ghoneim, H.S. El-Desoky, N.M. Zidan, Desalination 274 (2011) 22–30.
[69] J.R. Domínguez, T. González, P. Palo, J. Sánchez-Martín, Chem. Eng. J. 162 (2010) 1012–1018.
[70] O. García, E. Isarain-Chávez, S. Garcia-Segura, E. Brillas, J.M. Peralta-Hernández, Electrocatalysis 4 (2013) 224–234.
[71] J.M. Campos-Martin, G. Blanco-Brieva, J.L.G. Fierro, Angew. Chem. Int. Ed. 45 (2006) 6962–6984.
[72] D. Pletcher, Acta Chem. Scand. 53 (1999) 745–750.
[73] H.J.H. Fenton, J. Chem. Soc. Trans. 65 (1894) 899–910.
[74] F. Haber, J. Weiss, Proc. R. Soc. Lond. Ser. A Math. Phys. Sci. 147 (1934) 332–351.
[75] Y. Sun, J.J. Pignatello, Environ. Sci. Technol. 27 (1993) 304–310.
[76] S. Bouafia-Chergui, N. Oturan, H. Khalaf, M.A. Oturan, J. Environ. Sci. Health Pt. A: Toxic/Hazard. Subst. Environ. Eng. 45 (2010) 622–629.
[77] P. Wardman, L.P. Candeias, Radiat. Res. 145 (1996) 523–531.
[78] L.P. Candeias, M.R.L. Stratford, P. Wardman, Free Radic. Res. 20 (1994) 241–249.
[79] A.D. Bokare, W. Choi, J. Hazard. Mater. 275 (2014) 121–135.
[80] S. Malato, P. Fernández-Ibáñez, M.I. Maldonado, J. Blanco, W. Gernjak, Catal. Today 147 (2009) 1–59.
[81] E. Brillas, J.C. Calpe, J. Casado, Water Res. 34 (2000) 2253–2262.
[82] M.A. Oturan, J. Appl. Electrochem. 30 (2000) 475–482.

[83] E. Isarain-Chávez, C. Arias, P.L. Cabot, F. Centellas, R.M. Rodríguez, J.A. Garrido, E. Brillas, Appl. Catal. B: Environ. 96 (2010) 361–369.
[84] I. Sirés, J.A. Garrido, R.M. Rodríguez, E. Brillas, N. Oturan, M.A. Oturan, Appl. Catal. B: Environ. 72 (2007) 382–394.
[85] N. Kishimoto, T. Kitamura, M. Kato, H. Otsu, Water Res. 47 (2013) 1919–1927.
[86] N. Kishimoto, T. Kitamura, Y. Nakamura, Water Sci. Technol. 72 (2015) 850–857.
[87] N. Kishimoto, E. Sugimura, Water Sci. Technol. 62 (2010) 2321–2329.
[88] E. Brillas, R. Sauleda, J. Casado, J. Electrochem. Soc. 144 (1997) 2374–2379.
[89] Y.-H. Huang, G.-H. Huang, S.-N. Lee, S.-M. Lin, inventors. Industrial Technology Research Institute, assignee. Method of wastewater treatment by electrolysis and oxidization. United States Patent 6126838 A. 2000 October 3.
[90] K. Pratap, A.T. Lemley, J. Agric. Food. Chem. 42 (1994) 209–215.
[91] R.J. Scrudato, J.R. Chiarenzelli, inventors. The Research Foundation of State University of New York, assignee. Electrochemical peroxidation of contaminated liquids and slurries. United States Patent 6045707 A. 2000.
[92] D.A. Saltmiras, A.T. Lemley, J. Agric. Food. Chem. 48 (2000) 6149–6157.
[93] E. Brillas, R. Sauleda, J. Casado, J. Electrochem. Soc. 145 (1998) 759–765.
[94] B. Boye, M.M. Dieng, E. Brillas, J. Electroanal. Chem. 557 (2003) 135–146.
[95] C. Flox, P.L. Cabot, F. Centellas, J.A. Garrido, R.M. Rodríguez, C. Arias, E. Brillas, Appl. Catal. B: Environ. 75 (2007) 17–28.
[96] R. Salazar, S. Garcia-Segura, M.S. Ureta-Zañartu, E. Brillas, Electrochim. Acta 56 (2011) 6371–6379.
[97] L.C. Almeida, S. Garcia-Segura, C. Arias, N. Bocchi, E. Brillas, Chemosphere 89 (2012) 751–758.
[98] S. Garcia-Segura, E.B. Cavalcanti, E. Brillas, Appl. Catal. B: Environ. 144 (2014) 588–598.
[99] A. Thiam, I. Sirés, E. Brillas, Water Res. 81 (2015) 178–187.
[100] O. Horváth, K.L. Stevenson, Charge Transfer Photochemistry of Coordination Compounds, VCH, New York, United States, 1992.
[101] Y. Zuo, J. Hoigne, Environ. Sci. Technol. 26 (1992) 1014–1022.
[102] B.C. Faust, R.G. Zepp, Environ. Sci. Technol. 27 (1993) 2517–2522.
[103] J.H. Baxendale, J.A. Wilson, Trans. Faraday Soc. 53 (1957) 344–356.
[104] R. Venkatadri, R.W. Peters, Hazard. Waste Hazard. Mater. 10 (1993) 107–149.
[105] C. Flox, S. Ammar, C. Arias, E. Brillas, A.V. Vargas-Zavala, R. Abdelhedi, Appl. Catal. B: Environ. 67 (2006) 93–104.
[106] N. Borràs, C. Arias, R. Oliver, E. Brillas, J. Electroanal. Chem. 689 (2013) 158–167.
[107] A. El-Ghenymy, N. Oturan, M.A. Oturan, J.A. Garrido, P.L. Cabot, F. Centellas, R.M. Rodríguez, E. Brillas, Chem. Eng. J. 234 (2013) 115–123.
[108] F.C. Moreira, R.A.R. Boaventura, E. Brillas, V.J.P. Vilar, Appl. Catal. B: Environ. 162 (2015) 34–44.
[109] Y.-T. Lin, C. Liang, J.-H. Chen, Chemosphere 82 (2011) 1168–1172.
[110] B.G. Oliver, J.H. Carey, Environ. Sci. Technol. 11 (1977) 893–895.
[111] C. Flox, J.A. Garrido, R.M. Rodríguez, P.L. Cabot, F. Centellas, C. Arias, E. Brillas, Catal. Today 129 (2007) 29–36.
[112] S. Hammami, N. Oturan, N. Bellakhal, M. Dachraoui, M.A. Oturan, J. Electroanal. Chem. 610 (2007) 75–84.
[113] E. Isarain-Chávez, R.M. Rodríguez, J.A. Garrido, C. Arias, F. Centellas, P.L. Cabot, E. Brillas, Electrochim. Acta 56 (2010) 215–221.
[114] A. El-Ghenymy, R.M. Rodríguez, C. Arias, F. Centellas, J.A. Garrido, P.L. Cabot, E. Brillas, J. Electroanal. Chem. 701 (2013) 7–13.
[115] L. Labiadh, M.A. Oturan, M. Panizza, N.B. Hamadi, S. Ammar, J. Hazard. Mater. 297 (2015) 34–41.
[116] M. Iranifam, M. Zarei, A.R. Khataee, J. Electroanal. Chem. 659 (2011) 107–112.
[117] J. Wu, H. Zhang, N. Oturan, Y. Wang, L. Chen, M.A. Oturan, Chemosphere 87 (2012) 614–620.
[118] A. Khataee, H. Marandizadeh, M. Zarei, S. Aber, B. Vahid, Y. Hanifehpour, S.W. Joo, Curr. Nanosci. 9 (2013) 387–393.
[119] M. Hamza, R. Abdelhedi, E. Brillas, I. Sirés, J. Electroanal. Chem. 627 (2009) 41–50.
[120] E.B. Cavalcanti, S.G. Segura, F. Centellas, E. Brillas, Water Res. 47 (2013) 1803–1815.
[121] L.M. Da Silva, I.C. Gonçalves, J.J.S. Teles, D.V. Franco, Electrochim. Acta 146 (2014) 714–732.
[122] H.T. Madsen, E.G. Søgaard, J. Muff, Chem. Eng. J. 276 (2015) 358–364.
[123] S. Garcia-Segura, E. Brillas, Electrochim. Acta 140 (2014) 384–395.
[124] R. Vargas, S. Díaz, L. Viele, O. Núñez, C. Borrás, J. Mostany, B.R. Scharifker, Appl. Catal. B: Environ. 144 (2013) 107–111.
[125] V. Orescanin, R. Kollar, K. Nad, I.L. Mikelic, S.F. Gustek, J. Environ. Sci. Health Pt. A: Toxic/Hazard. Subst. Environ. Eng. 48 (2013) 1543–1547.
[126] A.E. Martell, R.M. Smith, Critical Stability Constants, Vols. 1–6, Plenum Press, New York, United States, 1974, 1975, 1976, 1977, 1982, 1989.
[127] P. Neta, R.E. Huie, A.B. Ross, J. Phys. Chem. Ref. Data Reprints 17 (1988) 1027–1247.
[128] J. De Laat, G. Truong Le, B. Legube, Chemosphere 55 (2004) 715–723.
[129] C. Carvalho, A. Fernandes, A. Lopes, H. Pinheiro, I. Gonçalves, Chemosphere 67 (2007) 1316–1324.
[130] N. Daneshvar, S. Aber, V. Vatanpour, M.H. Rasoulifard, J. Electroanal. Chem. 615 (2008) 165–174.
[131] A. Thiam, I. Sirés, J.A. Garrido, R.M. Rodríguez, E. Brillas, J. Hazard. Mater. 290 (2015) 34–42.
[132] Y. Fan, Z. Ai, L. Zhang, J. Hazard. Mater. 176 (2010) 678–684.
[133] F.C. Moreira, S. Garcia-Segura, R.A.R. Boaventura, E. Brillas, V.J.P. Vilar, Appl. Catal. B: Environ. 160–161 (2014) 492–505.
[134] T. González, J.R. Domínguez, P. Palo, J. Sánchez-Martín, E.M. Cuerda-Correa, Desalination 280 (2011) 197–202.
[135] B. Boye, M.M. Dieng, E. Brillas, Environ. Sci. Technol. 36 (2002) 3030–3035.
[136] A. Serra, X. Domènech, C. Arias, E. Brillas, J. Peral, Appl. Catal. B: Environ. 89 (2009) 12–21.
[137] A. Fernandes, M.J. Pacheco, L. Ciríaco, A. Lopes, J. Hazard. Mater. 199–200 (2012) 82–87.
[138] V.S. Antonin, S. Garcia-Segura, M.C. Santos, E. Brillas, J. Electroanal. Chem. 747 (2015) 1–11.
[139] M. Skoumal, C. Arias, P.L. Cabot, F. Centellas, J.A. Garrido, R.M. Rodríguez, E. Brillas, Chemosphere 71 (2008) 1718–1729.
[140] E. Tsantaki, T. Velegraki, A. Katsaounis, D. Mantzavinos, J. Hazard. Mater. 207-208 (2012) 91–96.
[141] A.Y. Sychev, V.G. Isak, Russ. Chem. Rev. 64 (1995) 1105–1129.
[142] D. Mansour, F. Fourcade, N. Bellakhal, M. Dachraoui, D. Hauchard, A. Amrane, Water Air Soil Pollut. 223 (2012) 2023–2034.
[143] A. Santos, P. Yustos, S. Rodriguez, E. Simon, F. Garcia-Ochoa, J. Hazard. Mater. 146 (2007) 595–601.
[144] A. El-Ghenymy, J.A. Garrido, R.M. Rodríguez, P.L. Cabot, F. Centellas, C. Arias, E. Brillas, J. Electroanal. Chem. 689 (2013) 149–157.
[145] A. El-Ghenymy, F. Centellas, J.A. Garrido, R.M. Rodríguez, I. Sirés, P.L. Cabot, E. Brillas, Electrochim. Acta 130 (2014) 568–576.
[146] A.K. Abdessalem, M.A. Oturan, N. Oturan, N. Bellakhal, M. Dachraoui, Int. J. Environ. Anal. Chem. 90 (2010) 468–477.
[147] S. Garcia-Segura, J. Keller, E. Brillas, J. Radjenovic, J. Hazard. Mater. 283 (2015) 551–557.
[148] M. Skoumal, R.M. Rodríguez, P.L. Cabot, F. Centellas, J.A. Garrido, C. Arias, E. Brillas, Electrochim. Acta 54 (2009) 2077–2085.
[149] C.-T. Wang, W.-L. Chou, M.-H. Chung, Y.-M. Kuo, Desalination 253 (2010) 129–134.
[150] L.C. Almeida, S. Garcia-Segura, N. Bocchi, E. Brillas, Appl. Catal. B: Environ. 103 (2011) 21–30.
[151] S. Garcia-Segura, L.C. Almeida, N. Bocchi, E. Brillas, J. Hazard. Mater. 194 (2011) 109–118.
[152] F.C. Moreira, J. Soler, A. Fonseca, I. Saraiva, R.A.R. Boaventura, E. Brillas, V.J.P. Vilar, Appl. Catal. B: Environ. 182 (2016) 161–171.
[153] J.J. Pignatello, Environ. Sci. Technol. 26 (1992) 944–951.
[154] R.E. Meeker, inventors. Stabilization of hydrogen peroxide. United States Patent 3208825 A. 1965 September 28.
[155] E. Guinea, C. Arias, P.L. Cabot, J.A. Garrido, R.M. Rodríguez, F. Centellas, E. Brillas, Water Res. 42 (2008) 499–511.
[156] A.R. Khataee, M. Zarei, L. Moradkhannejhad, Desalination 258 (2010) 112–119.
[157] Y. Sun, J.J. Pignatello, J. Agric. Food. Chem. 40 (1992) 322–327.
[158] A. Safarzadeh-Amiri, J.R. Bolton, S.R. Cater, Water Res. 31 (1997) 787–798.
[159] R.M. Smith, A.E. Martell, Sci. Total Environ. 64 (1987) 125–147.
[160] A.P.S. Batista, R.F.P. Nogueira, J. Photochem. Photobiol. A: Chem. 232 (2012) 8–13.
[161] E. Brillas, M.A. Baños, M. Skoumal, P.L. Cabot, J.A. Garrido, R.M. Rodríguez, Chemosphere 68 (2007) 199–209.
[162] E. Rosales, M. Pazos, M.A. Longo, M.A. Sanromán, Chem. Eng. J. 155 (2009) 62–67.
[163] B. Gözmen, B. Kayan, A.M. Gizir, A. Hesenov, J. Hazard. Mater. 168 (2009) 129–136.
[164] E.S. Galbavy, K. Ram, C. Anastasio, J. Photochem. Photobiol. A: Chem. 209 (2010) 186–192.
[165] E. Forgacs, T. Cserháti, G. Oros, Environ. Int. 30 (2004) 953–971.
[166] S. Garcia-Segura, F. Centellas, C. Arias, J.A. Garrido, R.M. Rodríguez, P.L. Cabot, E. Brillas, Electrochim. Acta 58 (2011) 303–311.
[167] F.C. Moreira, S. Garcia-Segura, V.J.P. Vilar, R.A.R. Boaventura, E. Brillas, Appl. Catal. B: Environ. 142–143 (2013) 877–890.
[168] A.M.S. Solano, S. Garcia-Segura, C.A. Martínez-Huitle, E. Brillas, Appl. Catal. B: Environ. 168–169 (2015) 559–571.
[169] J.M. Peralta-Hernández, Y. Meas-Vong, F.J. Rodríguez, T.W. Chapman, M.I. Maldonado, L.A. Godínez, Dyes Pigm. 76 (2008) 656–662.
[170] E.J. Ruiz, A. Hernández-Ramírez, J.M. Peralta-Hernández, C. Arias, E. Brillas, Chem. Eng. J. 171 (2011) 385–392.
[171] X. Florenza, A.M.S. Solano, F. Centellas, C.A. Martínez-Huitle, E. Brillas, S. Garcia-Segura, Electrochim. Acta 142 (2014) 276–288.
[172] Y. Juang, E. Nurhayati, C. Huang, J.R. Pan, S. Huang, Sep. Purif. Technol. 120 (2013) 289–295.
[173] B. Elias, L. Guihard, S. Nicolas, F. Fourcade, A. Amrane, Environ. Prog. Sustain. Energy 30 (2011) 160–167.
[174] J.L. Nava, I. Sirés, E. Brillas, Environ. Sci. Pollut. Res. 21 (2014) 8485–8492.
[175] E. Rosales, O. Iglesias, M. Pazos, M.A. Sanromán, J. Hazard. Mater. 213–214 (2012) 369–377.
[176] A.K. Abdessalem, N. Bellakhal, N. Oturan, M. Dachraoui, M.A. Oturan, Desalination 250 (2010) 450–455.
[177] M.A. Oturan, M. Pimentel, N. Oturan, I. Sirés, Electrochim. Acta 54 (2008) 173–182.
[178] N. Oturan, E. Brillas, M. Oturan, Environ. Chem. Lett. 10 (2012) 165–170.
[179] N. Oturan, M.A. Oturan, Agron. Sustain. Dev. 25 (2005) 267–270.
[180] A. Dhaouadi, N. Adhoum, J. Electroanal. Chem. 637 (2009) 33–42.

[181] B.R. Garza-Campos, J.L. Guzmán-Mar, L.H. Reyes, E. Brillas, A. Hernández-Ramírez, E.J. Ruiz-Ruiz, Chemosphere 97 (2014) 26–33.
[182] N. Oturan, S. Trajkovska, M.A. Oturan, M. Couderchet, J.-J. Aaron, Chemosphere 73 (2008) 1550–1556.
[183] A.R.F. Pipi, I. Sirés, A.R. De Andrade, E. Brillas, Chemosphere 109 (2014) 49–55.
[184] A. Da Pozzo, C. Merli, I. Sirés, J.A. Garrido, R.M. Rodríguez, E. Brillas, Environ. Chem. Lett. 3 (2005) 7–11.
[185] A. Babuponnusami, K. Muthukumar, Chem. Eng. J. 183 (2012) 1–9.
[186] K. Kümmerer, Chemosphere 45 (2001) 957–969.
[187] O.A.H. Jones, N. Voulvoulis, J.N. Lester, Crit. Rev. Environ. Sci. Technol. 35 (2005) 401–427.
[188] I. Sirés, F. Centellas, J.A. Garrido, R.M. Rodríguez, C. Arias, P.L. Cabot, E. Brillas, Appl. Catal. B: Environ. 72 (2007) 373–381.
[189] A. Dirany, I. Sirés, N. Oturan, M.A. Oturan, Chemosphere 81 (2010) 594–602.
[190] F. Ferrag-Siagh, F. Fourcade, I. Soutrel, H. Aït-Amar, H. Djelal, A. Amrane, J. Chem. Technol. Biotechnol. 88 (2013) 1380–1386.
[191] E. Isarain-Chávez, R.M. Rodríguez, P.L. Cabot, F. Centellas, C. Arias, J.A. Garrido, E. Brillas, Water Res. 45 (2011) 4119–4130.
[192] A. El-Ghenymy, P.L. Cabot, F. Centellas, J.A. Garrido, R.M. Rodríguez, C. Arias, E. Brillas, Chemosphere 91 (2013) 1324–1331.
[193] H. Olvera-Vargas, N. Oturan, M.A. Oturan, E. Brillas, Sep. Purif. Technol. 146 (2015) 127–135.
[194] F. Sopaj, N. Oturan, J. Pinson, F. Podvorica, M.A. Oturan, Appl. Catal. B: Environ. 199 (2016) 331–341.
[195] E. Brillas, S. Garcia-Segura, M. Skoumal, C. Arias, Chemosphere 79 (2010) 605–612.
[196] K. Rajeshwar, J.G. Ibanez, Environmental Electrochemistry: Fundamentals and Application in Pollution Abatement, Academic Press, San Diego, United States, 1997.
[197] E. Brillas, E. Mur, R. Sauleda, L. Sànchez, J. Peral, X. Domènech, J. Casado, Appl. Catal. B: Environ. 16 (1998) 31–42.
[198] Z. Rappoport, The Chemistry of Phenols, John Wiley & Sons Ltd, West Sussex, England, 2003.
[199] M. Pimentel, N. Oturan, M. Dezotti, M.A. Oturan, Appl. Catal. B: Environ. 83 (2008) 140–149.
[200] C. Flox, C. Arias, E. Brillas, A. Savall, K. Groenen-Serrano, Chemosphere 74 (2009) 1340–1347.
[201] E. Guinea, F. Centellas, J.A. Garrido, R.M. Rodríguez, C. Arias, P.-L. Cabot, E. Brillas, Appl. Catal. B: Environ. 89 (2009) 459–468.
[202] S. Garcia-Segura, E. Brillas, Water Res. 45 (2011) 2975–2984.
[203] H. Patel, R.T. Vashi, Characterization and Treatment of Textile Wastewater, 1st ed., Elsevier, United States, 2015.
[204] S.S. Vaghela, A.D. Jethva, B.B. Mehta, S.P. Dave, S. Adimurthy, G. Ramachandraiah, Environ. Sci. Technol. 39 (2005) 2848–2855.
[205] J.R. Domínguez, T. González, P. Palo, J. Sánchez-Martín, M.A. Rodrigo, C. Sáez, Water Air Soil Pollut. 223 (2012) 2685–2694.
[206] B. Kasprzyk-Hordern, R.M. Dinsdale, A.J. Guwy, Water Res. 43 (2009) 363–380.
[207] E. Dialynas, D. Mantzavinos, E. Diamadopoulos, Water Res. 42 (2008) 4603–4608.
[208] G. Pérez, A.R. Fernández-Alba, A.M. Urtiaga, I. Ortiz, Water Res. 44 (2010) 2763–2772.
[209] J. Radjenovic, A. Bagastyo, R.A. Rozendal, Y. Mu, J. Keller, K. Rabaey, Water Res. 45 (2011) 1579–1586.
[210] K. Van Hege, M. Verhaege, W. Verstraete, Electrochem. Commun. 4 (2002) 296–300.
[211] K. Van Hege, M. Verhaege, W. Verstraete, Water Res. 38 (2004) 1550–1558.
[212] G. Tchobanoglous, F. Kreith, Handbook of Solid Waste Management, 2nd ed., McGraw-Hill, New York, United States, 2002.
[213] D. Fatta, A. Papadopoulos, M. Loizidou, Environ. Geochem. Health 21 (1999) 175–190.
[214] S.R. Qasim, W. Chiang, Sanitary Landfill Leachate – Generation, Control and Treatment, CRC Press LLC, Boca Raton, United States, 1994.
[215] A. Cabeza, A. Urtiaga, M.-J. Rivero, I. Ortiz, J. Hazard. Mater. 144 (2007) 715–719.
[216] A. Urtiaga, A. Rueda, Á. Anglada, I. Ortiz, J. Hazard. Mater. 166 (2009) 1530–1534.
[217] H. Zhang, Y. Li, X. Wu, Y. Zhang, D. Zhang, Waste Manage. 30 (2010) 2096–2102.
[218] N. Nageswara Rao, M. Rohit, G. Nitin, P.N. Parameswaran, J.K. Astik, Chemosphere 76 (2009) 1206–1212.
[219] N. Oturan, E.D. van Hullebusch, H. Zhang, L. Mazeas, H. Budzinski, K. Le Menach, M.A. Oturan, Environ. Sci. Technol. 49 (2015) 12187–12196.
[220] A. Anglada, A.M. Urtiaga, I. Ortiz, J. Hazard. Mater. 181 (2010) 729–735.
[221] A. Fernandes, D. Santos, M.J. Pacheco, L. Ciríaco, A. Lopes, Appl. Catal. B: Environ. 148–149 (2014) 288–294.
[222] M. Panizza, C.A. Martinez-Huitle, Chemosphere 90 (2013) 1455–1460.
[223] J. Chapman, P. Baker, S. Wills, Winery Wastewater Handbook: Production, Impacts and Management, Winetitles, Adelaide, Australia, 2001.
[224] F.C. Moreira, R.A.R. Boaventura, E. Brillas, V.J.P. Vilar, Water Res. 75 (2015) 95–108.
[225] C. Salazar, I. Sirés, R. Salazar, H.D. Mansilla, C.A. Zaror, J. Chem. Technol. Biotechnol. 90 (2015) 2017–2026.
[226] Y. Laor, J.A. Koziel, L. Cai, U. Ravid, J. Air Waste Manage. Assoc. 58 (2008) 1187–1197.
[227] B. Borbón, M.T. Oropeza-Guzman, E. Brillas, I. Sirés, Environ. Sci. Pollut. Res. 21 (2014) 8573–8584.
[228] P.D. Saha, P.K. Banerjee, Treatability Studies of Tannery Wastewater: Treatment of Tannery Wastewater Using Chemical and Bioremediation Techniques, LAP Lambert Academic Publishing, Saarbrücken, Germany, 2012.
[229] E. Isarain-Chávez, C. De La Rosa, L.A. Godínez, E. Brillas, J.M. Peralta-Hernández, J. Electroanal. Chem. 713 (2014) 62–69.
[230] M. Panizza, G. Cerisola, in: D.V. Zinger (Ed.), Advances in Chemistry Research, vol. 2, Nova Science, New York, United States, 2006, pp. 1–38.
[231] F. Cardarelli, Materials Handbook: A Concise Desktop Reference, 2nd ed., Springer-Verlag London Limited, London, United Kingdom, 2008.
[232] H. Olvera-Vargas, N. Oturan, C.T. Aravindakumar, M.M.S. Paul, V.K. Sharma, M.A. Oturan, Environ. Sci. Pollut. Res. 21 (2014) 8379–8386.
[233] A. Özcan, Y. Şahin, A.S. Koparal, M.A. Oturan, J. Hazard. Mater. 153 (2008) 718–727.